

**ASYNCHRONOUS REPRESENTATION AND  
PROCESSING OF ANALOG SPARSE SIGNALS  
USING A TIME-SCALE FRAMEWORK**

by

**Azime Can-Cimino**

B.Sc in Electrical and Electronics Eng., Istanbul University, 2005

M.Sc in Electrical and Electronics Eng., Istanbul University, 2008

Submitted to the Graduate Faculty of  
the Swanson School of Engineering in partial fulfillment  
of the requirements for the degree of

**Doctor of Philosophy**

University of Pittsburgh

2014

UNIVERSITY OF PITTSBURGH  
SWANSON SCHOOL OF ENGINEERING

This dissertation was presented

by

Azime Can-Cimino

It was defended on

March 24, 2014

and approved by

Luis F. Chaparro, Ph.D., Professor, Department of Electrical and Computer Engineering

Amro A. El-Jaroudi, Ph.D., Professor, Department of Electrical and Computer Engineering

Ervin Sejdić, Ph.D., Professor, Department of Electrical and Computer Engineering

Juan J. Manfredi, Ph.D., Professor, Department of Mathematics

Zhi-Hong Mao, Ph.D., Professor, Department of Electrical and Computer Engineering

Mingui Sun, Ph.D., Professor, Department of Neurological Surgery

Dissertation Director: Luis F. Chaparro, Ph.D., Professor, Department of Electrical and  
Computer Engineering

Copyright © by Azime Can-Cimino  
2014

# ASYNCHRONOUS REPRESENTATION AND PROCESSING OF ANALOG SPARSE SIGNALS USING A TIME-SCALE FRAMEWORK

Azime Can-Cimino, PhD

University of Pittsburgh, 2014

In this dissertation we investigate the problem of asynchronous representation and processing of analog sparse signals using a time-scale framework. Recently, in the design of signal representations the focus has been on the use of application-driven constraints for optimality purposes. Appearing in many fields such as neuroscience, implantable biomedical diagnostic devices, and sensor network applications, sparse or burst-like signals are of great interest.

A common challenge in the representation of such signals is that they exhibit non-stationary behavior with frequency-varying spectra. By ignoring that the maximum frequency of their spectra is changing with time, uniformly sampling sparse signals collects samples in quiescent segments and results in high power dissipation. Also, continuous monitoring of signals challenges data acquisition, storage, and processing; especially if remote monitoring is desired, as this would require that a large number of samples be generated, stored and transmitted. Power consumption and the type of processing imposed by the size of the devices in the aforementioned applications has motivated the use of asynchronous approaches in our research. First, we work on establishing a new paradigm for the representation of analog sparse signals using a time-frequency representation. Second, we develop a scale-based signal decomposition framework which uses filter-bank structures for the representation-analysis-compression scheme of the sparse information. Using an asynchronous signal decomposition scheme leads to reduced computational requirements and lower power consumption; thus it is promising for hardware implementation. In addition, the proposed algorithm does not require prior knowledge of the bandwidth of the signal and

the effect of noise can still be alleviated. Finally, we consider the synthesis step, where the target signal is reconstructed from compressed data. We implement a perfect reconstruction filter bank based on Slepian wavelets to use in the reconstruction of sparse signals from non-uniform samples.

In this work, experiments on primary biomedical signal applications, such as electrocardiogram (EEG), swallowing signals and heart sound recordings have achieved significant improvements over traditional methods in the sensing and processing of sparse data. The results are also promising in applications including compression and denoising.

## TABLE OF CONTENTS

<b>PREFACE</b> . . . . .	xii
<b>1.0 INTRODUCTION</b> . . . . .	1
<b>2.0 BACKGROUND</b> . . . . .	4
2.1 Examples of Non-Uniform Sampling . . . . .	5
2.1.1 Level-Crossing Sampling . . . . .	5
2.1.2 Asynchronous Sigma Delta Modulation . . . . .	7
2.2 Wavelet Transform and Multiresolution Analysis . . . . .	9
2.3 Bases with Time and Frequency Localizations . . . . .	17
2.3.1 Haar Bases . . . . .	21
2.3.2 Slepian Functions . . . . .	24
2.4 Perfect Reconstruction Filter Banks . . . . .	31
<b>3.0 ANALYSIS OF ANALOG TIME-SPARSE SIGNALS</b> . . . . .	35
3.1 Asynchronous Analysis with ASDM . . . . .	37
3.2 Signal Decomposers . . . . .	43
3.2.1 Cascade Decomposers . . . . .	44
3.2.2 Parallel Decomposer . . . . .	50
3.3 Modified ASDM Bank of Filters . . . . .	53
3.3.1 Modified ASDM as a Non-uniform Sampler . . . . .	53
3.3.2 Asynchronous Analysis with MASDM . . . . .	54
<b>4.0 SYNTHESIS OF SPARSE SIGNALS</b> . . . . .	57
4.1 Slepian Sequences for Regularized Reconstruction . . . . .	58
4.2 Modulated Slepian Sequences for Regularized Reconstruction . . . . .	60

<b>5.0 WAVELET BASES FOR SPARSE SIGNALS</b> . . . . .	63
5.1 FIR Biorthogonal Filters for the Slepian Wavelet Transform . . . . .	65
5.2 Multiresolution Analysis with the Slepian Scaling Functions . . . . .	76
5.3 Incorporating Slepian Wavelets into Asynchronous Decomposers . . . . .	90
5.4 Conclusions . . . . .	93
<b>6.0 FUTURE WORK</b> . . . . .	97
<b>BIBLIOGRAPHY</b> . . . . .	98

## LIST OF FIGURES

1	Level-crossing Sampling . . . . .	6
2	Asynchronous sigma delta, and its signals $y(t)$ and $z(t)$ . . . . .	7
3	Nested Vector Spaces spanned by the Scaling Functions . . . . .	11
4	Wavelet Spaces $\{ W_j \}$ . . . . .	14
5	Haar Wavelet Function . . . . .	21
6	Haar Scaling and Wavelet functions for different scales . . . . .	22
7	Haar analysis and synthesis filter banks . . . . .	23
8	Slepian Spectral Decomposition obtained with four Slepian functions . . . . .	26
9	The four most bandlimited Slepian functions and their spectra ( $N = 100$ , $NW = 2$ ). . . . .	27
10	Slepian Wavelets . . . . .	30
11	Reconstruction and Compression with Slepian wavelets . . . . .	30
12	Two channel multi-rate filter bank . . . . .	33
13	Different scale parameters: (a) $\kappa_i$ , (b) $2\kappa_i$ , (c) $\frac{\kappa_i}{2}$ . . . . .	40
14	Left: definition of $\alpha_k$ and $\beta_k$ corresponding to consecutive pulses of $z(t)$ ; Right (a)–(d): effect of scale parameter $\kappa$ as it decreases. . . . .	41
15	A module of the asynchronous low-frequency decomposer . . . . .	43
16	Low-Frequency Decomposer . . . . .	44
17	High-Frequency Decomposer . . . . .	44
18	Input to the (a) first, (b) second, (c) 5th and (d) 8th module, respectively. . . . .	46
19	Reconstruction of test signal $x_1(t)$ (dark signal) with additive noise SNR=3 dB. . . . .	46

20	(a) Recorded and (b) Reconstructed Swallowing Data: type dry, cross correlation between the reconstructed signal and original signal 84.7 . . . . .	47
21	Left: phonocardiogram recording of a heart sound without noise (a); reconstructed signal (b); and reconstruction error (c). Right: phonocardiogram recording with additive noise (d); reconstructed signal (e); and reconstruction error (f). . . . .	48
22	Left: Spectrum of phonocardiogram recording of a heart sound without noise (a); reconstructed signal (b); and reconstruction error (c). Right: Spectrum of phonocardiogram recording with additive noise (d); reconstructed signal (e); and reconstruction error (f). . . . .	49
23	Multilevel signal components for noiseless recording, (a) and (b); histograms of the averages for the components, (c) and (d). . . . .	50
24	Left: High-frequency decomposition for synthetic signal composed of four sinusoids: (a)–(b) original signal and its spectrum, (c)–(h) $d_i(t)$ components, (i) $f_L(t)$ component. Right: Low-frequency decomposition for speech signal: (a)–(b) original signal and its spectrum, (c)–(h) $e_i(t)$ components, (i) $g_M(t)$ component. . . . .	51
25	Bank-of-filters decomposer . . . . .	52
26	Resulting $d_i(t)$ 's on parallel decomposer configuration . . . . .	52
27	Modified Asynchronous Sigma Delta Modulator . . . . .	53
28	Non-uniform samples obtained using Modified ASDM . . . . .	54
29	Asynchronous Decomposer . . . . .	55
30	The equivalent filters . . . . .	56
31	(a) Iterative estimator output (b) Quantization Error with SNR=17.94dB . . . . .	59
32	Right: Spectra of analyzed signal and of Discrete Slepian Sequences; left: Modulated-Discrete Slepian Sequences . . . . .	61
33	Reconstructed signal and error: (left) Modulated-Slepian reconstruction for SNR= 25.95dB, $M = 120$ , $\epsilon = 2 \times 10^{-4}$ , (middle) baseband Slepian reconstruction (SNR=15.20 dB, $M=600$ , $\epsilon = 2 \times 10^{-4}$ ) (right) Piecewise Cubic Interpolator (SNR= 10.89 dB) . . . . .	62

34	Two-channel filter banks leading to Slepian wavelets . . . . .	65
35	(a) First Slepian function and convolutions of it with itself, (b) Refinement Equation verification . . . . .	68
36	Wavelet Transform with filter banks . . . . .	70
37	$\pi$ -bandlimited Biorthogonal Slepian scaling functions $\phi$ and and corresponding wavelets $\psi$ : (a) N=2 DPSS sequence; (b)-(d) N=3 DPSS sequence; (e)-(h) N=4 DPSS sequence . . . . .	73
38	Dual Slepian scaling functions $\tilde{\phi}$ and wavelets $\tilde{\psi}$ based on different lengths L: (a) length-2; (b) length-5; (c) length-9; (d) length-13; (e) length-4; (f) length-8; (g) length-16, (h) length-20 . . . . .	74
39	Different lengths decomposition and reconstruction filters: (a) $2 \times 2$ ; (b) $3 \times 5$ ; (c) $3 \times 9$ ; (d) $3 \times 13$ ; (e) $4 \times 4$ ; (f) $4 \times 8$ ; (g) $4 \times 16$ ; (b) $4 \times 20$ where $M \times N$ denotes length- $M$ decomposition filter and length- $N$ reconstruction filter . . . . .	75
40	(a) First Slepian function $\phi(t) = \varphi_{0,\pi,\tau}(t)$ and, (b) its Fourier transform $\hat{\theta}(\omega)$ . . . . .	76
41	Decomposition of a discrete approximation $A_{j+1}x$ into an approximation at a coarser resolution and detail $D_jx$ . . . . .	79
42	Coarse approximations $a_j[n]$ at at resolutions 1, 1/2, 1/4, 1/8, 1/16 and 1/32 of the signal shown at the bottom . . . . .	79
43	Multi-resolution discrete approximations of an discontinuous signal: (a) Coarse approximations $A_jx$ with different resolution scaling function, (b) Detail approximation with wavelets. The top gives the coarse approximation at resolution 1/32 . . . . .	80
44	Wavelet function $\psi(t)$ and, Right: its Fourier transform $\hat{\psi}(\omega)$ . . . . .	81
45	Frequency splitting in a $j = 2$ scale approximation . . . . .	82
46	(a) Top: Piecewise constant function, Bottom: Gaussian White noise added ( $SNR = 21.8dB$ ); (b) Top: Wiener Filter estimation ( $SNR = 26.6dB$ ), Bottom: Estimation reconstructed from thresholded wavelet coefficients of Slepian length-2 wavelet ( $SNR = 38.9dB$ ); (c) Slepian wavelet transform of the clean signal: (d) Slepian wavelet transform of noisy signal . . . . .	85
47	Slepian wavelet transform of a smooth signal with short live irregularities . . . . .	86

48	Wavelet Enhancement:(a) Noisy signal, (b)Reconstruction with Daubechies length-5 wavelets, (c) Reconstruction with Slepian length-5wavelets . . . . .	86
49	Wavelet denoising (a) with Haar wavelet, Top: Noisy chirp signal, Middle: Coarse approximation, Bottom: Details; (b) with Slepian wavelet Top: Noisy chirp signal, Middle: Coarse approximation, Bottom: Details . . . . .	87
50	Piecewise regular signal representation: (a) original signal; (b) Fourier basis approximation (notice the Gibbs ringing at the discontinuities in the original signal); (c) <i>Length</i> – 20 Slepian wavelet (Gibb’s ringing still present); (d) <i>Length</i> – 2 Slepian wavelet (there is smoothing at the discontinuities); (e) <i>Length</i> – 7 Slepian wavelet . . . . .	88
51	Heisenberg rectangles that indicate where the energy of the basis is mostly concentrated (a) A local Slepian basis divides the time axis with smooth windows where modulation translates these windows in frequency: (b) Wavelet basis divides the frequency into octave bandwidths . . . . .	91
52	Biorthogonal Slepian wavelet basis performance on sparse signal . . . . .	92
53	A sparse data: (a) the original signal with samples, 38% samples; (b) Sample positions; (c) Interpolation with long–length Slepian wavelets, $SNR = 14.2dB$ ( $N = 17, W = \pi$ rad/sec); (d) Interpolation with short–length Slepian wavelets, $SNR = 11.6dB$ ( $N = 4, W = \pi$ rad/sec) . . . . .	95
54	A sparse data: (a) the original signal with samples, 21% samples; (b) Interpolation of samples in (a) with long–length Slepian wavelets, $SNR = 11.4dB$ ( $N = 17, W = \pi$ rad/sec); (c) the original signal with samples, 42% samples; (d) Interpolation of samples in (c) with short–length Slepian wavelets $SNR = 11.6dB$ ( $N = 4, W = \pi$ rad/sec) . . . . .	96

## PREFACE

I am thankful to my wonderful husband Matthew Cimino for all of his support. I used to think I should acknowledge french press coffee in my thesis for all its help in the long days that I didn't move away from my desk. It was only after meeting him that it became possible to have the same productivity without drinking five cups of coffee a day. I am grateful for the peace and inspiration that he has brought into my life.

I am grateful to my families here and miles away. I am thankful to my loving grandmother and mother for all their support in all of my endeavors.

I always felt lucky to work with Dr. Chaparro and have him as an advisor. He was always patient while helping with the problems I struggled on. He is an inspiring and insightful mentor. Both for his guidance and time I would like to thank him.

I also would like to thank Dr. El-Nokali, Dr. Jaroudi, and my committee members for their help in my studies.

I dedicate this thesis to my father.

## 1.0 INTRODUCTION

This thesis investigates asynchronous representation and retrieval of sparse signals and their applications to biomedical signal processing. After the two introductory chapters, the thesis splits into three parts that present the contributions of this work on sparse signal processing.

Chapter 2 is the introductory chapter where we explain the theory that we based our research on. Chapters 3 and 4 offer a comprehensive discussion of the asynchronous analysis and reconstruction of non-stationary signals within a time-scale framework. In Chapter 3, we discuss the class of analysis methods for sampling and representation of sparse signals. Specifically we consider a filter-bank set up that takes advantage of the sparsity of the data in order to compressively represent the information. We then propose an implementable wavelet-like scale based decomposition scheme that returns a small number of scale parameters.

Next, in Chapter 4, we suggest methods to retrieve information from highly non-uniform samples. The reconstruction from non-uniform samples is well known. However, there is room for improvements. We suggest improvements on the existing techniques on sparse signals in order to handle robust reconstructions with a reduced computational complexity. We generalize the concept by construction of multi-scale approximations that follow from the proposed analysis model in the first part of the work. In section 4.2 we obtained the reconstruction of highly non-uniform sampled signals by connecting the sinc and the Slepian functions—a more appropriate basis. Then in section 4.2, we propose a practical scheme that is based on modulated Slepian functions to achieve low-complexity and low-error solutions for the reconstruction problem. Our approach results in a robust and computationally efficient implementation.

In the second part of the thesis, Chapter 5, we discuss Slepian wavelet bases and implement a perfect reconstruction filter bank based on Slepian wavelets to use in the representation of sparse signals. In general, wavelets have shown to be good tools for representation of smooth or piece-wise smooth signals in many applications. Despite the optimality of wavelets in representing piecewise smooth functions, limited capacity of these algorithms to model the dependency between wavelet coefficients across scales makes them perform far from optimal for sparse signals. By incorporating the Slepian wavelets into the proposed asynchronous schemes we obtain wavelet expansion coefficients from non-uniform samples and, relate the coefficients in different scales to derive a multi resolution analysis.

The presented work is a novel approach in applying and combining recent research results from asynchronous signal processing, sampling theory and Slepian wavelets. Its key contributions can be grouped under the following items:

- A new paradigm for the representation of analog sparse signals is established using time-scale representations. We have shown that it is possible to obtain efficient analysis of the sparse information with a new understanding of the interaction of continuous-time and discrete-time signal processing.
- We develop a scale-based asynchronous signal decomposition framework which uses filter-bank structures for the representation-analysis-compression scheme of the sparse information. Using an asynchronous signal decomposition scheme leads to reduced computational requirements and power consumption compared to current synchronous techniques; thus, it is promising for practical hardware implementation.
- A novel signal-dependent non-uniform sampling technique using an Asynchronous Sigma Delta Modulator is derived.
- We implement a perfect reconstruction filter bank based on Slepian wavelets.
- We establish information retrieval using highly non-uniform samples with a computationally low-cost algorithm that exploits Slepian wavelets.

Related publications:

1. A. Can, E. Sejdić and L. F. Chaparro, “ Asynchronous Processing of Sparse Signals,” *IET Signal Processing*, vol. 8, Issue 3, May 2014.

2. L. F. Chaparro, E. Sejdić, A. Can, O. Alkishiwo, S. Senay and A. Akan, "Asynchronous Processing of Non-stationary Signals in a Time-frequency Context," *Signal Processing Magazine, IEEE*, vol.30, pages: 42 – 52, Nov 2013
3. E. Sejdić, A. Can, L. F. Chaparro, C. M. Steele, and T. Chau, "Compressive Sampling of Swallowing Accelerometry Signals Using Time-Frequency Dictionaries Based on Modulated Discrete Prolate Spheroidal Sequences," *Eurasip Journal on Advances in Signal Processing*, vol.101, 2012.
4. Can, A. and L.F. Chaparro, "Asynchronous sampling and reconstruction of analog sparse signals," *Sensing Technology Applications (SPIE)*, May 5-9 2014, Maryland, USA
5. Can, A. and Chaparro, L. F., "Asynchronous Bank of Filters for Sparse Signal Decomposition," *21th European Sig. Proc. Conf. (EUSIPCO)*, Sept. 9-13, 2013, Marrakech, Morocco.
6. Can, A. and Sejdić, E. and Alkishiwo, O. and Chaparro, L.F. , "Compressive asynchronous decomposition of heart sounds," pp.736-739, *Statistical Signal Processing Workshop, 2012 IEEE (SSP)*, Aug. 5-8, 2012, Michigan, USA.
7. Can, A. and Sejdić, E. and Chaparro, L. F., "Asynchronous sampling and reconstruction of sparse signals," pp. 854-858, *20th European Sig. Proc. Conf. (EUSIPCO)*, Aug. 27-31, 2012, Bucharest, Romania.
8. Can, A. and Sejdić, E. and Chaparro, L. F., "An asynchronous scale decomposition for biomedical signals," pp. 1-6, *IEEE Signal Proc. in Medicine and Biology Symposium (SPMB)*, Dec. 10, 2011, Brooklyn, New York, USA.

## 2.0 BACKGROUND

This chapter reviews the theoretical basis for this thesis. The target signals under consideration are sparse signals. Over the course of our analysis, we are concerned about the concise representation of the information, starting from the sampling to coding and eventually transmission stages. Besides the sparse nature, one of the common aspect of the signals that we deal with is their non-stationarity. Conceptually, non-stationarity relates to the variation over time of the statistics of the signal. Thus in sampling and representation of non-stationary signals one has to take into account that the frequency content is changing. Ignorance of this change can results in a redundancy in sample sizes. A more appropriate approach is to make the sampling and representation signal-dependent. Hence we first wanted to review the signal-dependent processing techniques Level Crossing Sampling (LCS) and Asynchronous Sigma Delta Modulation (ASDM) in section 2.1.1 and section 2.1.2 respectively.

Then we look at the wavelet transform in section 2.2, which enables the analysis of the different frequency components within a signal using variable size windows. We provide the main aspects of multi resolution analysis that is fundamental in wavelet representation.

In addition to signal characteristics and localization in time and frequency (and in space for 2-d), localization of a basis is an important aspect in the designing of tools for information extraction. In section 2.3 we consider the basis that allow us to develop localized techniques. First considered was a Haar basis, which has the shortest time support among all other wavelets basis. A Slepian basis was then considered which yields the most concentrated waveform in a desired bandwidth.

Lastly, perfect reconstruction filter banks are included in section 2.4, which enable us to implement wavelet transforms.

## 2.1 EXAMPLES OF NON-UNIFORM SAMPLING

Uniform sampling is done at a rate dictated by the highest frequency component of the input. When the input is slower or not changing, the resulting higher than needed sampling rate provides redundant information at the cost of high power dissipation [1,2]. In many situations uniform sampling, connected to the Shannon-Nyquist sampling theory, either cannot be implemented or is not appropriate. For instance, when the nodes of a sensor network have limited sensing and processing power, non-uniform sampling is needed. In other situations, uniform sampling is not desirable due to the required high sampling rates and complex processing. This is the case, for continuous monitoring in health-related sensing where signal exhibit sparse nature in time. They are almost zero most of the time and changes occur at brief intervals; which challenges the analog to digital conversion given the high sampling rates required. Asynchronous sampling methods are an efficient alternative in these cases.

Asynchronous, i.e., without clocks, techniques alleviate the problem of power consumption. Instead of using analog to digital converters to sample and quantize the signal, asynchronous systems either acquire samples only when the signal reaches certain values, as in level-crossing sampling, or convert the amplitude of the signal into a binary signal with zero-crossing values proportional to the signal amplitude, as in time-encoding using asynchronous sigma delta modulator (ASDM).

### 2.1.1 Level-Crossing Sampling

Among several nonuniform sampling approaches proposed over the years, level-crossing sampling (LC sampling) has recently received attention from the circuits and systems community [3]. The scheme generates samples of the signal by recording the time instants at which the signal crosses a predefined quantization level. Resulting time instants are non-uniformly distributed as can be seen in Fig. 1. The advantage of level crossing is that samples are only collected when there is significant information in the signal, i.e. change. A drawback of LC sampling however, is that a set of quantization levels needs to be specified *a-priori* and that the sampling times and the corresponding amplitudes must be kept. Moreover, only

a multilevel reconstruction of the original signal is possible. In spite of this drawback, the LC sampling is not hampered by aliasing (no frequency content of the signal is considered) or quantization error (when the sample value coincides with one of the quantization levels), and can be processed in continuous-time [4].

For a given set of quantization levels  $\{q_i\}_{-N \leq i \leq N}$ , typically taken as uniform levels, the output of the level-crossing sampler,  $x_{lc}(t)$ ,  $0 \leq t \leq T$ , is approximated by a multilevel signal

$$x_{lc}(t) = \sum_{i=-N}^N q_i [u(t - \tau_i) - u(t - \tau_{i+1})] \quad (2.1)$$

where  $u(t) = 1, t > 0$  is unit-step function. Here,  $\tau_{i+1} > \tau_i$  and  $\tau_i$  corresponds to the time at which the signal coincides with a level  $q_i$ . This multi-level approximation of  $x(t)$  depends on the chosen quantization levels, and the times at which the signal coincides with these levels are not uniform. A possible advantage of this multi-level representation is that it can be converted into continuous-time binary signals which can be processed in continuous-time [1, 4, 5]. As we show next, the assignment of the quantization levels can be made adaptive by considering local averages of the signal. Such a method is possible using the asynchronous sigma delta modulator. Moreover, by using the ASDM the original signal can be recovered by approximating a resulting integral equation.

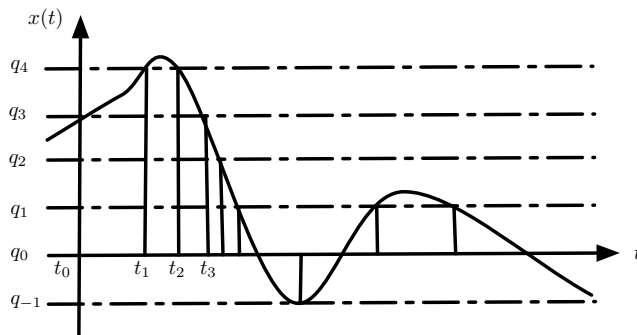


Figure 1: Level-crossing Sampling

### 2.1.2 Asynchronous Sigma Delta Modulation

The ASDM is a way of implementing non-uniform sampling. This modulator, shown in Fig. 2, is a nonlinear feedback system consisting of an integrator and a Schmitt trigger [6]. It maps the amplitude information of a bounded input signal  $x(t)$  into a time sequence  $\{t_k\}$  generated by the zero crossings of the binary output of the ASDM. For a bounded input  $x(t)$ ,  $|x(t)| < c$ , the output of the ASDM is a binary signal  $z(t)$  with values of  $+b$  or  $-b$ , and its zero-crossing times are directly related to the amplitude of  $x(t)$ .

Indeed, the output of the integrator in  $[t_k, t_{k+1}]$  is given by

$$y(t) = y(t_k) + \frac{1}{\kappa} \int_{t_k}^{t_{k+1}} [x(\tau) - z(\tau)] d\tau \quad (2.2)$$

The bias  $\pm b$  is chosen to be bigger than the bound  $c$  of the input signal  $x(t)$  to obtain increasing/decreasing function of time when integrated.

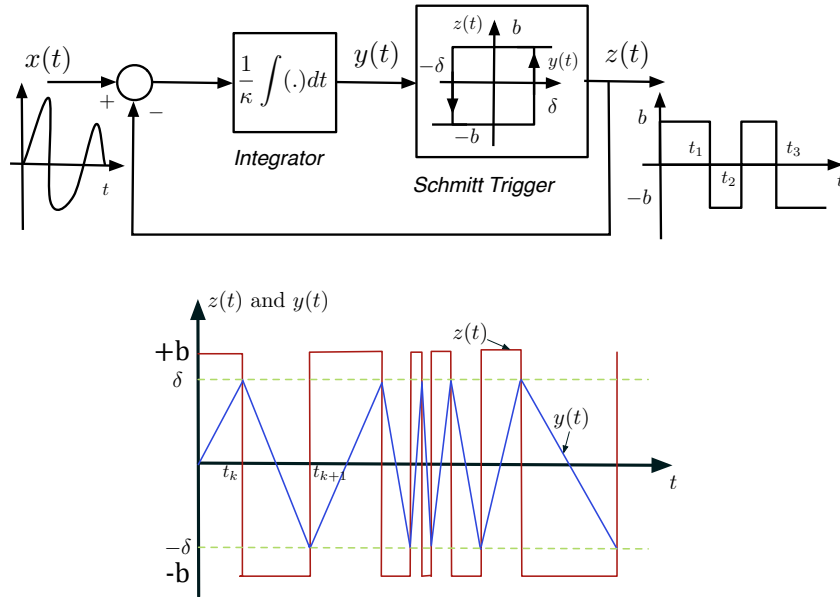


Figure 2: Asynchronous sigma delta, and its signals  $y(t)$  and  $z(t)$ .

When the output of the integrator reaches predefined values  $\pm\delta$  the output  $z(t)$  is triggered to the opposite state, see bottom of Fig. 2. How fast the triggering occurs is related to

the value of  $\kappa$ , which is somehow connected to the maximum frequency of the input signal. The information carried by the amplitude of  $x(t)$  is carried out by the zero-crossing times of the binary output signal  $z(t)$ . The zero-crossing times as well as the design parameters  $\{\kappa, \delta, b\}$  (strictly positive real numbers) depend on the nature of the signal.

Assuming that the initial state for  $[y(t_k), z(t_k)]$  is  $[\delta, b]$ , at some time  $t_{k+1} > t_k$  the output of the integrator,  $y(t)$ , reaches the triggering threshold  $-\delta$  so that according to (2.2):

$$-\delta = \delta + \frac{1}{\kappa} \int_{t_k}^{t_{k+1}} [x(\tau) - b] d\tau \quad \text{or} \quad \int_{t_k}^{t_{k+1}} x(\tau) d\tau = b(t_{k+1} - t_k) - 2\delta\kappa$$

Similarly starting with  $[y(t_{k+1}), z(t_{k+1})]$  at state  $[-\delta, -b]$ , we have at time  $t_{k+2}$  :

$$\delta = -\delta + \frac{1}{\kappa} \int_{t_{k+1}}^{t_{k+2}} [x(\tau) + b] d\tau \quad \text{or} \quad \int_{t_{k+1}}^{t_{k+2}} x(\tau) d\tau = -b(t_{k+2} - t_{k+1}) + 2\delta\kappa$$

Thus, for an increasing sequence  $\{t_k\}$ ,  $k \in \mathbb{Z}$ , we have from above

$$\int_{t_k}^{t_{k+1}} x(\tau) d\tau = (-1)^k [-b(t_{k+1} - t_k) + 2\kappa\delta] \quad (2.3)$$

It is of interest to note here that

- by approximating the integral using the trapezoidal rule and assuming a representation of the signal it is possible to obtain a uniform representation of the original signal using the zero-crossing times [7],
- a multilevel signal can be represented by zero-crossings using the above theory. For instance, consider that the multilevel signal is

$$x(t) = q \quad \tau_0 \leq t \leq \tau_1$$

If we let  $t_0 = \tau_0$  and  $t_2 = \tau_1$ , and fix  $b$  and  $\delta$  we then have for two consecutive pulses of the ASDM output using the integral equation above

$$\begin{aligned} q(t_1 - \tau_0) &= b(t_1 - \tau_0) - 2\kappa\delta \\ q(\tau_1 - t_1) &= -b(\tau_1 - t_1) + 2\kappa\delta \end{aligned}$$

Adding these two equations and replacing  $t_0$  and  $t_2$  we obtain a value for  $t_1$  by solving for it in

$$q(\tau_1 - \tau_0) = -b(\tau_1 + \tau_0) + 2bt_1 \quad \text{or} \quad t_1 = \frac{b(\tau_1 + \tau_0) + q(\tau_1 - \tau_0)}{2b}$$

and for that value, the value of  $\kappa$  for the ASDM is

$$\begin{aligned} \kappa &= (b - q) \frac{t_1 - \tau_0}{2\delta} \\ &= (q + b) \frac{b(\tau_1 + \tau_0) - q(\tau_1 - \tau_0)}{4b\delta} - \frac{\tau_0}{2\delta} \end{aligned}$$

This provides the connection of the ASDM with the level-crossing (LC) sampler as a non-uniform sampler, and that  $\kappa$  is connected to the frequency content of the signal. If we have the multilevel signal from the LC given by equation (2.1) we could for each  $i$  obtain an intermediate zero crossing and represent the multilevel signal by a binary signal with the resulting zero crossings.

We would like to use these two items in the representation of sparse signals.

## 2.2 WAVELET TRANSFORM AND MULTIREOLUTION ANALYSIS

Over the course of our analysis, we are concerned with the concise representation of information, starting from sampling to coding, and eventually transmission stages. Besides the sparse nature, one of the common aspect of the signals that we deal with is their non-stationarity. Hence, we use techniques that enable us to analyze them on more than one dimension and track their changing pattern in time. One of such techniques, which is the focus of this work, is the wavelet transform [8–13]. Here, we give the fundamental aspects of Wavelet Transform through a multi resolution perspective.

The wavelet transform enables the analysis of the different frequency components within a signal using variable size windows in contrast to fixed size windows in the Short-time Fourier Transform (STFT). In general without *a-priori* knowledge of the specific frequency content of the signal, determining an appropriate window size is a problem for STFT [14]. The

wavelet transform does not have this drawback. It uses variable window lengths by scaling a basis. Also uniform shifting of the scaled basis provides localization. The continuous wavelet transform of a signal  $x(t)$  can be expressed as

$$d(j, k) = \langle x, \psi_j \rangle = 2^{j/2} \int_{-\infty}^{\infty} x(t) \psi_j^*(t) dt \quad (2.4)$$

where  $\psi_j(t) = \psi(2^j t - k)$ . The symbol  $j > 0$  represents the scaling parameter which reflects the time and frequency resolutions of the basis  $\psi(2^j t - k)$ . As the scale  $j$  increases the width of the time window shortens hence the time resolution increases and the frequency resolution decreases. The index  $k$  is the translation parameter for uniformly shifting the scaled wavelet along the time axis. Through increasing scale and time shifts it is possible to catch the sudden changes at different locations of the analyzed signal. Similarly, by using large scales we can analyze low frequency components. This adaptive aspect is appealing for our analysis and motivated our early work, i.e. the asynchronous decomposers (see section 3) can detect the transient components in the scale domain.

The efficiency of the wavelet transform and optimality of a particular wavelet depends on the application. Different wavelet families are adapted for different applications. The focus of our work is on Slepian wavelets, first proposed by [15]. In addition to exhibit a multi-scale structure, they preserve the high energy concentration property inherited from Slepian functions. The definitions and details of Slepian basis functions are given in Section 2.3.2. The following lists some appealing aspects of wavelets for our analysis:

- The wavelet transform allows precise local description of signal behavior [8]. A wavelet expansion coefficient are indicative of the local features. That helps us to identify and get rid of the local noise or distortion caused by sensor imperfections or the noise in the given sensing environment.
- Wavelets are adjustable that they can be designed depending on the application.
- Wavelet analysis is well-suited for transient signals. Again, the localization aspect of wavelets allows a transient event to be modeled with a small number of coefficients [14].
- The magnitude of the expansion coefficients drops off rapidly with  $j$  and  $k$  for a large class of signals. This behavior makes wavelet analysis an attractive tool for compression and de-noising.

- Multi resolution analysis provides an insight to understand the effects of changing scale. Our proposed techniques exhibit a multi-resolution behavior where the signal is studied at different levels of resolution or scales. This allows us to process only the relevant details in a sparse signal. The main idea behind this is to use wavelet bases as a tool to describe the information in a signal from **coarse**–to **fine**–resolution in frequency.

A milestone in the development of the wavelet theory is the introduction of the multi-resolution analysis (MRA) [16]. In 1989 when Mallat and Meyer [16] have introduced the theory of multiresolution signal decomposition using wavelet bases. The framework makes it possible to construct wavelets and design their associated scaling functions without the need of continuous waveforms. By multiresolution approach, the wavelet is upstaged by a new basis, in addition to wavelet basis, so called the scaling. Scaling functions approximate a signal at many resolutions, with a factor of two between each, while the wavelets encode the information between the resolutions. Mallat suggested a bank of filters that computes the fast wavelet transform. These filters also provide an implementable procedure to synthesize wavelet bases. The algorithm requires order of operations that is the same size with the length of the signal. Section 2.4 shows that multi resolution approximations can be completely described as the part that retrieves the loss of information across resolutions.

MRA consists of a sequence of successive approximation spaces of different resolution as illustrated in the Fig. 3 [12]. The spaces denoted by  $V_j$  and so called approximation

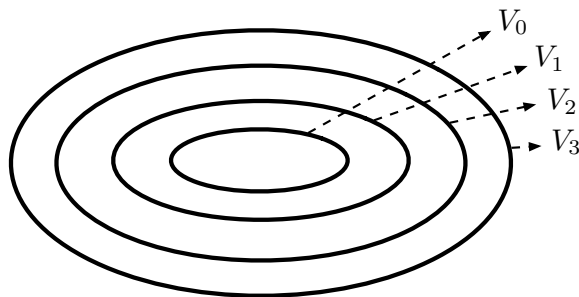


Figure 3: Nested Vector Spaces spanned by the Scaling Functions

spaces represent the set of all possible approximations of a signal at the resolution  $2^j$ . For simplicity, the common choice of resolution difference between is taken as 2. Approximation

of a function in these different resolution spaces is obtained by projection operator,  $A_j$ . Key ingredients of MRA spaces are [17]:

- $A_j$  is an orthogonal projection in order to have the closest approximation of a signal at a resolution of interest.

$$\forall g(t) \in V_j, \| A_j x(t) - x(t) \| \leq \| g(t) - x(t) \|$$

- *Shift-invariance*: The approximation of a signal,  $A_j x(t)$  can be represented by  $2^j$  samples per unit length. When the signal is shifted by a length proportional to  $2^{-j}$ ,  $A_j x(t)$  is shifted by the same amount.
- *Causality*: The approximation of a signal at a resolution  $2^j$  contains all the necessary information to compute the same signal at a coarser resolution, i.e.,

$$\begin{aligned} \forall j \in \mathbb{Z}, \quad V_j &\subset V_{j+1} \\ \forall j \in \mathbb{Z}, \quad x(t) \in V_j &\Leftrightarrow x(2t) \in V_{j+1} \end{aligned}$$

A detailed explanation of the properties of the projection operator  $A_j$  and vector spaces can be found in Mallat's paper [17]. There he introduces the scaling function, a unique function  $\phi(t) \in L^2\mathbb{R}$ , such that if  $\phi_j(t) = 2^j \phi(2^j t)$  for  $\forall j \in \mathbb{Z}$ , then it can be used as an orthonormal basis of  $V_j$ . In other words, one can build an orthonormal basis for any resolution level by dilating and translating a function  $\phi(t)$ . Thus the orthogonal projection on  $V_j$  can be computed as,

$$\forall x(t) \in L^2(\mathbb{R}), A_j x(t) = 2^{-j} \sum_{n=-\infty}^{\infty} \langle x(t), \phi_j(t) \rangle \phi_j^*(t) \quad (2.5)$$

This inner product can be interpreted as a convolution product that is evaluated at  $2^{-j}n$ , hence we can rewrite the approximation as,

$$A_j x = (x(t) * \phi_j(-t))|_{t=2^{-j}n} \quad (2.6)$$

Since  $\sqrt{2^{-j}}\phi_j(t-2^{-j}n)_{n \in \mathbb{Z}}$ ,  $\phi(t)$  is a orthonormal family of functions,  $\phi(t)$  can be considered as a low pass filter. Hence we can obtain  $A_j x$  by low pass filtering and then sampling uniformly

at the rate  $2^j$ . Let the subspace spanned by scaling function and its integer translates is denoted as,

$$V_0 = \overline{\text{Span } \phi(t-k)} \quad \text{so that} \quad x(t) = \sum_k a_k \phi(t-k) \quad \text{for any } x(t) \in V_0 \quad (2.7)$$

Equation (2.7) gives the flexibility of expressing a function in different resolution spaces. The relationship of the spanned spaces is depicted in Fig. 3,

$$\dots \subset V_{-2} \subset V_{-1} \subset V_0 \subset V_1 \subset V_2 \subset \dots \subset L^2 \quad (2.8)$$

with  $V_{-\infty} = 0$ ,  $V_{\infty} = L^2$  [12]. As depicted in Fig. 3, if  $\phi(t)$  is in  $V_0$ , it is also in  $V_1$ , the space spanned by  $\phi(2t)$ . This means we can express  $\phi(t)$  using  $V_1$  basis as well.

$$\phi(t) = \sum_n h_0(n) \sqrt{2} \phi(2t-n), \quad n \in Z \quad (2.9)$$

This recursive relation is also known as the *refinement* equation for scaling functions. Using scaling property of MRA spaces, if  $x(t) \in V_j$ , then it can be expanded onto a finer space. In other words, the space that contains the high resolution signals contains the lower resolutions as well. More generally, for  $j > 0$ , as we increase the value of  $j$  the span gets larger since  $\phi_j(t)$  is narrower, and the translation steps gets smaller. Therefore, it represents a finer detail. Likewise, for  $j < 0$   $\phi_j(t)$  is wider and is translated into larger steps. So, these wider scaling functions represent only coarse information, and the space they span is smaller.

Increasing the scale  $j$  will increase the size of the subspace spanned by  $\phi_j$  and will result in finer approximations of the signal. However a signal can be better described by not only increasing the scale, but by defining a different set of functions  $\psi_j(t)$  which span the differences between the spaces spanned by various scales of the scaling function, see Fig. 4 [12]. If we define an orthogonal complement of  $V_j$  in  $V_{j+1}$  as  $W_j$ , we can expand  $V_{j+1}$  in terms of its subspaces as,

$$V_{j+1} = V_j \oplus W_j \quad (2.10)$$

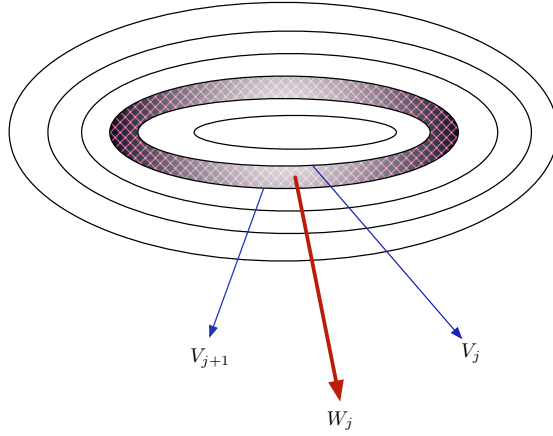


Figure 4: Wavelet Spaces  $\{ W_j \}$

In general this yields

$$L^2 = V_0 \oplus W_0 \oplus W_1 \oplus \dots \quad (2.11)$$

when  $V_0$  is the initial space spanned by the scaling function  $\phi(t - k)$ . The initial space can be chosen differently/arbitrarily as well, for example as

$$L^2 = V_4 \oplus W_4 \oplus W_5 \oplus \dots \quad (2.12)$$

or we can start from a coarser space

$$\begin{aligned} L^2 &= V_{-3} \oplus W_{-3} \oplus W_{-2} \oplus \dots \quad \text{or even} \\ L^2 &= \dots \oplus W_{-1} \oplus W_0 \oplus W_1 \oplus W_2 \oplus \dots \end{aligned}$$

We can also define  $V_0$  using wavelet spaces [12],

$$V_0 = \dots \oplus W_{-\infty} \oplus \dots \oplus W_{-1} \quad (2.13)$$

Since wavelets reside in the space spanned by the next narrower scaling function,  $W_0 \subset V_1$ , they can be expressed by (similar to Eq. 2.9)

$$\psi(t) = \sum_n h_1(n) \sqrt{2} \phi(2t - n), \quad n \in Z \quad (2.14)$$

This so called wavelet equation is also fundamental in the design of filter banks that implement the wavelet transform. Using bases  $\phi(t)$  and  $\psi(t)$  and their scaled and shifted versions we can represent a signal at a desired resolution. For instance, if we start with an initial scale  $j_0$ , the first summation gives a coarse approximation of  $f(t)$  at the starting scale  $j_0$  and for each increasing index  $j$  in the second summation, a finer resolution is added, which adds increasing detail.

$$L^2 = V_{j_0} \oplus W_{j_0} \oplus W_{j_0+1} \oplus \dots \quad (2.15)$$

The choice of  $j_0$  sets the coarsest scale whose space is spanned by  $\phi_{j_0}(t - k)$ . The rest of  $L^2(R)$  is spanned by the wavelets which provide the high resolution details of the signal. It can be 0 as in Eq. (2.11), 10 as in Eq. (2.12), or it can be  $-\infty$  as in Eq. (2.8) where no scaling functions are used. In practice, where one is given only the samples of the signal, not the signal itself, the highest resolution can be achieved at sample level.

In many applications, one never has to deal directly with the scaling functions or the wavelets. Only the coefficients  $h_0(n)$  and  $h_1(n)$  are needed for defining the dilation equations (2.9) and (2.14). In addition,  $a_{j_0}(k)$  and  $d_j(k)$  are needed to perform the expansion (2.23). To work directly with the coefficients, we express lower scale expansion coefficients in terms of those at higher scales. Starting with the basic recursion (2.9)

$$\phi(t) = \sum_n h_0(n) \sqrt{2} \phi(2t - n), \quad n \in Z \quad (2.16)$$

and by assuming a unique solution exists, we scale and translate the time variable as

$$\phi(2^j t - k) = \sum_n h_0(n) \sqrt{2} \phi(2(2^j t - k) - n) = \sum_n h_0(n) \sqrt{2} \phi(2^{j+1} t - 2k - n) \quad (2.17)$$

If we do change of variables  $m = 2k + n$ , then

$$\phi(2^j t - k) = \sum_m h_0(m - 2k) \sqrt{2} \phi(2^{j+1} t - m) \quad (2.18)$$

Using,

$$V_j = \text{Span}_k \{2^{j/2} \phi_k(2^j t - k)\} \quad (2.19)$$

then

$$x(t) \in V_{j+1} \Rightarrow x(t) = \sum_k a_{j+1}(k) 2^{(j+1)/2} \phi(2^{(j+1)} t - k). \quad (2.20)$$

This relationship expressible at a scale of  $j + 1$  with scaling functions only and no wavelets. At one scale lower resolution wavelets are necessary for the "details" not available at a scale of  $j$ .

$$x(t) = \sum_k a_j(k) 2^{j/2} \phi(2^j t - k) + \sum_k d_j(k) 2^{j/2} \psi(2^j t - k) \quad (2.21)$$

If  $\phi_{j,k}(t)$  and  $\psi_{j,k}(t)$  are orthonormal, the  $j$  level scaling can be found by taking the inner product [12],

$$a_j(k) = \langle f(t), \phi_{j,k}(t) \rangle = \int x(t) 2^{j/2} \phi(2^j t - k) dt$$

Following this, it is possible to relate approximation coefficients and wavelet coefficients among scales:

$$\begin{aligned} a_j(k) &= \sum_m h_0(m - 2k) a_{j+1}(m) \\ d_j(k) &= \sum_m h_1(m - 2k) a_{j+1}(m) \end{aligned}$$

For a finite length- $N$  the relation between  $h_0(n)$  and  $h_1(n)$  is [13],

$$h_1(n) = (-1)^n h(N - 1 - n) \quad (2.22)$$

The overall wavelet expansion using scaling and wavelet functions can be made as in [12],

$$\begin{aligned} x(t) &= \sum_k a_{j_0}(k) \phi_{j_0,k}(t) + \sum_{j=j_0}^{\infty} \sum_k d_j(k) \psi_{j,k}(t) \\ &= \sum_k a_{j_0}(k) 2^{j_0/2} \phi(2^{j_0/2} t - k) + \sum_{j=j_0}^{\infty} \sum_k d_j(k) 2^{j_0/2} \psi(2^{j_0/2} t - k) \end{aligned} \quad (2.23)$$

## 2.3 BASES WITH TIME AND FREQUENCY LOCALIZATIONS

Sparsity is an important concept, as it naturally or by means of a transform appears in many applications in signal processing and in communication systems. Our focus is on time–sparse signals. In general 1-d sparse signals have only a limited number of samples in time or limited coefficients in a transform domain. We can also classify band limited signals as sparse since they behave sparse in frequency where the non-zero coefficients appear consecutively. Also in many applications signals exhibit a sparse behavior or a sparse representation can otherwise be obtained in a transform domain.

Localization in time and frequency of a signal is an important aspect in designing tools for information extraction and processing. In order to analyze, approximate, enhance, compress and/or estimate the information one needs to consider time–frequency behavior of the signal. Transform domain techniques and expansion of information over bases has always been a major field of research in signal processing. Bases enables the ability to represent and transform the information into another domain, where some aspects of the signals are more prominent. Hence, localization properties of bases are important.

We have performed linear and affine expansions using inner products through our analysis of non stationary signals. Frame theory [18] helps to assess completeness, stability and redundancy of such representations. For this reason we start with a brief section of definitions from frame theory as a reference for later sections.

- A family of vectors  $\{\theta_n\}_{n \in \Delta}$  is a **frame** of a Hilbert space  $\mathbb{H}$  if there exists two positive constants  $A$  and  $B$  such that for any  $x \in \mathbb{H}$  [8],

$$A\|x\|^2 \leq \sum_{n \in \Delta} |\langle x, \theta_n \rangle|^2 \leq B\|x\|^2 \quad (2.24)$$

where the index set  $\Delta$  might be finite or infinite.

If  $A = B$  the frame is called *tight*. A frame defines a complete and stable signal representation, though it can also be redundant. When the frame vectors are normalized,  $\|\theta_n\| = 1$ ,

the redundancy in this representation is measured by the frame bounds,  $A$  and  $B$  [8]. If the  $\{\theta_n\}_{n \in \Delta}$  are linearly independent [10],

$$A \leq 1 \leq B$$

If  $A = B = 1$  the frame is an orthonormal basis.  $A$  can be regarded as a minimum redundancy factor, if  $A > 1$  then the frame is redundant.

Frame coefficients,  $\langle x, \theta_n \rangle$ , is calculated using a pseudo inverse that is expressed with a "dual frame". If we denote  $\langle x, \theta_n \rangle$  by an operator  $T$ , the pseudo inverse,  $\tilde{T}^{-1}$ , is the left inverse  $\tilde{T}^{-1} = (T^*T)^{-1}T^*$ . We can classify the bases of Hilbert Spaces  $\mathbb{H}$  we have used in 2 groups: Orthonormal basis and Riesz Basis.

- **Orthonormal Basis:** A family  $\{\theta_n\}_{n \in N}$  is an orthonormal basis if it is normal,  $\|\theta_n\| = 1$ , and if it is orthogonal  $\langle \theta_n, \theta_m \rangle = 0$  for  $n \neq m$ . Then, if for  $x \in \mathbb{H}$  there exists a sequence  $\lambda_n$  such that

$$\lim_{N \rightarrow \infty} \left\| x - \sum_{n=0}^N \lambda_n \theta_n \right\| = 0$$

A Hilbert space that admits an orthogonal basis is said to be separable. For example the family of Diracs  $\{\theta_n[k] = \delta[k - n]\}$  is an orthonormal basis of Hilbert space  $\mathbb{I}^2(\mathbb{Z})$  hence it is separable.  $L^2(\mathbb{R})$  is also a separable Hilbert space and wavelets are used to construct the orthonormal basis.

Orthonogonality makes it easy to calculate this sequence, called also by orthogonal expansion coefficients,

$$\lambda_n = \frac{\langle x, \theta_n \rangle}{\|\theta_n\|^2}$$

Hence an orthogonal expansion is developed:  $x = \sum_{n=0}^{\infty} \frac{\langle x, \theta_n \rangle}{\|\theta_n\|^2} \theta_n$ . Computing the inner product of  $y \in \mathbb{H}$  yields Parseval equation for orthonormal bases:

$$\langle x, y \rangle = \sum_{n=0}^{\infty} \langle x, \theta_n \rangle \langle y, \theta_n \rangle^*$$

When  $y = x$ , we get an energy conservation called the Plancherel formula [8]:

$$\|x\|^2 = \sum_{n=0}^{\infty} |\lambda_n|^2. \tag{2.25}$$

- **Riesz Bases:** We can still impose a partial energy equivalence to guarantee the stability of the basis by loosening the orthogonality [8]. The linear independent but not orthogonal basis of  $\mathbb{H}$  is called a Riesz basis if for any  $x \in \mathbb{H}$  we can find a sequence  $\lambda_n$  with  $y = \sum_{n=0}^{\infty} \lambda_n \theta_n$ , there exist  $A > 0$  and  $B > 0$  that satisfies [8],

$$\frac{\|x\|^2}{B} \leq \sum_n |\lambda_n|^2 \leq \frac{\|x\|^2}{A} \quad (2.26)$$

A given signal from some space  $S$  can be expressed as a linear combination of a set of elementary functions  $\{\psi_i\}_{i \in \mathbb{Z}}$ . In this was we can express  $x$  as a weighted summation,

$$x = \sum_i c_i \psi_i \quad (2.27)$$

If we can write all the signals in  $S$  as in 2.27, the set  $\psi_i$  is considered to be complete for a particular space and there also exists a dual set  $\{\tilde{\psi}_i\}_{i \in \mathbb{Z}}$  such that the expansion coefficients are calculated as

$$c_i = \langle x, \tilde{\psi}_i \rangle \quad (2.28)$$

- If the set is complete and  $\{\psi_i\}$  is an orthonormal basis for  $S$ , the basis and its dual are the same  $\psi_i = \tilde{\psi}_i$  and

$$\langle \psi_i, \psi_j \rangle = \delta[i - j].$$

- If the set is complete and the vectors  $\{\psi_i\}$  are linearly independent but not orthonormal, the basis and its dual satisfy

$$\langle \psi_i, \tilde{\psi}_j \rangle = \delta[i - j]$$

$\psi_i$  is called biorthogonal basis.

- If the set is complete but the vectors  $\{\psi_i\}$  are linearly dependent (redundant) then we do not have a basis but an overdetermined representation called a frame.

The goodness of the basis depends on the class of signals we would like to represent. While orthogonal bases are computationally convenient, the more general cases of nonorthogonal and biorthogonal bases are as important. In particular we will see that we can form efficient biorthogonal bases using Slepian functions. We have also used overdetermined expansions onto linearly dependent bases in the asynchronous decomposition schemes.

Fourier bases for periodic signals and sinc expansions for band-limited signals are the best known orthogonal transforms. However, these expansion techniques perform poorly on non-stationary signals as the bases do not have good localization in time. We are interested in the analysis of non-stationary signals where there is a time variation of the frequencies. We would like to track the local behavior of the signal with bases that will reveal the time-frequency structure of the signal. While the sinc function has a  $1/t$  decay in time, Fourier bases have no decay in time. Because of the poor time localization they have, choice of these basis functions spreads the local effect over large regions of the transform domain. For example, a long recorded accelerometer signal could be corrupted entirely in the Fourier domain from an error of jittering the sensor at any point in the recording.

There have also been more localized solutions for signal analysis such as the short-time Fourier transform. Windowed Fourier transforms and wavelets are two important methods in the analysis of non-stationary signals. Both methods correlate the signal with a family of basis functions that have good time localizations. Our search for efficient bases started with multi-resolution approximations. The wavelet transform allows one to achieve good resolution both in time and frequency, and to look at signals at different resolutions. In the following subsections we consider basis functions which are well concentrated in time, frequency, or in both. We start with the Haar functions. Haar basis functions are the first wavelets and were the only one for a long time [19]. It has very good time localization but a bad frequency resolution as a consequence. Haar basis has a decay of  $1/w$  in frequency. Because it is trivial, the Haar basis are widely used as a localized wavelet basis especially in the analysis of irregularities and detection of discontinuities in 1-d [20] as well as in 2-d signals [21]. Our adaptation of Haar basis in the representation of multi-level signals resulted in our proposed scale based decomposition schemes [22]. Its basic structure makes it easy to visualize the wavelets and multi resolution analysis features. We first presented Haar basis

in the following section 2.3.1. Then we look at the general wavelet framework where Haar can be considered as a subset. It is clear that representation of a signal can be facilitated if a basis of functions can be found that are concentrated both in time and frequency domains at the same time, such as Slepian functions. Hence, second we consider Slepian basis.

### 2.3.1 Haar Bases

Haar basis functions have the shortest time support hence they provide bad frequency resolution. Nevertheless, they match the structure of the data (piece-wise constant) that we would like to represent. We use Haar wavelets in the compression of the multi-level signals appearing in the proposed decomposers. Since Haar bases are discontinuous as multi-level signals, they can provide the sparsest approximation to these multi-level signals. Most of the coefficients appear very close to zero. We think such compressed representation is promising for continuous transmission of the information. Moreover, having the shortest time support among all other wavelets, makes them appealing in the detection of short-lived irregularities or abnormalities in the signal in time.

We depict Haar scaling function and Haar wavelet in Fig. 5. It is clear from the illus-

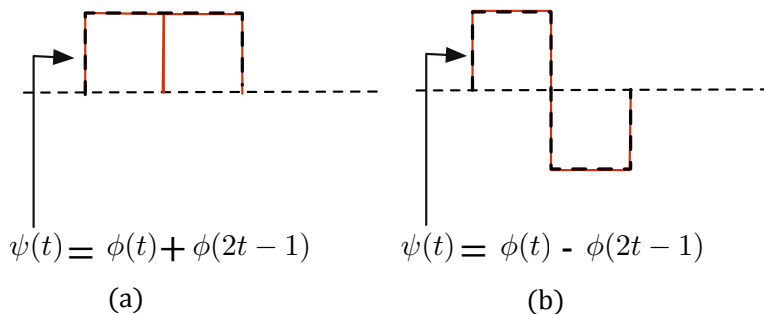


Figure 5: Haar Wavelet Function

tration that the expansion coefficients for the Haar scaling function using Eq.(2.9) would be  $h_0(0) = 1/\sqrt{2}$  and  $h_0(1) = 1/\sqrt{2}$ . Similarly for Haar wavelet, the expansion coefficients are  $h_1(0) = 1/\sqrt{2}$  and  $h_1(1) = -1/\sqrt{2}$ . In Fig. 6 we depict how shifting and scaling appears in three consecutive scales. This illustration is taken from [12]. We also show below how to implement the discrete Haar transform using filter banks. This approach will also be

fundamental in the implementation of Slepian wavelets. The basis functions in the discrete case are [10],

$$\psi_{2k}[n] = \begin{cases} \frac{1}{\sqrt{2}} & n = 2k, 2k + 1, \\ 0 & \text{otherwise,} \end{cases} \quad \psi_{2k+1}[n] = \begin{cases} \frac{1}{\sqrt{2}} & n = 2k, \\ \frac{-1}{\sqrt{2}} & n = 2k + 1, \\ 0 & \text{otherwise.} \end{cases} \quad (2.29)$$

defined as translates of each other, i.e.

$$\psi_{2k}[n] = \psi_0[n - 2k], \quad \psi_{2k+1}[n] = \psi_1[n - 2k]$$

The expansion is

$$x[n] = \sum_{k \in \mathbb{Z}} d[k] \psi_k[n], \quad (2.30)$$

As the basis function  $\{\psi_k(t)\}_{k \in \mathbb{Z}}$  is orthonormal, the expansion coefficients can be found easily,

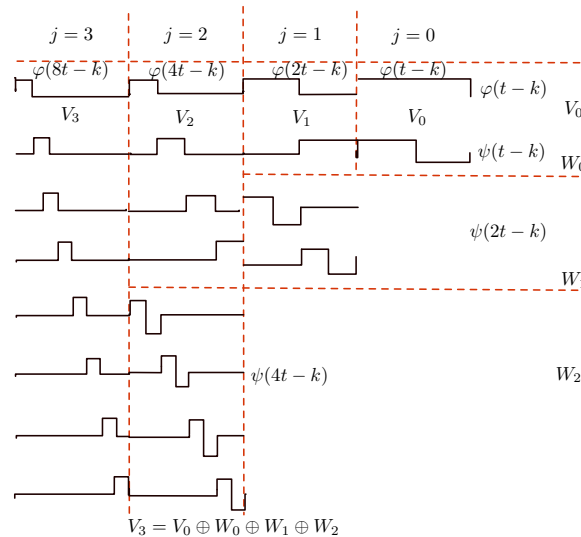


Figure 6: Haar Scaling and Wavelet functions for different scales

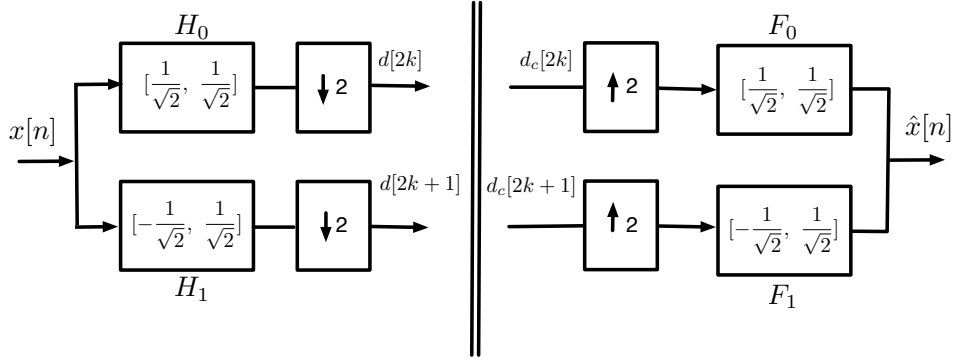


Figure 7: Haar analysis and synthesis filter banks

$$d[2k] = \langle \psi_{2k}, x \rangle = \frac{1}{\sqrt{2}} (x[2k] + x[2k + 1]), \quad (2.31)$$

$$d[2k + 1] = \langle \psi_{2k+1}, x \rangle = \frac{1}{\sqrt{2}} (x[2k] - x[2k + 1]). \quad (2.32)$$

The first projection is onto the subspace spanned by  $\psi_{2k}[n]$  and the latter is onto the subspace spanned by  $\psi_{2k+1}[n]$ . Equation 2.30 can be split into two parts,

$$x[n] = \sum_{k \in \mathbb{Z}} d[2k] \psi_{2k}[n] + \sum_{k \in \mathbb{Z}} d[2k + 1] \psi_{2k+1}[n] \quad (2.33)$$

The first part in the summation is the average, or coarse version, and the latter is the known as the *detail* component of the signal. Another way of considering this transform is through convolution. Let  $h_0[n]$  and  $h_1[n]$  be an FIR filter with the following impulse responses,

$$h_0[n] = \begin{cases} \frac{1}{\sqrt{2}} & n = -1, 0, \\ 0 & \text{otherwise,} \end{cases} \quad h_1[n] = \begin{cases} -\frac{1}{\sqrt{2}} & n = -1, \\ \frac{1}{\sqrt{2}} & n = 0, \\ 0 & \text{otherwise.} \end{cases} \quad (2.34)$$

Expansion coefficients in 2.31 follow from a convolution of  $x[n]$  with the given filters at instants  $2k$  and  $2k + 1$  evaluated at even indices,

$$\begin{aligned} d[2k] &= x[n] * h_0[n] \Big|_{n=2k} = \sum_{m \in \mathbb{Z}} h_0[2k - m]x[m] \\ d[2k + 1] &= x[n] * h_1[n] \Big|_{n=2k} = \sum_{m \in \mathbb{Z}} h_1[2k - m]x[m] \end{aligned}$$

Notice that the response of the analysis filters are the time reversed versions of the basis functions  $h_0[n] = \psi_0[-n]$  and  $h_1[n] = \psi_1[-n]$ . Overall expansion steps can be modeled by an analysis filter bank as illustrated in Fig. 7. The double vertical lines represent the compression step in our algorithm and  $d_c$  denoted the compressed coefficients. In the reconstruction part, the synthesis filters are designed using perfect reconstruction in the orthogonal filter banks, i.e.  $f_0[n] = \psi_0[n]$ ,  $f_1[n] = \psi_1[n]$ . They are obtained to be the time-reversed version of each other, i.e.  $f_i[n] = h_i[-n]$ .

Two wavelets used in our sparse signal analysis are the Haar and the Slepian wavelets. As shown above, the Haar transform is very significant when signals are represented by binary or multilevel functions as it is the case in the ASDM representation and the LC sampling. On the other hand, if the signals are sparse but not binary or multilevel we need a wavelet representation such as the Slepian to allow accurate representation of narrow pulses. In the following we summarize some of the properties of the Haar and the Slepian wavelets of interest in our work.

### 2.3.2 Slepian Functions

The energy concentration of a signal in a given time interval  $[-T/2, T/2]$  can be expressed as [23],

$$\alpha^2(T) := \frac{\int_{-T/2}^{T/2} x^2(t)dt}{\int_{-\infty}^{\infty} x^2(t)dt} \quad (2.35)$$

and energy concentration of its spectrum concentration to a given band  $[W, W]$ ,

$$\beta^2(W) := \frac{\int_{-W}^W |X(\Omega)|^2 d\Omega}{\int_{-\infty}^{\infty} |X(\Omega)|^2 d\Omega} \quad (2.36)$$

Slepian, Landau and Pollak considered [24–26] how large  $\alpha^2(T)$  can be for a band limited signal  $x(t)$ . They proposed Prolate Spheroidal Wave Functions (PSWF) which are time limited and at the same time maximally concentrated to a certain bandwidth. We adopted the name “Slepian function” hereafter for PSWF in honor of David Slepian. The Slepian functions  $\{\varphi_{m,W,\tau}(t)\}_{n=0}^{\infty}$  are the most time-concentrated orthonormal basis for  $W$ -band-limited functions. We have used Walter’s notation for Slepian functions [27]. The time concentration is denoted by the parameter  $\tau$  and the parameter  $\sigma$  indicates the frequency support. They are defined in different ways in literature, one of which is a solution of the following integral equation,

$$\int_{-\tau}^{\tau} \varphi_{n,\sigma,\tau}(x) \frac{1}{T} \operatorname{sinc}\left(\frac{t-x}{T}\right) dx = \lambda_{n,\sigma,\tau} \varphi_{n,\sigma,\tau}(t). \quad (2.37)$$

They are the eigenfunctions of the operator. Their good localizations properties make them favorable for time–frequency signal analysis.

A main feature of wavelets is that they are time-limited functions. A function that has good localization both in time and frequency would be a good candidate as a wavelet basis. Slepian wavelets first proposed by Shen and Walter [15]. In this section, we aim to convey the reasoning behind this choice, first by giving the theory of Slepian functions and then the definition of the Slepian wavelets Shen and Walter introduced. Our derivations on Slepian wavelets, provided in Chapter 5, are based on filter banks.

The Slepian functions  $\varphi_{n,\sigma,\tau}$  can also be represented as the solution of a energy concentration optimization problem on the interval  $[-\tau, \tau]$  of a signal  $x(t)$

$$\begin{aligned} \max \quad & \int_{-\tau}^{\tau} \|x(t)\|^2 dt \\ \text{subject to} \quad & \|\varphi_{n,\sigma,\tau}(t)\|^2 = 1. \end{aligned}$$

The function  $\varphi_{0,\sigma,\tau}$ , which is the first Slepian function provides the maximum energy concentration on the time interval  $[-\tau, \tau]$ . Similarly,  $\varphi_{1,\sigma,\tau}$  has the maximum energy concentration among those orthogonal to  $\varphi_{0,\sigma,\tau}$ . The first subindex denotes which Slepian function is referred (such as first one is the most time-concentrated). The second index reflects the frequency concentration interval  $[-\sigma, \sigma]$  and the last one is for time concentration  $[-\tau, \tau]$  respectively [28].

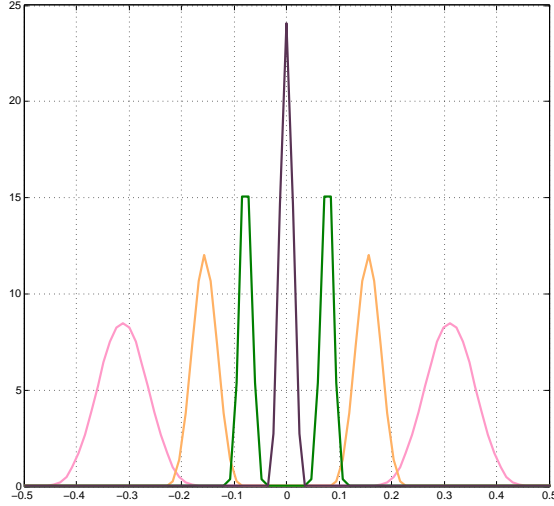


Figure 8: Slepian Spectral Decomposition obtained with four Slepian functions

As the Slepian functions provide high-energy concentration, they are promising candidates for a wavelet basis where the efficiency of the transform is directly related to the time-bandwidth localization of the basis. This basis choice provides the sparsity in the transform domain. It increases as we use well-localized functions, hence the transform results in reduced redundancy and high compression. Moreover, Slepian wavelets enables spectral decomposition. An illustration of this behavior can be seen in Fig. 8. Some of the properties of the Slepian functions which are used for the description of the wavelet setting are:

- The Slepian functions are orthogonal in finite and infinite support domains,

$$(i) \quad \int_{-\tau}^{\tau} \varphi_{n,\sigma,\tau}(t) \varphi_{m,\sigma,\tau}(t) dt = \lambda_{n,\sigma,\tau} \delta_{nm}$$

$$(ii) \quad \int_{-\infty}^{\infty} \varphi_{n,\sigma,\tau}(t) \varphi_{m,\sigma,\tau}(t) dt = \delta_{nm}$$

Thus,  $\{\varphi_{n,\sigma,\tau}(t)\}$  constitutes an orthogonal basis of  $L^2(-\tau, \tau)$ , and an orthonormal basis for the subspace  $B_\sigma$  of  $L^2(-\infty, \infty)$  [29]. These relations also hold in the discrete domain as well

$$T \sum_{n=0}^{\infty} \varphi_{n,\sigma,\tau}(kT) \varphi_{n,\sigma,\tau}(mT) = \delta_{mk}$$

$$T \sum_{k=-\infty}^{\infty} \varphi_{n,\sigma,\tau}(kT) \varphi_{m,\sigma,\tau}(mT) = \delta_{mn}$$

where  $T$  is the sampling period. Because of this orthogonality one can use the Slepian functions as basis for a orthogonal series expansion of any  $\sigma$ -band limited function [30],

$$f(t) = \sum_{n=0}^{\infty} c_n \varphi_{n,\sigma,\tau}(t) \quad \text{where}$$

$$c_n = \sum_{k=-\infty}^{\infty} T f(kT) \varphi_{n,\sigma,\tau}(kT)$$

- The Fourier transform of  $\varphi_{n,\sigma,\tau}$  is given by

$$\hat{\varphi}_{n,\sigma,\tau}(\omega) = (-1)^n \sqrt{\frac{2\pi\tau}{\sigma\lambda_{n,\sigma,\tau}}} \varphi_{n,\sigma,\tau}\left(\frac{\tau\omega}{\sigma}\right) [u(\omega + \sigma) - u(\omega - \sigma)] \quad (2.38)$$

and has support in  $(-\sigma, \sigma)$  in frequency [31]. The MATLAB function *dps* generates discrete Slepian functions. In Fig. 9 we display the first four Slepian functions, and their Fourier transforms. In the figure  $N$  is the length of the Slepian sequence and  $NW$  is the time bandwidth product of the sequence.

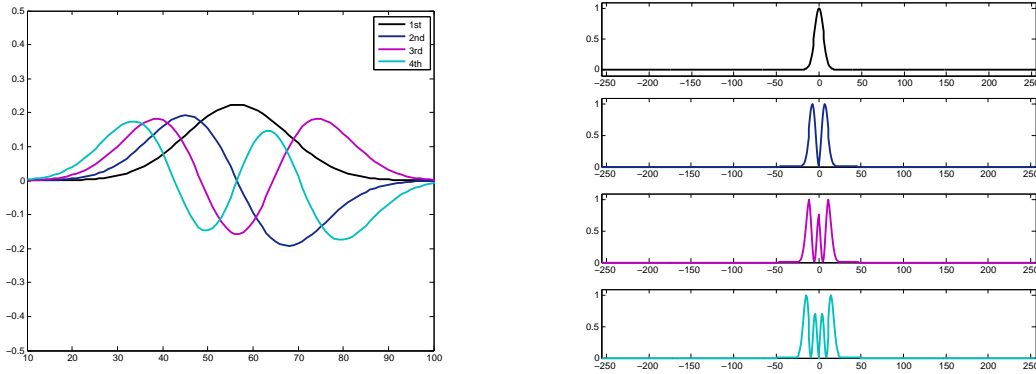


Figure 9: The four most bandlimited Slepian functions and their spectra ( $N = 100$ ,  $NW = 2$ ).

- The relationships between the Slepian functions at different scales are obtained by a change of scale in the integral equation (2.37) to get [15],

$$\varphi_{n,\sigma\tau,1}(t) = \sqrt{\tau} \varphi_{n,\sigma,\tau}(\tau t) \quad (2.39)$$

Shen and Walter suggests use the expression (2.39) to get a relation between  $\pi$  and  $2\pi$ -band limited Slepian functions as,

$$\varphi_{n,\pi,\tau}(t) = \sum_{k=0}^{\infty} h_{n,k} \varphi_{n,2\pi,\tau}(t) \quad (2.40)$$

where

$$h_{n,k} = \sum_{p=-\infty}^{\infty} \varphi_{n,\pi,\tau}(p/2) \varphi_{n,2\pi,\tau}(p/2) \quad (2.41)$$

This can be regarded as a dilation equation as it relates the various nested subspaces  $V_m = B_{2^m\pi}$  in a multiresolution analysis (MRA) [15]. For  $f \in V_0$ , by using Eq. (2.39) coarse spaces of MRA are defined as follows,

$$f(t) = \sum_{k=0}^{\infty} a_k^0 \varphi_{n,\pi,\tau}(t) \quad (2.42)$$

or a detailed represent the function in one degree finer scale,  $V_1$ , can be written as,

$$f(t) = \sum_{k=0}^{\infty} a_k^1 \varphi_{n,2\pi,\tau}(t) \quad (2.43)$$

then the coefficients are related by

$$a_n^0 = \sum_{k=0}^{\infty} h_{n,k} a_k^1 \quad (2.44)$$

where  $h_{n,k}$  are given by Eq. 2.41 and

$$a_k^1 = \sum_{n=0}^{\infty} h_{n,k} a_n^0 \quad (2.45)$$

These relations hold and can be extended to other scales,  $V_m$ , as well. In this section we consider Shen and Walter's [15, 29] wavelets proposed for MRA analysis of  $\pi$ -bandlimited functions. Our wavelet constructions differ from these findings. The main deviation comes from the implementation of the wavelet transform, where we used a filter bank approach. We adapt the same scaling function proposed by Shen and Walter that is the first Slepian function. However, our wavelet function associated with the Slepian scaling function is different than the one they suggest. Nevertheless we included Shen and Walter's as a reference and comparison. As Shen and Walter suggests, the notation changes slightly to avoid so

many subscripts in defining basis for nested MRA spaces. Sticking with their notation,  $\varphi_n^m$  is the Slepian function with bandwidth  $W = 2^m\pi$  and again note that the time concentration interval is  $[-\tau, \tau]$ .

It has been shown that  $\{\varphi_n^m\}$  enables MRA and it constitute an unconditional basis of  $V_m$  [15]. The dilation equation relating the various scales is, based on 2.39,

$$\varphi_n^m(t) = \sum_{k=0}^{\infty} h_{n,k}^m \varphi_k^{m+1}(t) \quad \text{where} \quad \phi_n^m(t) := \varphi_{n,2^m\pi,\tau}(t)$$

where the coefficients are given by [29],

$$\begin{aligned} h_{n,k}^m &= \int_{-\infty}^{\infty} \varphi_n^m(t) \varphi_k^{m+1}(t) \\ &= \sum_{j=-\infty}^{\infty} 2^{-m-1} \varphi_n^m(2^{-m-1}j) \varphi_k^{m+1}(2^{-m-1}j) \end{aligned}$$

The next step is to find a wavelet basis that will span the space  $W_m$  that is the orthogonal complement of  $V_m$  in  $V_{m+1}$ . It is suggested the basis for this orthogonal space be [15],

$$\begin{aligned} \psi_{2n}^m(t) &:= \cos\left(\frac{3\pi}{2}2^m t\right) \varphi_n^{m-1}(t) \\ \psi_{2n+1}^m(t) &:= \sin\left(\frac{3\pi}{2}2^m t\right) \varphi_n^{m-1}(t) \end{aligned}$$

The first three Slepian functions and their associated wavelets are shown in Fig. 10.

To illustrate the nice spectral-feature of Slepian wavelets, shown in Fig. 8, we have performed a signal recovery from wavelet coefficients. We pick the first Slepian function as the scaling function, which has a spectrum depicted in red color on the right hand side plot of Fig. 11. This is the basis that spans the coarsest space  $V_0$ . Then we form a wavelet by modulating this scaling function so that the wavelet and the scaling function are orthogonal to each other. The magenta spectrum line belongs to coarsest wavelet, i.e., the one spanning the  $W_0$  space, and the black and green lines indicate the scale 1 ( $j = 1$ ) and scale 2, respectively. As the signal we want to represent, with a blue spectrum line falls onto wavelet basis frequency-tile (notice the overlap blue-input and magenta-scale 1 wavelet lines), we obtained a good reconstruction, depicted in left hand side plot of Fig. 11. We see that

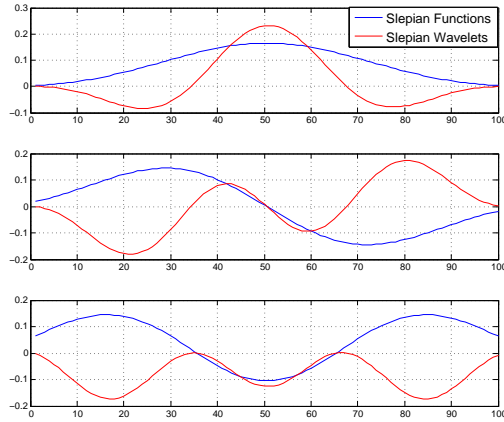


Figure 10: Slepian Wavelets

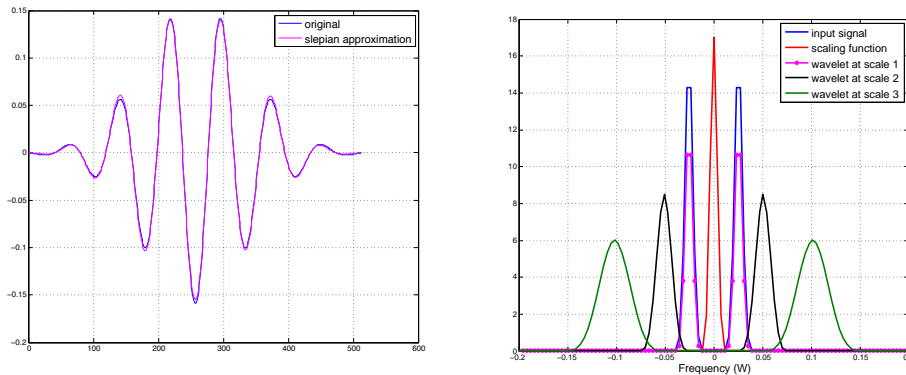


Figure 11: Reconstruction and Compression with Slepian wavelets

when both Slepian wavelets and the signal occupy the same band, the representation is very accurate and sparse.

The key steps of this representation are: **first** to generate the first Slepian sequence according to the input signals time-frequency support (Slepian functions return the most possible concentrated sequence in this interval); **second** to design a wavelet basis with respect to this scaling function. The second step is a matter of arranging the modulation

ratio so that scaling function and wavelets are orthogonal in the frequency domain. Besides providing the low-error reconstruction, the wavelet transform resulted in high-compression for this example. The original input signal has 512 samples, while the associated wavelet coefficients are:  $[-0.0000 \quad -1.3475 \quad -0.0036 \quad -0.0038 \quad -0.0000 \quad 0.0001 \quad 0.0001 \quad -0.0000]$ . As expected, the dominant coefficient corresponds to the scale-1 wavelet. Further compression, for this particular case, is achievable by ignoring the rest of the coefficients except the second one.

## 2.4 PERFECT RECONSTRUCTION FILTER BANKS

Filter banks are a computationally attractive approach in the implementation of the wavelet transform. The iterated filter bank structure enables to represent continuous time wavelets with a finite number of sequences and their shifted versions [9, 32–34]. Our goal in this section is to highlight the link between the filter bank structure and the construction of orthonormal, biorthogonal and overcomplete sets of wavelet basis functions based on it.

In 1976 Croisier et al. discovered quadrature mirror filters (QMF) which are non-ideal yet split a signal into two subsampled signals and obtain alias-free reconstruction. The study of classical multi rate banks has become a major topic in signal processing since then. Subband coding [35–37] with a critically sampled filter banks can avoid the redundancy in expansions such as in the STFT. Except the simple Haar filter, a QMF has an infinite impulse response (IIR) [8]. In 1984, Smith and Barnwell [38] and Mintzer [39] found the first orthogonal solution with a finite impulse response (FIR) and showed the necessary and sufficient conditions for obtaining perfect reconstitution [10]. These FIR filters are called conjugate mirror filters. The theory was completed by the biorthogonal equations of Vetterli [40–42] and the general paraunitary matrix theory [43]. In this work, we follow this digital signal processing approach based on Mallat’s [17] multi resolution and filter bank theory. This approach gives a framework enables to perform wavelet decompositions [9] and establishes the link between wavelets and filter banks.

Earlier, a two channel filter bank was discussed in the discrete Haar transform in section 2.3. The filter bank structure sketched in Fig. 7 implements an orthonormal series expansion of discrete signals. We have seen that in order to obtain perfect reconstruction,  $\hat{x}[n] = x[n]$ , analysis and synthesis filters should be time-reversed versions of each other, i.e.  $f_i[n] = h_i[-n]$  for this orthogonal case. They are also named as mirror image filters in literature. However, this condition can be relaxed by letting the expansion be biorthogonal [10]. In fact in literature the term “perfect reconstruction filter bank” is used for the filter that enables biorthogonal expansions [11]. In the case of biorthogonal filter banks, analysis and synthesis filters will not be simply time reversed each other anymore. We have four different filters;  $h, g$  for analysis and  $\tilde{h}, \tilde{g}$  for synthesis, as depicted in Fig. 12 to implement biorthogonal expansions. We will show the necessary and sufficient conditions on filters [13] that guarantee perfect reconstruction.

Biorthogonal filter bank structure is composed of four different filters as depicted in Fig. 12. The analysis bank filters  $h, g$ , are the inverse of the synthesis bank filters  $\tilde{h}, \tilde{g}$ . Here, we have only depicted the two-channel filter bank with one step decomposition. But different structures are possible, such as the ones iterates on the first channel, or on the second, or on many channels. In the Fig. 12 the down-sampling operators are decimators and the up sampling operators are expanders. This class of filter bank is important, it leads to biorthogonal scaling and wavelet bases in which Slepian wavelets fall in. By perfect reconstruction we mean the input of the filter bank  $x$  is same with the output  $\tilde{x}$ . If causal filters are employed we may also expect some delay in the perfect reconstruction case, i.e.  $\tilde{x}_0[n] = x_0[n - l]$ . It has been shown by Vetterli [40] that perfect reconstruction without implicit pole/zero cancelation, which may cause internal instability of the filter bank system, can only be achieved when both analysis and synthesis filters have finite length. Hence we put the emphasis on filters with finite impulse response (FIR). Also FIR filter banks are preferable to obtain faster computations. As it can be seen from Fig. 12 two channel multi rate filter bank convolves a signal  $x_0$  with 2 filters and subsamples by 2 the output:

$$x_1[n] = x_0[n] * h[2n]$$

$$d_1[n] = x_0[n] * g[2n]$$

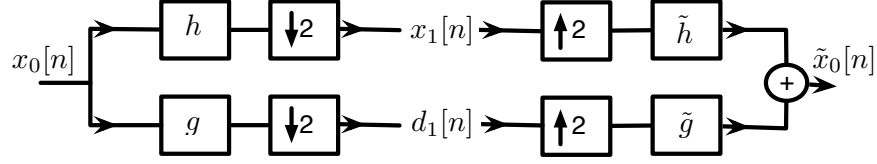


Figure 12: Two channel multi-rate filter bank

As we considered all the filters to be *FIR*, the above convolution can be written as

$$x_1[n] = \sum_k x_0[k] * h[2n - k] \quad (2.46)$$

$$d_1[n] = \sum_k x_0[k] * g[2n - k] \quad (2.47)$$

Then  $x_1$  and  $d_1$  are up sampled and using another set of filters  $\{\tilde{h}, \tilde{g}\}$ , the output  $\tilde{x}_0$  is obtained by filtering the up sampled signals as depicted in Fig. 12. This second set of filters  $\tilde{h}$  and  $\tilde{g}$  are called dual filters. If we denote the up sampled parts as  $x^u[n]$  such as,

$$x^u[n] = \begin{cases} x[\ell] & \text{if } n = 2\ell, \\ 0 & \text{if } n = 2\ell + 1 \end{cases}$$

Then we can write the reconstructed signal as,

$$\tilde{x}_0[m] = \sum_n \left[ x_1^u[n] \tilde{h}[2n - m] + d_1^u[n] \tilde{g}[2n - m] \right] \quad (2.48)$$

In order to have perfect reconstruction [13], i.e.  $x_0[n] = \tilde{x}_0[n]$ ,

$$\sum_n \left[ h[2n - k] \tilde{h}[2n - m] + g[2n - k] \tilde{g}[2n - m] \right] = \delta(m - k) \quad (2.49)$$

The analysis of this filter bank structure can be easily performed in the frequency domain and/or z-domain. Downsampling followed by up-sampling by 2 nulls out the odd-indexed coefficients. We recognize that down-sampling by 2 makes frequencies that are  $\pi$  apart indistinguishable. Also non-ideal filters cause amplitude and phase distortions on the input. This distortion is not recoverable using only the first or second channel alone. But combination of both channels helps to get rid of the aliasing caused by downsampling and up

sampling operation. The synthesis filters are adapted to the analysis filters to cancel the reconstruction errors. Eq. 2.46 in z-domain:

$$\begin{aligned} X_1[z^2] &= \frac{1}{2} [H(z)X_0(z) + H(-z)X_0(-z)] \\ D_1[z^2] &= \frac{1}{2} [G(z)X_0(z) + G(-z)X_0(-z)] \end{aligned} \quad (2.50)$$

If we denote  $h[-n]$  with  $\bar{h}[n]$ , i.e.  $\bar{h}[n] = h[-n]$ , Eq. 2.46 becomes,

$$\tilde{X}_0[z] = \tilde{H}(z)X_1(z^2) + \tilde{G}(z)D_1(z^2) \quad (2.51)$$

Then Eq. 2.49,

$$\frac{1}{2} [H(z)\tilde{H}(z) + G(z)\tilde{G}(z)] = 1 \quad (2.52)$$

and

$$\frac{1}{2} [H(-z)\tilde{H}(z) - G(-z)\tilde{G}(z)] = 0 \quad (2.53)$$

To make Eq. 2.53 hold we can pick  $\tilde{H}(z) = G(-z)P(z)$  and  $\tilde{G}(z) = H(-z)P(z)$  where  $P(z)$  polynomial in  $z$ . Substituting this in Eq. 2.52,

$$P(z) [H(z)G(-z) + H(-z)G(z)] = 2.$$

The only possible solutions to this are [13],

$$P(z) = \alpha z^k \quad (2.54)$$

$$H(z)G(-z) + H(-z)G(z) = 2\alpha^{-1}z^k, \quad \alpha \neq 0$$

$$\tilde{H}(z) = \alpha z^k G(-z) \quad (2.55)$$

$$\tilde{G}(z) = \alpha z^k H(-z)$$

Conditions 2.54 and 2.55 are necessary and sufficient conditions for perfect reconstruction [13].

### 3.0 ANALYSIS OF ANALOG TIME–SPARSE SIGNALS

Signals from practical applications are realizations of non–stationary processes and as such are difficult to represent and to process. Time–sparse signals exhibit non–stationary behavior. Conceptually, non–stationarity relates to the variation over time of the statistics of the signal. Thus the representation and processing of non–stationary signals is typically done assuming that the statistics either do not change with time (stationarity) or that remain constant in short time intervals (local stationarity). To consider the time–variability, non–stationary behavior needs to be connected to joint time–frequency spectral characterization even though the analysis is complicated by the inverse time and frequency relationship as set by the uncertainty principle [44]. According to the Wold–Cramer representation [45], a non–stationary process can be thought of as the output of a time–varying system. As such, the distribution of the power of a non–stationary signal is a function of time and frequency [46, 47]. Therefore to process synchronously non–stationary signals, according to the Nyquist–Shannon sampling theory, it is necessary that they be sampled using a continuously varying sampling period. However, conventional synchronous processing assumes the signal being processed is band–limited and thus sampled uniformly with a sampling period that depends on the maximum frequency present in the signal. By ignoring that the frequency content is changing with time unnecessary samples are collected in segments of the signal where the signal is quiescent. A more appropriate approach would be to make the process signal–dependent [1].

Besides the signal–dependence of the processing, power consumption and type of processing are issues of great importance in many biomedical and sensor network applications that also need to be considered. In brain computer interfacing, for instance, the size of the devices, the difficulty in replacing batteries, possible harms to the patient from high frequen-

cies generated by fast clocks, and the high power cost incurred in data transmission point to the need for asynchronous methodologies [3, 48–51], and analog processing [5].

Lebesgue sum, instead of Riemann sum used in uniform sampling, provide the rational for level-crossing (LC) sampling [3, 50] — a signal-dependent approach. For a fixed set of quantization levels, the LC sampler acquires a sample whenever the signal coincides with one of those levels. Level-crossing sampling is independent of the Nyquist–Shannon band-limited signal constraint and has no quantization error in the amplitude. Although very efficient in the collection of significant data from the signal, LC sampling requires an *a priori* set of quantization levels and results in non-uniform sampling where for each sample we need to know not only the value of the sample but also the time at which it occurs. Selecting quantization levels that depend on the signal, rather than fixed levels, as is commonly done, is an issue of research interest [7, 50].

The LC technique is a well-known asynchronous technique addressing common problems of synchronous processing [7, 52, 53]. Though it has three main drawbacks. It requires both amplitude and time for each of the samples and selecting appropriate quantization levels, and it lacks a reconstruction error measure. In this section, we show that sampling and reconstruction using an asynchronous sigma delta modulator (ASDM) improve on these three issues. This leads to the consideration of non-uniform, signal-dependent level-crossing and asynchronous sigma delta modulator (ASDM) based sampling. More importantly, the multi-level representation obtained through ASDM provides a way to process these analog signals digitally [5] — a desirable processing in many applications.

A different approach to sampling and reconstruction of non-stationary signals, while satisfying the signal dependence and the low-power consumption, is possible using the Asynchronous Sigma Delta Modulator (ASDM) [49, 54]. The ASDM is a non-linear feedback system that maps a bounded analog input signal into a binary output signal with zero-crossing times that depend on the amplitude of the signal. It can be shown that the ASDM operation is an adaptive LC sampling scheme [7]. Moreover, using duty-cycle modulation we obtain a multi-level representation of an analog signal in terms of localized averages — computed in windows with supports that depend on the amplitude of the signal. Such representation allows us to obtain a signal decomposition that generalizes the Haar wavelet

representation [55]. As we will show, this is accomplished by latticing the time–frequency plane choosing fixed frequency ranges and allowing the time–windows to be set by the signal in each of these frequency ranges.

Our main objective is to propose improvements on the existing techniques for asynchronous processing of non–stationary signals, while pointing to their time–scale framework. As such, we have organized the chapters as follows.

In section 3.1 is a comprehensive discussion of the asynchronous processing with ASDM is given within a time–scale framework. Power consumption and type of processing imposed by the size of the devices in many applications motivate the use of asynchronous, rather than conventional synchronous, approaches. We show how ASDM can be thought of an optimal LC sampler. More importantly changing a parameter, will soon be called “scale parameter”, representation of the signal in different resolutions became possible. Then, in section 3.2 we consider two decomposition procedures that exploits scale based behavior to compressively represent sparse information. Simulations with actual signals illustrate the decomposition algorithms for representation and compression applications.

In section 3.3, the non–uniform sampling required by the time–variation of the frequencies in non–stationary signals is presented. We introduce modified the asynchronous Sigma delta modulator (MASDM) and propose improvements on the non–uniform sampling. Using MASDM in the decompositions schemes, a localized decomposition that generalizes the Haar wavelet representation of analog non–stationary signals is discussed.

Simulations are given to illustrate the main topic in each of the sections. Important applications of these procedures are the compression and processing of biomedical signals as it will be illustrated. Conclusions will follow.

### 3.1 ASYNCHRONOUS ANALYSIS WITH ASDM

In this section, we provide a comprehensive discussion of the asynchronous representation and analysis of non–stationary signals. Power consumption and type of processing imposed by the size of the devices in many applications motivate the use of asynchronous, rather than

conventional synchronous, approaches. An alternative asynchronous approach to LC technique is Asynchronous Sigma Delta Modulator (ASDM) [54]. The ASDM structure enables signal dependent clock-free analysis of non-stationary signals with a low-power consumption. We show that sampling and reconstruction using ASDM improves on the LC sampler.

An ASDM [49] is a nonlinear feedback system that operates at low power and consists of an integrator and a Schmitt trigger. It has been used to time encode a bounded and band-limited analog signal into a continuous-time signal with binary amplitude [49], see Fig. 2. For a amplitude bounded signal  $x(t)$ ,  $|x(t)| \leq c$ , and an appropriate value of the scale parameter  $\kappa$ , the ASDM maps the amplitude of  $x(t)$  into a binary signal  $z(t)$  of amplitude  $\pm b$ . If in  $t_k \leq t \leq t_{k+1}$  the output of the Schmitt trigger is the binary signal  $z(t) = b(-1)^{k+1}[u(t - t_k) - u(t - t_{k+1})]$  where  $u(t)$  is the unit-step function and  $b > c$ , the output of the integrator  $y(t)$  is bounded, i.e.,  $|y(t)| < \delta$ . Thus, the difference  $y(t_{k+1}) - y(t_k) = \pm 2\delta$  is equal to

$$\frac{1}{\kappa} \left[ \int_{t_k}^{t_{k+1}} x(\tau) d\tau - (-1)^{k+1} b(t_{k+1} - t_k) \right]$$

and gives the integral equation [49]:

$$\int_{t_k}^{t_{k+1}} x(\tau) d\tau = (-1)^k [-b(t_{k+1} - t_k) + 2\kappa\delta]. \quad (3.1)$$

relating the amplitude information of  $x(t)$  to the duration of the pulses in  $z(t)$  — or equivalently to the zero-crossing times  $\{t_k\}$ . There are several ways to exploit this relation. The main reading from this relation is that for fixed design parameters  $\kappa, \delta, b$  the output waveform is directly related to the input amplitude and its change rate. Input modulates the output, in other words output is encoded with inputs amplitude. If amplitude information of the the input can be encoded in zero-crossing of output, one can reconstruct the  $x(t)$  from  $t_k$ . For band-limited signals, perfect reconstruction from non-uniform samples can be attained provided that the zero-crossing times  $\{t_k\}$  satisfy the condition [49]:

$$\max_k (t_{k+1} - t_k) \leq T_N \quad (3.2)$$

where  $T_N \leq (1/2f_{max})$  is the Nyquist sampling period for a band-limited signal with maximum frequency  $f_{max}$ .

Note that one can also approximate the integral (3.1) to obtain an approximation of the signal using the zero-crossing times [54]. These two reason have been the main use of this circuitry.

We wanted to read more into this relation (3.1). We explore the effect of design parameters. As  $\kappa$  and  $\delta$  appears as a product in the equations, they have the similar effect. Hence we fix one of them, i.e.  $\delta$ . Also for implementation concerns, as both *delta* and *b* are Schmitt trigger's parameters, it would be also easier to freely change the integrator parameter  $\kappa$ . Intuitively one would expect as we increase  $\kappa$ , it would take longer for Schmitt trigger to reach its thresholds. And this is observed by simulation, see in Fig. 13.

Using and Eq. 3.1 we can write,

$$\frac{2\kappa\delta}{b+c} \leq t_{k+1} - t_k \leq \frac{2\kappa\delta}{b-c} \leq T_N \quad (3.3)$$

which gives a way to choose the scale parameter  $\kappa$  in terms of the Nyquist sampling rate. Letting  $\delta = 0.5$  we have

$$\kappa \leq T_N(b-c) \leq \frac{b-c}{2f_{max}} \quad (3.4)$$

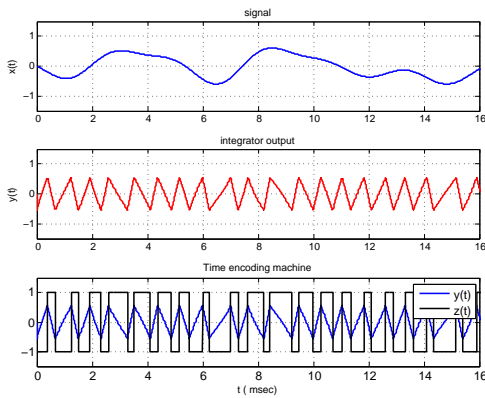
indicating the scale parameter  $\kappa$  depends not only on the maximum frequency of the signal but on the difference in amplitude of the signal,  $c$ , and the choice of  $b$ .

The sequence of binary rectangular pulses  $z(t)$  is characterized by the duty-cycle  $0 < \alpha_k/T_k < 1$  of two consecutive pulses of duration  $T_k = \alpha_k + \beta_k$  where  $\alpha_k = t_{k+1} - t_k$  and  $\beta_k = t_{k+2} - t_{k+1}$ . Letting

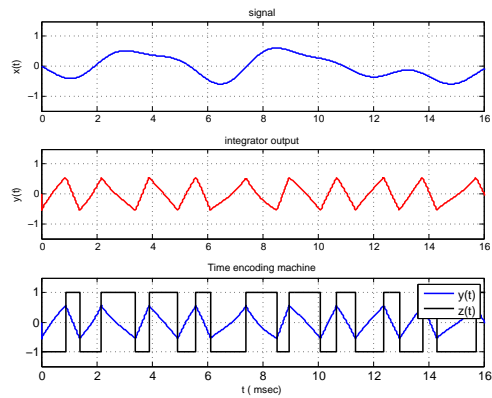
$$\zeta_k = \frac{\alpha_k - \beta_k}{\alpha_k + \beta_k}$$

we have that the duty cycle  $\alpha_k/T_k = (1 + \zeta_k)/2$  where, as shown next,  $\zeta_k$  is the local average of  $x(t)$  in  $t_k \leq t \leq t_{k+1}$ . Indeed, the integral equation (3.1) can also be written in terms of  $z(t)$  as

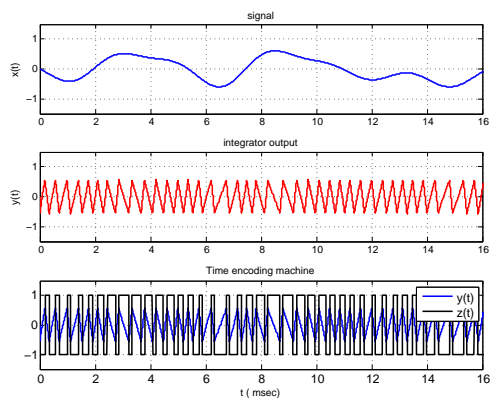
$$\int_{t_k}^{t_{k+1}} x(\tau) d\tau = (-1)^{k+1} \int_{t_k}^{t_{k+1}} z(\tau) d\tau + 2(-1)^k \kappa \delta.$$



(a)



(b)



(c)

Figure 13: Different scale parameters: (a)  $\kappa_i$ , (b)  $2\kappa_i$ , (c)  $\frac{\kappa_i}{2}$

Input-output relationship can be used to get local estimate of the signal average  $\zeta_k$  in  $[t_k, t_{k+2}]$ :

$$\frac{1}{T_k} \int_{t_k}^{t_{k+2}} x(\tau) d\tau = \frac{(-1)^{k+1}}{T_k} \left[ \underbrace{\int_{t_k}^{t_{k+1}} z(t) dt}_{\alpha_k} - \underbrace{\int_{t_{k+1}}^{t_{k+2}} z(t) dt}_{\beta_k} \right]$$

where as indicate above  $T_k = t_{k+2} - t_k = \alpha_k + \beta_k$ . As we could relate the zero crossings to the local averages, we can easily relate the effect of  $\kappa$  on these local averages, see Fig. 14. Thus, for a bounded and band-limited analog signal the corresponding scale parameter

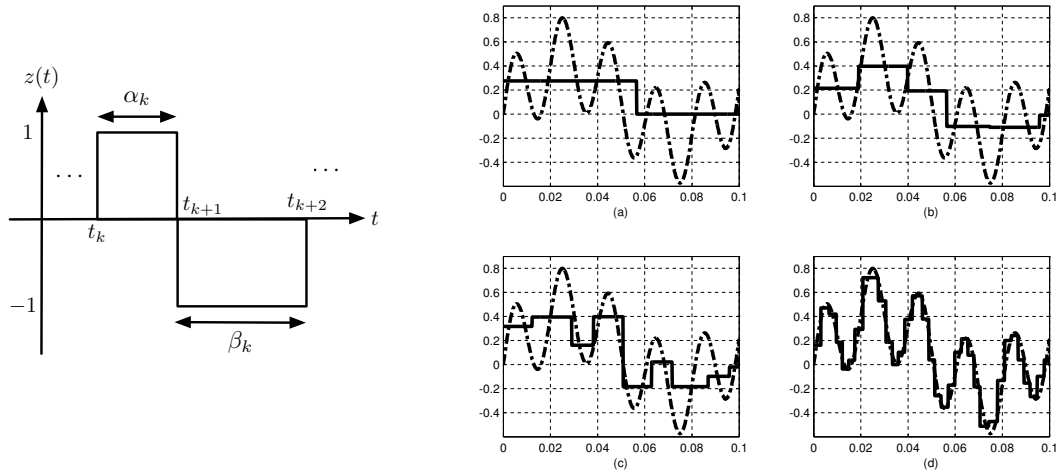


Figure 14: Left: definition of  $\alpha_k$  and  $\beta_k$  corresponding to consecutive pulses of  $z(t)$ ; Right (a)–(d): effect of scale parameter  $\kappa$  as it decreases.

determines the width of an appropriate window — according to the non-uniform zero-crossing times — to compute an estimate of the local average. Thus, the ASDM provides

either a representation of its input  $x(t)$  by its binary output  $z(t)$  and the integral equation, or a sequence of local averages  $\{\zeta_k\}$  at non-uniform times  $\{t_{2k}\}$ . Different from the LC sampler, the ASDM only requires the sample times, the quantization levels are set by the amplitude of the signal. The only drawback of this approach for general signals is the condition that the input signal be band-limited so as to obtain an appropriate value for  $\kappa$ . A possible alternative to avoid this is to lattice the time-frequency plane by arbitrary frequency windows and for the signal component in each of these ranges to have arbitrary time windows according to their amplitude. This results in an asynchronous decomposition which we discuss next. The local-average approximation obtained above for a scale parameter  $\kappa$  of the ASDM is similar to the Haar wavelet representation [11] but with the distinction that the time-windows are signal-dependent instead of being fixed. Indeed, it is possible to generate pulses with duty-cycle determined by the sequence  $\{\alpha_k, \beta_k\}$ . Indeed, if  $\nu(t) = u(t) - u(t - 0.5)$  is a scaling function the wavelet function can be defined as

$$\psi_{\alpha_k, \beta_k, t_k, t_{k+1}}(t) = \nu\left(\frac{0.5t}{\alpha_k} - t_k\right) - \nu\left(\frac{0.5t}{\beta_k} - t_{k+1}\right)$$

So that local averages are found as

$$\zeta_k = \frac{1}{t_{k+2} - t_k} \int_{t_k}^{t_{k+2}} \psi_{\alpha_k, \beta_k, t_k, t_{k+1}}(t) z(t) dt \quad (3.5)$$

giving an approximation for  $x(t)$  similar to the one given by a wavelet representation:

$$\hat{x}(t) = \sum_{k \text{ even}} \zeta_k p_k(t) \quad (3.6)$$

for unit pulse  $p_k(t) = u(t - t_k) - u(t - t_{k+2})$ . This is a generalization of the Haar wavelet for a particular value of the scale  $\kappa$ . As such, our representation has the properties of wavelet representations.

For a scale parameter  $\kappa$  for the ASDM, the resulting set of local averages  $\{\zeta_k\}$  — depending on the zero-crossing times  $\{t_k\}$  or  $\{\alpha_k, \beta_k\}$  — provide the multi-level approximation (3.6) of  $x(t)$ . Considering that  $\zeta_k$  is the best mean-square estimator of the signal in  $[t_k, t_{k+2}]$  when no data is provided, the ASDM can be thought of an optimal LC sampler. More importantly, using different values of  $\kappa$  allows us to obtain different scale representations of the signal.

### 3.2 SIGNAL DECOMPOSERS

The scale decomposition is obtained by latticing the time–frequency plane so that the frequency axis is segmented to obtain related scale parameters  $\{\kappa_\ell\}$ , and the time axis is divided according to the width of the different time–windows determined by the scale parameters. For instance, to obtain a set of scales

$$\kappa_\ell = \frac{\kappa_1}{2^{\ell-1}} \quad \ell = 2, \dots, L$$

we would choose a narrow–band low–pass filter with bandwidth  $f_1$  such that  $\kappa_1 = (b - c)/f_1$  according to (3.4), and for the next modules we would choose low–pass filters of bandwidths  $2^{\ell-1}f_1$  (Hz),  $\ell = 2, \dots, L - 1$ , i.e., it is doubled at each module after the first to cover the bandwidth of the input signal. This is the equivalent of anti–aliasing filtering in the Shannon–Nyquist sampling theory. These scale low–pass filters allow us to obtain appropriate scale parameters for the ASDMs in the decomposer, as illustrated in 15.

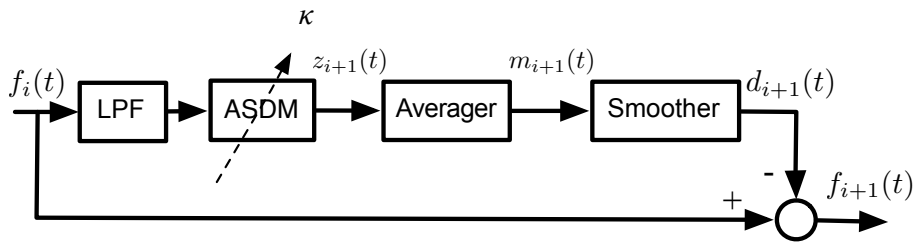


Figure 15: A module of the asynchronous low–frequency decomposer

We adopted this Fig. 15 as a module and performed two different realizations, cascade and parallel. Each configuration makes available different features in the analysis that are advantageous in specific applications. The common advantage in both configurations is that can be used for non-stationary signal analysis, especially for sparse signals in time, and for signals that are not necessarily band-limited.

### 3.2.1 Cascade Decomposers

The decomposers consists of  $L$  cascaded modules, one of them decomposes the signal into low-frequency components while the other provides the high-frequency components. Fig. 16 illustrates two modules of the low-frequency decomposer. The number of modules,  $L$ , is determined by the range of frequencies of interest in the signal. For a certain scale  $\kappa_\ell$ , determined by the maximum cutoff frequency of the corresponding scale filter, the ASDM maps the input signal into a sequence  $\{\alpha_{k,\ell}, \beta_{k,\ell}\}$  which the averager converts into local averages  $\{\zeta_{k,\ell}\}$ . The smoothing low-pass filter, after the averager, is used to avoid discontinuities that may occur when the multi-level signal  $d_\ell(t)$  is subtracted from the input signal of the corresponding module. Each of these modules operates similarly but at a different scale.

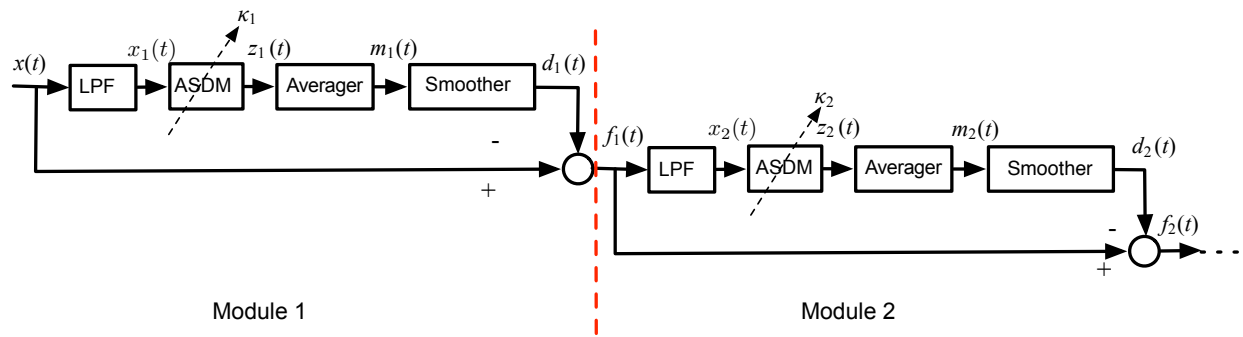


Figure 16: Low-Frequency Decomposer

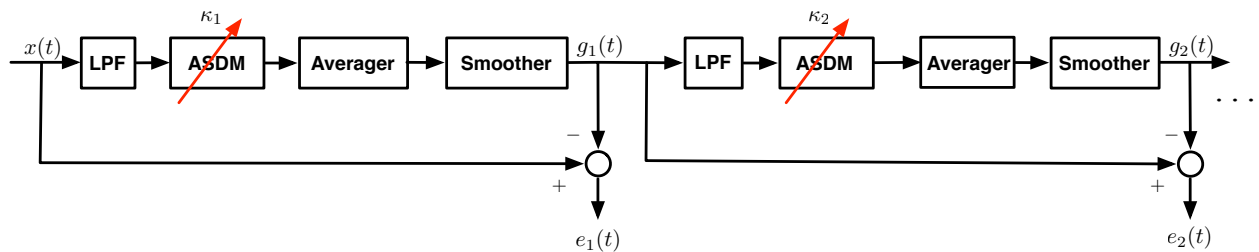


Figure 17: High-Frequency Decomposer

The input to the modules beyond the first one can be written sequentially as follows,

$$\begin{aligned}
f_1(t) &= x(t) - d_1(t) \\
f_2(t) &= f_1(t) - d_2(t) = x(t) - d_1(t) - d_2(t) \\
&\vdots \\
f_L(t) &= x(t) - \sum_{\ell=1}^L d_\ell(t).
\end{aligned} \tag{3.7}$$

We thus have the decomposition

$$x(t) = \sum_{\ell=1}^L d_\ell(t) + f_L(t) \approx \sum_{\ell=1}^L \sum_k \zeta_{k,\ell} p_k(t) + f_L(t) \tag{3.8}$$

where the  $\{d_\ell(t)\}$  are the low-frequency components of  $x(t)$  and of  $\{f_k(t)\}$ ,  $f_L(t)$  can be thought of as the error of the decomposition and as before  $p_k(t) = u(t - t_k) - u(t - t_{k+2})$ . The averages  $\{\zeta_{k,\ell}\}$  depend on the scale being used and are computed as in (3.5). This scale decomposition is analogous to a wavelet decomposition for analog signals. In terms of compression, the input signal  $x(t)$  can be equivalently represented by  $L$  sets of values  $\{\kappa_i, \zeta_{k,\ell}, i = 1, \dots, L$  from which we can generate the signal  $m_i(t), i = 1, \dots, L$ .

We have observed that  $f_L(t)$  approaches zero after a small number of modules  $L$ . Hence we can treat the output of the each block,  $f_i(t), i = 1, \dots, L$  as an error term in the representation since it is the difference between the original signal and decomposed parts. Because of the spectral behavior  $f_L(t)$  is called the "high-frequency component" and the smoothed averages  $\{d_\ell(t)\}$  are called the "low-frequency" components.

Here we illustrate this with a toy example: we consider a signal 1 sec. long and sampled at  $1kHz$  (in order to simulate the continuous-time).

$$x_1(t) = \sin(20\pi t) + \sin(10\pi t) + \sin(60\pi t)$$

For this signal  $L = 8$  modules and the following set of  $\kappa$  values are used consecutively

$$\kappa_i = [0.01, 0.0071, 0.0036, 0.0018, 0.0009, 0.0004, 0.0002, 0.0001].$$

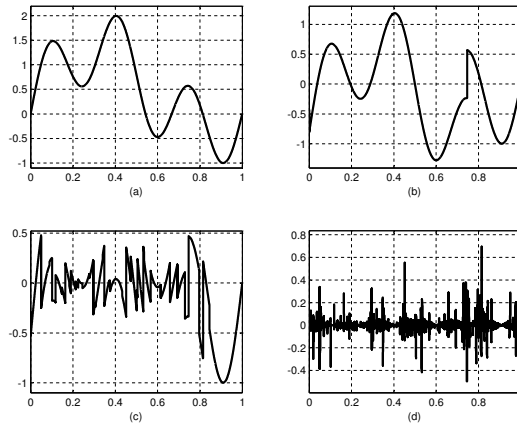


Figure 18: Input to the (a) first, (b) second, (c) 5th and (d) 8th module, respectively.

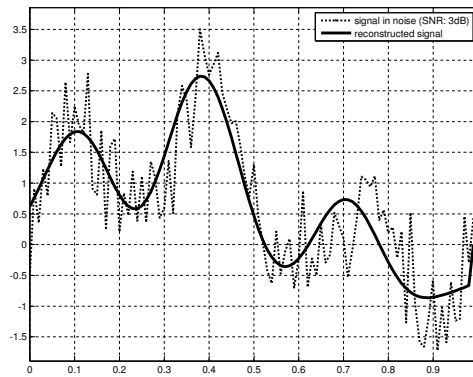


Figure 19: Reconstruction of test signal  $x_1(t)$  (dark signal) with additive noise  $SNR=3$  dB.

Figure 18 displays the components  $f_i(t)$  of this signal at different modules. After the 8<sup>th</sup> module, decomposition process is terminated since  $f_8(t)$ , looks like noise as shown in Fig. 18(d). The result for the reconstruction of the same signal with added noise ( $SNR = 3dB$ ) is plotted in Fig. 19. If we disregard the last term in the decomposition,  $f_L(t)$ , we observe a smoothing of the noise that is embedded in the signal.

This effect can be seen from Fig. 20 as well. Here we use an actual sparse signal. The recordings are swallowing signals a dual-axis accelerometer, are provided by [56]. The results

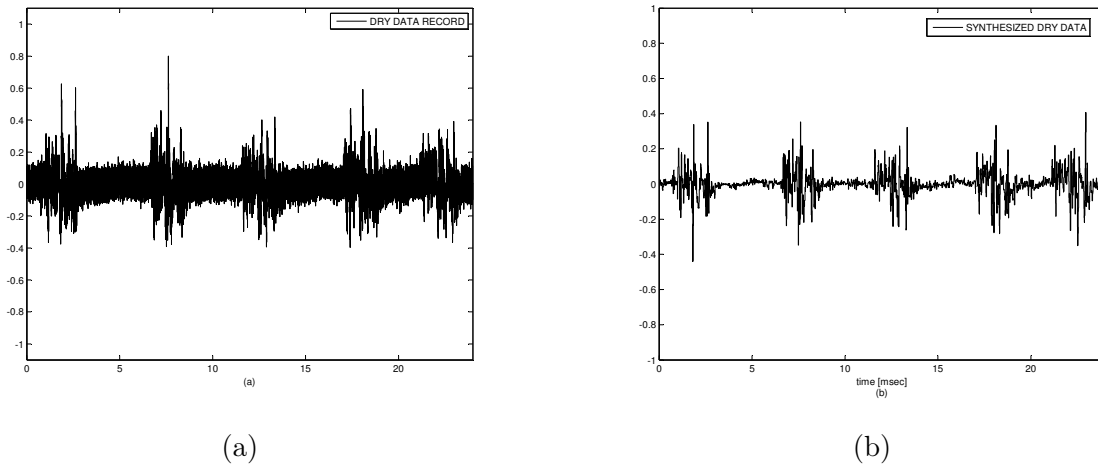


Figure 20: (a) Recorded and (b) Reconstructed Swallowing Data: type dry, cross correlation between the reconstructed signal and original signal 84.7

shown in Figs. 20 is obtained using

$$\kappa = [0.01, 0.005, 0.0025, 0.0013, 0.0006]$$

with  $L = 5$  modules of decomposer. It clearly depict that the proposed scheme can provide a denoised version of swallowing accelerometry signals. The similarity between the original and the reconstructed signal is found as 84.7%. Specifically, the location and the duration of swallows is clearer from the synthesized signals. Such denoised signals can be then used to segment these recordings more accurately.

This decomposition Eq.3.8 does seem analogous to the wavelet decomposition, but it is valid for continuous rather than discrete signal and it uses a scale rather than frequency to implement the decomposition.

To illustrate the performance of the decomposer we consider a phonocardiogram recording of a heart sound, shown on the top left of Fig. 21, and interpolated to approximate an

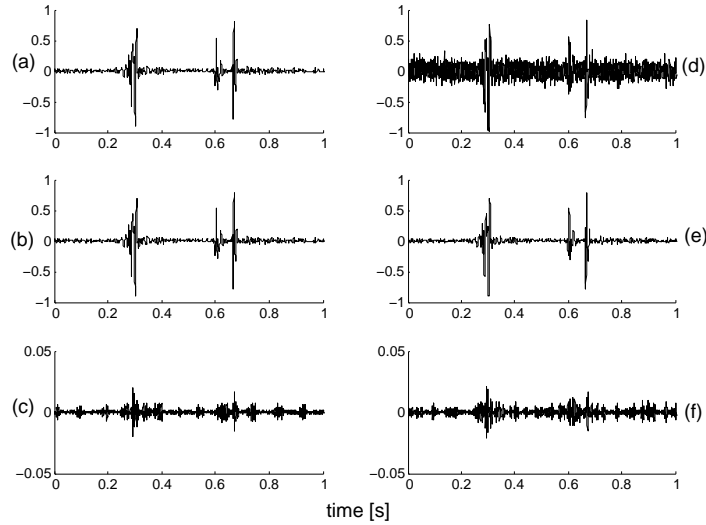


Figure 21: Left: phonocardiogram recording of a heart sound without noise (a); reconstructed signal (b); and reconstruction error (c). Right: phonocardiogram recording with additive noise (d); reconstructed signal (e); and reconstruction error (f).

analog signal in the simulation. In Figs. 21 and 22, we display the reconstruction of the original with and without additive noise. Similar to a wavelet representation, the decomposition algorithm is robust to additive, zero-mean noise. The reconstructed signal in both cases are very similar. For the noise-free recording, Fig. 23 displays the multilevel signals  $d_i$ ,  $i = 1, 2$ . The histograms on the right side of the figure show the prevalence of some averages. Selecting the most prevalent averages and the corresponding zero-crossing  $[t_k, t_{k+2}]$  provide a compressed representation of the signal. For the low-frequency decomposer we have followed a reasoning similar to wavelets analysis, and a dual of it would be the high-frequency

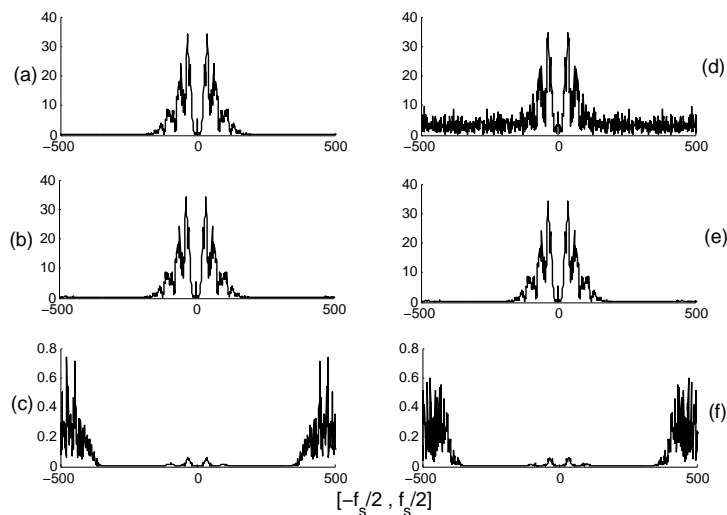


Figure 22: Left: Spectrum of phonocardiogram recording of a heart sound without noise (a); reconstructed signal (b); and reconstruction error (c). Right: Spectrum of phonocardiogram recording with additive noise (d); reconstructed signal (e); and reconstruction error (f).

decomposer shown in Fig. 17. The input is now expressed in terms of high-frequency terms  $\{e_i(t)\}$ ,

$$\begin{aligned}
 g_1(t) &= x(t) - e_1(t) \\
 g_2(t) &= x(t) - e_1(t) - e_2(t) \\
 &\vdots \\
 g_M(t) &= x(t) - \sum_{i=1}^M e_i(t)
 \end{aligned} \tag{3.9}$$

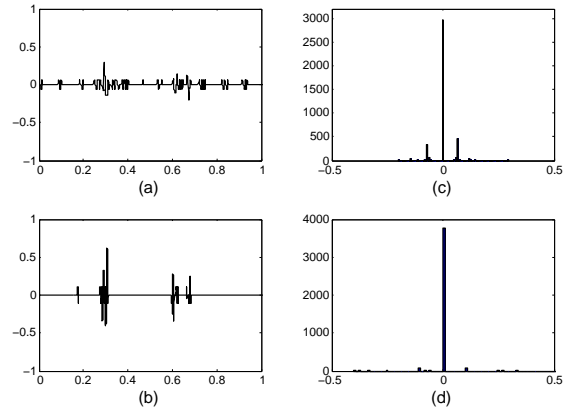


Figure 23: Multilevel signal components for noiseless recording, (a) and (b); histograms of the averages for the components, (c) and (d).

The decomposition in terms of high-frequency components is then given by

$$x(t) = \sum_{i=1}^m e_i(t) + g_M(t) \quad (3.10)$$

Fig. 24 illustrates the low- and the high-frequency decompositions. The advantage of these types of decompositions is apparent for signals that reside either in the low or in the high end of the frequency spectrum.

### 3.2.2 Parallel Decomposer

Asynchronous analysis can be also achieved by filtering the signal into different frequency bands and processing each separately. This approach is analogous to wavelet packets. A joint time-frequency lattice is constructed by determining frequency bands and letting the time windows, connected with the scale parameters, depend on the the maximum frequency

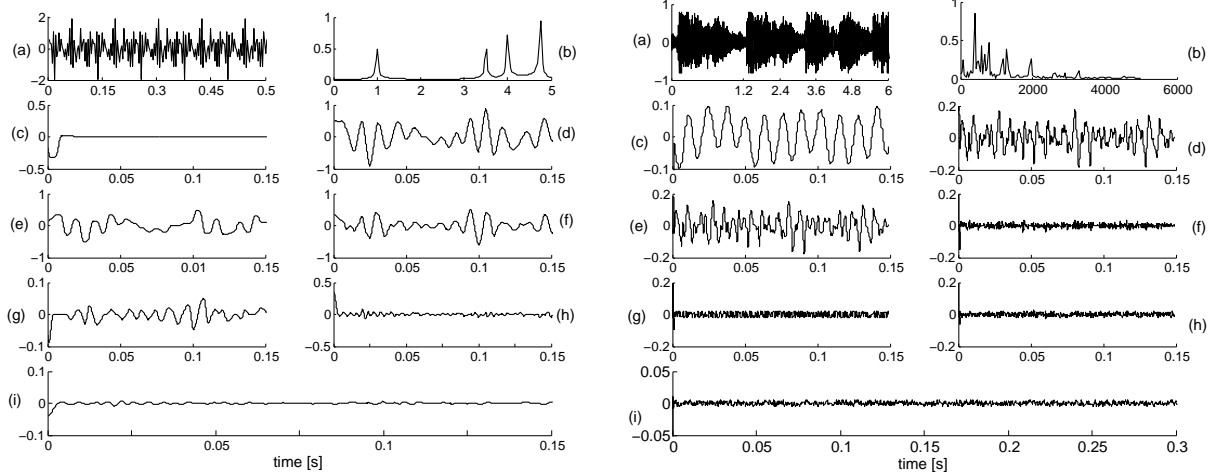


Figure 24: Left: High-frequency decomposition for synthetic signal composed of four sinusoids: (a)–(b) original signal and its spectrum, (c)–(h)  $d_i(t)$  components, (i)  $f_L(t)$  component. Right: Low-frequency decomposition for speech signal: (a)–(b) original signal and its spectrum, (c)–(h)  $e_i(t)$  components, (i)  $g_M(t)$  component.

of these bands and the amplitude of the signal being processed. The proposed bank-of-filters approach is shown in Fig. 25. The cutoff frequencies of the filters determine the values of  $\kappa_i$  for the  $i^{th}$  ASDM decomposer:

$$\kappa_i = \frac{\pi(1-c)}{\Omega_i}, \quad i = 0, 1, 2, \dots, M-1 \quad (3.11)$$

where  $\Omega_i$  is the cut-off frequency of the  $i^{th}$  filter, an  $M$  is the number of branches. The output of each of the the ASDM decomposers,  $z_\ell(t)$ , provides random sequence  $\{\alpha_{\ell,k}, \beta_{\ell,k}\}$  from which we can compute sequences of local averages and durations of the window  $\{\bar{x}_{\ell,k}, T_{\ell,k}\}$  for  $\ell = 1, 2, \dots, M, k = 1, 2, \dots, K$  where  $K$  corresponds to the number of pulses in each decomposition. For a non-deterministic signal  $\{\alpha_{\ell,k}\}$  are random, and as such their distributions characterize  $d_\ell(t)$  as well as the signal  $x(t)$ . The  $\{\bar{x}_{\ell,k}, T_{\ell,k}\}$  provide the same compression

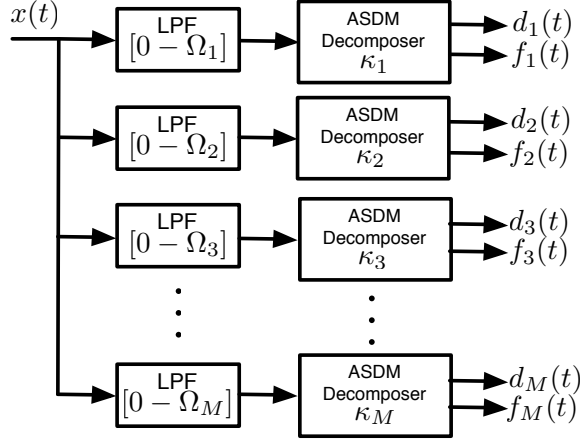


Figure 25: Bank-of-filters decomposer

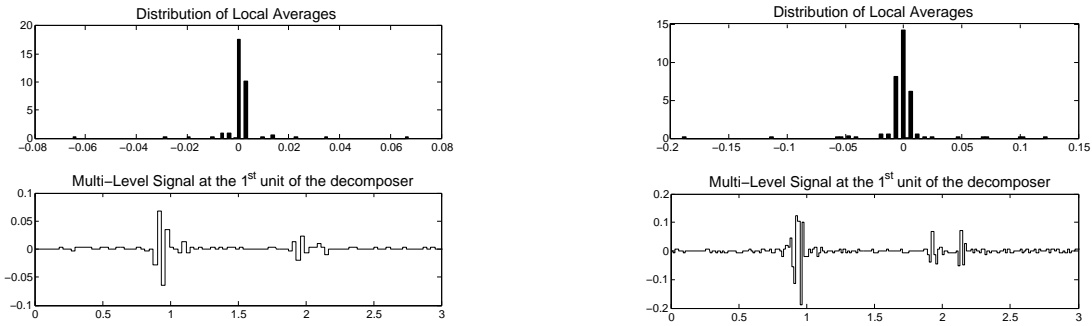


Figure 26: Resulting  $d_i(t)$ 's on parallel decomposer configuration

as the one provided by  $\{\alpha_{\ell,k}, \beta_{\ell,k}\}$  and the zero-crossings  $\{t_{\ell,k}\}$ . To obtain more compression we can consider the distribution of the  $\{\bar{x}_{\ell,k}\}$  or  $d_i(t)$  and use, similar to the process that motivated compressive sensing, a way to obtain a sparser signal by ignoring values clustered around one of the averages. In the following simulation of a Phonocardiograph recording of an actual heart sound, we emphasize this aspect of the parallel scheme by showing two decomposed low-frequency parts,  $d_1(t)$  and  $d_2(t)$ , and their histogram in Fig. 26. Parallel units take advantage of the sparsity in the signal and enable efficient representation using dominant local averages in each branch.

### 3.3 MODIFIED ASDM BANK OF FILTERS

#### 3.3.1 Modified ASDM as a Non-uniform Sampler

The motivation of this section is to search for a better solutions for encoding the information provided by the ASDM. Although the ASDM has appealing features such as being signal dependent and low-power information coder, its non-linear structure makes the recovery of the original information challenging [49, 54]. To overcome the challenge and sustain the advantages of ASDM signal dependent behavior, we consider a different approach to dealing with the integral equation (3.1). Let's assume that the input of the ASDM is the derivative of the signal,  $dx(t)/dt$ , rather than the signal itself. For this input equation (3.1) becomes

$$\int_{\tilde{t}_k}^{\tilde{t}_{k+1}} \frac{dx(\tau)}{d\tau} = (-1)^k [-(\tilde{t}_{k+1} - \tilde{t}_k) + \tilde{\kappa}] \quad (3.12)$$

This is equivalent to extracting the integrator from the feedforward loop in the model of

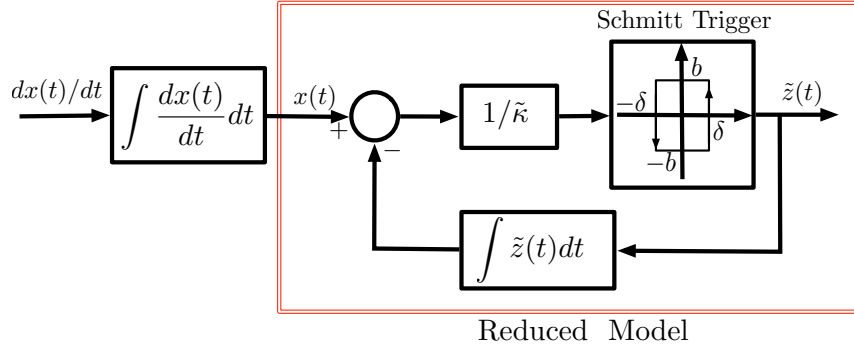


Figure 27: Modified Asynchronous Sigma Delta Modulator

Fig. 2 to obtain the equivalent feedback system shown in Fig. 27. The tilde symbol is used to indicate the parameters when the input is the derivative. This configuration has two interesting facts that simplify the analysis:

- \* First, letting the input be the derivative of the signal the integral equation is reduced to a first-order difference equation of which the input is a function of the zero-crossing times and a scale parameter of the ASDM:

$$x(\tilde{t}_{k+1}) - x(\tilde{t}_k) = (-1)^k [-(\tilde{t}_{k+1} - \tilde{t}_k) + \tilde{\kappa}]. \quad (3.13)$$

Using the modified ASDM (MASDM), we only need to keep the zero-crossing times to recursively obtain samples of the signal at non-uniform times from which to approximate the original signal, rather than solving the integral equation (3.1). Zero-crossing times and scale parameters of the modified ASDM in the synthesis part of the procedure provide the regeneration of the samples which can be interpolated to reconstruct the original signal. Non-uniform samples drawn from a sparse signal using MASDM is shown in Fig. 28.

\* Second, a reduced model can be used to avoid the derivative as input and reformulate the problem with respect to the signal itself, as highlighted in Fig. 27.

### 3.3.2 Asynchronous Analysis with MASDM

In this section we propose a bank of filters structure that uses the modified ASDM to analyze the signal at desired frequency ranges. The MASDM structure provides the zero-crossing times needed to recursively obtain non-uniform samples.

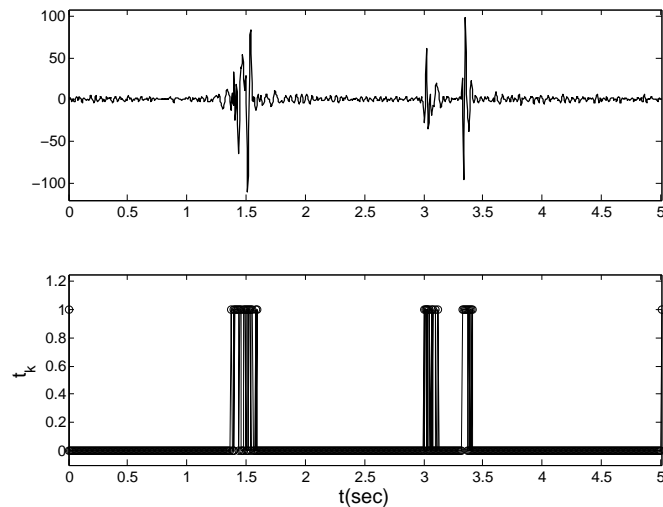


Figure 28: Non-uniform samples obtained using Modified ASDM

The recursive procedure reconstruction is given by Eq.(3.13) and requires that we set the parameters of the MASDM according to the derivative of the input. This can be done as follows:

- The amplitude bound in this case is on the derivative

$$c_d = \max \left| \frac{dx(t)}{dt} \right| < b.$$

where  $c_d$  is the maximum amplitude of the signal's derivative and  $b$  is the bias. For simplicity, the bias parameter  $b$  can be set to one, and the threshold parameter can be set to 0.5. This bound can be associated with the bound  $c$  of the signal itself. If we let the bound on  $x(t)$  be  $c$ , and assume  $x(t)$  is continuous we have,

$$c_d \leq \frac{2c}{T} \tag{3.14}$$

Here  $T \leq 1/(2f_{max})$  for perfect reconstruction where  $f_{max}$  is the maximum frequency of  $x(t)$ .

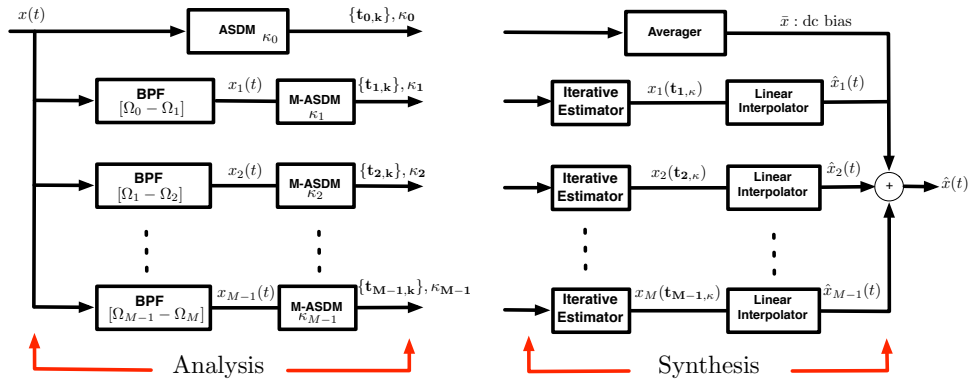


Figure 29: Asynchronous Decomposer

- Again, the lack of knowledge of  $f_{max}$  is an issue to be addressed by the proposed bank of filters. Using the bandwidth of the filters in the bank-of-filters the scale parameter should then satisfy in each branch

$$\tilde{\kappa}_i \leq \frac{\pi(1 - c_d)}{\Omega_i}, \quad i = 1, \dots, M$$

where  $\Omega_i$  is upper cut-off frequency of the filter in the  $i^{th}$  branch.

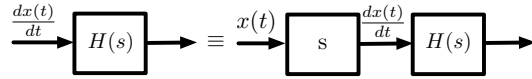


Figure 30: The equivalent filters

Note that the *reduced model*, see Fig. 27, avoids the derivative as an input by adding a zero to each of the filters to make  $x(t)$  the input rather than its derivative (as in Fig. 30) and the low-pass filters band-pass. We also need to include an extra branch to estimate the dc-bias, which is lost when the derivative is calculated, if the signal has any.

The dependence of the recursion on  $\tilde{\kappa}$  can be eliminated by considering evaluating (3.1) in two consecutive time intervals giving the following relation:

$$\int_{t_k}^{t_{k+2}} x(\tau) d\tau = t_{k+2} - 2t_{k+1} + t_k$$

and as such when replacing the signal by its derivative as the input in the ASDM we have

$$x(\tilde{t}_{k+2}) - x(\tilde{t}_k) = \tilde{t}_{k+2} - 2\tilde{t}_{k+1} + \tilde{t}_k$$

This not only eliminates the value of  $\tilde{\kappa}$  in the calculations but reduces the number of sample values  $\{x(\tilde{t}_k)\}$ .

We studied the decomposition and signal dependent sampling of sparse signals. A scale-based representation was obtained though two different asynchronous decomposition schemes, low- and high-frequency decomposers. Specifically, we proposed a bank-of-filters parallel decomposer using modified ASDM that behaves like a asynchronous analog to digital converter. Issues involving regularization and quantization in such recovery were discussed in details.

## 4.0 SYNTHESIS OF SPARSE SIGNALS

It has been shown that structured data, e.g. sparse signals, can be efficiently sampled at far below the Nyquist rate [22, 57]. However, despite the sparseness of the samples the reconstruction presents problems due to the typical ill-conditioning of the matrices involved [58], and so the methods are computationally expensive. Also, non-uniform sampling is not a preferred method for data acquisition, since both samples and their corresponding sample times are needed for reconstruction. We consider next an approach that allows us to compute the non-uniform samples recursively from the zero-crossing times.

Although the signal-dependent strategy provides an efficient sampling method for non-stationary and sparse signals, it complicates the signal reconstruction. Reconstruction based on the Nyquist-Shannon's sampling theory (also attributed to E. T. Whittaker and V. A. Kotelnikov) requires the signal to be band-limited. In practice, just like the assumption of stationarity, the band-limitedness condition on non-stationary signals is not appropriate: bandwidth is not an exact measure of the frequency content of a signal but rather a mathematical idealization, and the spectral representation of non-stationary signals is time-varying. Furthermore, Shannon's sinc interpolation for band-limited signals is not a well-posed problem. Fortunately, the sinc basis can be replaced by the prolate spheroidal wave (PSW) functions [24], which have better time and frequency localization than the sinc function [30, 51]. The PSW functions allow more compression in the sampling [51, 59] and whenever the signal has band-pass characteristics, modulated Slepian functions provide parsimonious representations.

Compressive sampling [60, 61] and matching pursuit [62] theories provide effective solutions to the problem of reconstructing a signal from its nonuniform samples. But again, they are primarily computationally expensive and often sub-optimal for the case of sparse data.

In matching pursuit bases are chosen from a redundant dictionary in order to best match the signal behavior.

In general searching a dictionary for best fit is computationally expensive. Forming a dictionary with well time and frequency concentrated bases increases the accuracy. We looked at bases dictionaries constructed with modulated Slepian sequences. The bases in the dictionary were obtained by modulation and varying of the bandwidth of discrete Slepian sequences. Using the proposed approach we carried out simulations on electrocardiogram and heart sound signals. The numerical analysis using real signals showed that modulated Slepian bases reconstruct more accurately than baseband Slepian functions [63,64].

In this section we suggest improvements on the existing techniques on sparse signals so as to be able to handle robust reconstructions with a reduced computational complexity. First, in section 4.1 we obtained reconstruction from non uniform samples using Slepian sequences. Then in section 4.2, we propose a practical scheme that is based on modulated Slepian functions to achieve low-complexity and low-error solutions for the reconstruction problem.

#### 4.1 SLEPIAN SEQUENCES FOR REGULARIZED RECONSTRUCTION

The above decomposers represent the signal using components in different frequency bands. To extend the scope of asynchronous processing we consider now the transmission and reconstruction of the asynchronously represented information using a bank of filters and the modified ASDM for the analysis and applying the Slepian sequences in the reconstruction. This would be analogous to analog-to-digital and digital-to-analog converters but for non-uniform sampling.

To use equation (3.15) to recover the non-uniform samples we need to transmit the zero crossings for each of the branches of the bank-of-filters (see Fig. 29). Naturally these values could be subjected to quantization error. The time elapsed between two consecutive samples is quantized according to a timer with a period of  $T_c$  seconds. Theoretically, the quantization error can be minimized as much as it is needed by simply reducing the  $T_c$ . In

this work, we adapted a method proposed by Roza [65] for sampling the asynchronous signal at a relatively low frequency. By using a clock with a sampling frequency of  $1/T_c$  on the modulated asynchronous signal, a sample-and-hold signal is obtained. We have observed reasonable quantization errors using a 8-bit quantizer. The reconstruction accuracy is shown in Figure (31). Here the signal used is an electroencephalography recording and the clock frequency is set to  $20kHz$ . The zero crossings corresponding to this signal are quantized with the eight-bit quantizer and then used to reconstruct the non-uniform samples.

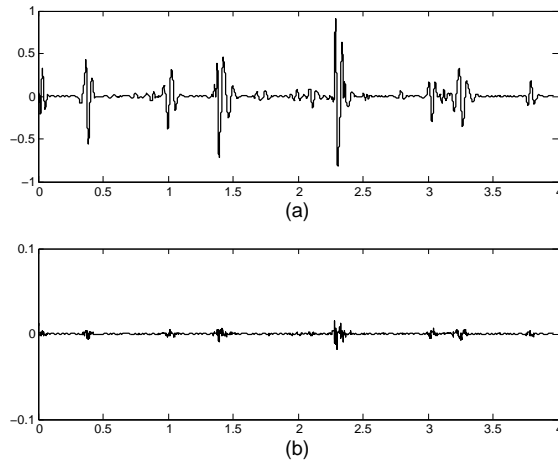


Figure 31: (a) Iterative estimator output (b) Quantization Error with SNR=17.94dB

Reconstruction from a non-uniform sampled signal is made possible by connecting the *sinc* and the Slepian functions — a more appropriate basis. To reconstruct the original signal we will use baseband as well as modulated Slepian functions for interpolation. Using non-uniform sampling instants  $\{t_k\}$  the  $M$ -dimensional Slepian projection is given by

$$\hat{x}(\hat{t}_k) = \Phi(\hat{t}_k)\gamma_M \quad (4.1)$$

where  $\hat{t}_k = t_k + \tau$ ,  $-\frac{T_c}{2} \leq \tau \leq \frac{T_c}{2}$ ,  $0 \leq k \leq N - 1$  for the actual zero-crossing  $t_k$  and  $\tau$  is the quantization error related to the sampling period  $T_c$  used in Roza's method. The projection coefficients  $\gamma_M$  can be obtained by the pseudo-inverse,

$$\gamma_M = [\Phi(\hat{t}_k)]^\dagger \hat{x}(\hat{t}_k). \quad (4.2)$$

Then the reconstructed signal is given by

$$x_r(t) = \Phi(\hat{t}_k)[\Phi(\hat{t}_k)]^\dagger \hat{x}(\hat{t}_k) \quad (4.3)$$

An inversion of  $N \times M$  Slepian matrix  $\Phi(\hat{t}_k)$  is highly ill-conditioned, especially when the sampling is non-uniform [66]. In order to gain numerically stable solutions we used Tikhonov regularization method [59, 67],

$$\gamma_{M\epsilon} = (\Phi(\hat{t}_k)^T \Phi(\hat{t}_k) + \epsilon I)^T \hat{x}(\hat{t}_k). \quad (4.4)$$

## 4.2 MODULATED SLEPIAN SEQUENCES FOR REGULARIZED RECONSTRUCTION

When both Slepian sequences and the signal under investigation occupy the same band, the representation is very accurate and sparse. There are two non ideal cases we can think of here:

- If the signal is not baseband, or has components that occupy a band centered around a frequency  $w_i > 0$
  - or the signal's bandwidth is much smaller than the band spanned by the Slepian sequenc.
- In this case, the representation is not as accurate or is redundant.

The second case can be solved by decreasing the Slepian sequence's frequency concentration. We can almost always achieve the same accuracy using a larger number of bases. Similarly for the first case we may want to increase the frequency concentration of our Slepian bases. This, however, will not result in accuracy as much as the second case since narrow band signals are more predictable [64, 68] than wider signals. In order to gain better bases, modulated discrete prolate spheroidal sequences (MDSS) are proposed in [63]. MDPSS can be written as,

$$\varphi_k^m(n, N, W) = \varphi_k(n, N, W) \times e^{j\omega_m n}. \quad (4.5)$$

The angular modulating frequency is  $\omega_m$ ,  $N$  is the time support and  $W$  is the frequency support of the sequence.  $\varphi_k(n, N, W)$  is the  $k^{\text{th}}$  DPSS satisfying:

$$\sum_{\ell=0}^{N-1} \frac{\sin(2\pi W(n-\ell))}{\pi(n-\ell)} \varphi_k(\ell, N, W) = \lambda_k(N, W) \varphi_k(n, N, W), \quad k = 0, 1, \dots, N-1 \quad (4.6)$$

with  $\lambda_k(N, W)$  begin ordered non-zero eigenvalues,

$$\lambda_0(N, W) > \lambda_1(N, W), \dots, \lambda_{N-1}(N, W) > 0.$$

Since 4.5 also satisfies the above relation 4.6, modulated sequences posses the properties of discrete prolate spheroidal sequences, e.g. they are doubly orthogonal and confined both in time and in frequency. The frequency concentration around frequency  $w_m$  depends on the baseband sequence frequency concentration  $W$ , i.e.  $[-W + \omega_m, W + \omega]$ . Hence we form a fine grid in frequency domain using narrow Slepian sequences and by modulating them. To illustrate the advantage of using modulated Slepian functions we consider the

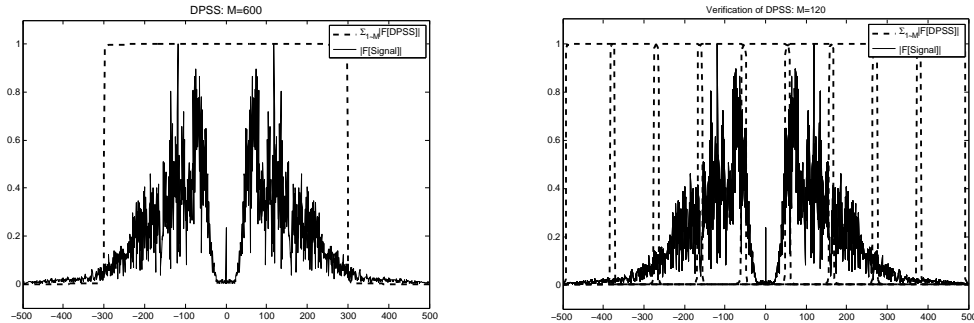


Figure 32: Right: Spectra of analyzed signal and of Discrete Slepian Sequences; left: Modulated–Discrete Slepian Sequences

processing of Phonocardiograph recordings of an actual heart sound containing the opening snap [69]. The heart sound is processed with the bank-of-filters, and zero-crossing times  $t_{i,k}$  are obtained at each branch, see Fig. 29. Performance comparison of different interpolation methods can be seen in Fig. 33. Its performance is compared with the piecewise linear interpolation which is known to be well suited for non uniform samples. Incorporating

Modulated Slepian functions [68], see Fig. 32, into filter–bank scheme provided the minimum error in the reconstruction as optimum time–frequency concentration is ensured in each band. Modulated Slepian functions also improved performance compared to interpolation using baseband Slepian functions.

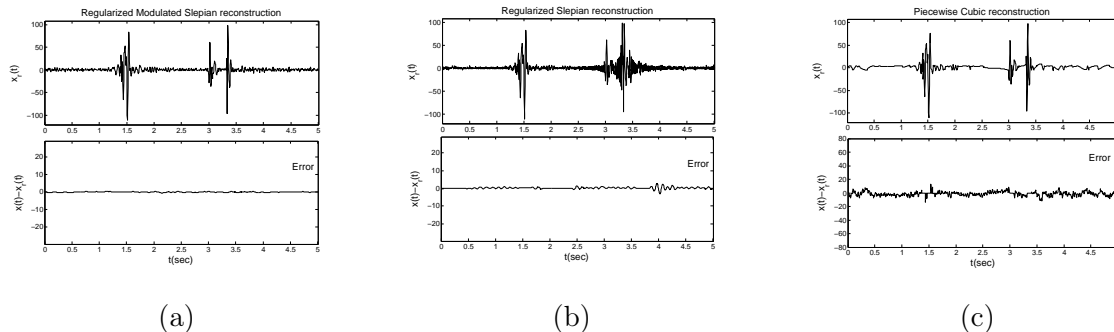


Figure 33: Reconstructed signal and error: (left) Modulated–Slepian reconstruction for SNR= 25.95dB,  $M = 120$ ,  $\epsilon = 2 \times 10^{-4}$ , (middle) baseband Slepian reconstruction (SNR=15.20 dB,  $M=600$ ,  $\epsilon = 2 \times 10^{-4}$ ) (right) Piecewise Cubic Interpolator (SNR= 10.89 dB)

In this section, we have analyzed experimentally the advantage of modulated Slepian functions on the interpolation from non–uniform samples. The accuracy of the interpolation with modulated Slepian interpolation showed promising results for the recovery of sparse signals from zero–crossings. In the following section we will show how to obtain similar performance but with reduced computational cost using Slepian wavelets.

## 5.0 WAVELET BASES FOR SPARSE SIGNALS

Slepian wavelets give a new way to express sparse signals that overcomes some limits of other representations. We blend desirable properties of Slepian functions with ideas from wavelets, along with an efficient algorithm to compute expansion. Such wavelets are capable of quickly capturing the essence of a data set with a small number of coefficients. Owing to the localization properties of Slepian wavelets, instead of spreading the information among all the scales, it is very well concentrated. As most of the coefficients are zero, no redundancy is built into the representation of sparse signals.

In this chapter, we present a multi resolution representation based on Slepian wavelet for interpreting sparse information. We first look at the projection of a function using Slepian scaling functions to different resolution scales and obtain a scale related approximation. Then we define Slepian wavelets looking at the difference between two consecutive resolution spaces. They are formed to span the intermediary space between aforementioned spaces spanned by the scaling function. Finally we obtain a complete multiresolution approximation using the Slepian wavelets. This section is presented around two main axes; 1) a critical review of the Slepian wavelets and 2) their particular relevance in the reconstruction of sparse signals from its non-uniform samples.

Expansion of signals in terms of wavelets and perfect reconstruction filter banks have proven to be equivalent forms in signal representation, see Section 2.4. We have adapted the later one, as it yields implementable systems. This equivalent expansion has a multi resolution property enabling us to form an important framework both for the decomposition schemes we have proposed earlier, and also for the analysis of non-stationary signals using wavelet bases. We have pursued on the biorthogonal structures [13, 42] as they enable perfect reconstruction and efficient implementations with FIR filters. Using biorthogonal

filters banks based on Slepian functions we obtained wavelets that are symmetric, causal and implementable in real-time.

The first use of Slepian functions as wavelets were proposed by Shen and Walter [15]. First Slepian function with bandwidth of  $\pi$  used as a scaling function, and they obtained a MRA analysis of the space of band limited signals [31] using continuous time Slepian wavelets. Though we have benefited on their derivations, our approach differs in implementation. We have performed all computations over discrete signals with biorthogonal Slepian filters. Shen and Walter's findings in [15] simplified our mathematical analysis, though our discretizations yield fast numerical algorithms. Yet, we would like to mention their work in [28] where they exploit a natural connection between sinc and Slepian functions to obtain formulas to digitize band limited signals. A sampling theorem based on Slepian functions is provided and MRA based on Slepian functions is suggested. All derivations in this work is based on scaling functions, wavelets were not introduced. They suggest the corresponding wavelets in their further studies by modulating the scaling function [29]. This gives an orthogonal complementary of the scaling function in the frequency domain. We will see in this section that our wavelet bases differ from their approach as well.

Mallat's MRA spaces are built by a scaling function that is orthogonal to its integer translates. The proposed scaling function in the Shen's study is not orthogonal to its integer translates but they do constitute a Riesz basis for the space of  $\pi$ -bandlimited signals. In [70] Slepian wavelets are used for the image reconstruction in computerized tomography. There the method was proven to outperform in quality of the reconstruction and computational complexity, many other wavelet based methods suggested concerning the same problem. Mondal and Percival in [71] investigates wavelet variance analysis of Gaussian time series using Slepian wavelets. They derive a statistical theory for Slepian-based wavelet variances for irregularly sampled time series. They also show that, for regularly sampled Gaussian time series, Slepian-based wavelet variances are comparable to Daubechies-based variances.

## 5.1 FIR BIORTHOGONAL FILTERS FOR THE SLEPIAN WAVELET TRANSFORM

In this section we introduce biorthogonal wavelet basis sets,  $\phi(t), \tilde{\phi}(t), \psi(t), \tilde{\psi}(t)$ , to be used in the multi-resolution analysis of  $\pi$  bandlimited signals. Scaling function  $\phi(t)$  is taken as the first Slepian function that has a maximum concentration on a desired interval [26]. Then using this scaling function we derive a dual basis,  $\tilde{\phi}(t)$ , which allows us to constitute a biorthogonal system  $\{\phi, \tilde{\phi}\}$  which enables dyadic signal expansions,

$$x(t) = \sum_j \langle \phi_j(t), x(t) \rangle \tilde{\phi}_j(t) = \sum_j \langle \tilde{\phi}_j(t), x(t) \rangle \phi_j$$

of any  $\pi$ -bandlimited function  $x$ . Here we consider dilated versions of the basis by indexing with  $j$ . Corresponding wavelets  $\psi(t), \tilde{\psi}(t)$  are constructed with two pairs of analysis filters  $\{h[n], g[n]\}_{n \in \mathbb{Z}}$  and synthesis filters  $\{\tilde{h}[n], \tilde{g}[n]\}_{n \in \mathbb{Z}}$ , as illustrated in Fig. 34.

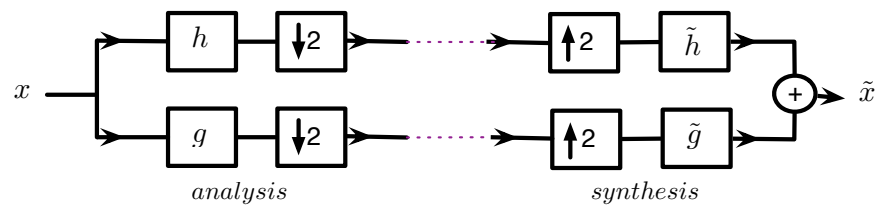


Figure 34: Two-channel filter banks leading to Slepian wavelets

The heart of building a perfect reconstruction scheme,  $\tilde{x} = x$ , depicted in Fig. 34 is the choice of  $h[n]$  and  $\tilde{h}[n]$  [11], which we rely on Slepian biorthogonal wavelets. For clarity we organized our derivations into five steps in this section,

- Defining the Slepian scaling function  $\phi$ ,
- Obtaining a dual scaling function  $\tilde{\phi}$  that is biorthogonal to  $\phi$ ,
- Using  $\phi$  and  $\tilde{\phi}$  to obtain filters (or expansion coefficients)  $h$  and  $\tilde{h}$ ,
- Utilizing perfect reconstruction rules to find  $g$  and  $\tilde{g}$ ,
- Using  $g$  and  $\tilde{g}$  to derive wavelets  $\psi$  and  $\tilde{\psi}$ .

First we start by defining the scaling function  $\phi(t)$ . Our scaling function is the first Slepian function  $\phi(t) := \varphi_{0,\pi,\tau}(t)$ , a low-pass waveform. The first subindex denotes that this is the first Slepian function (which has the maximum concentration among the others); the second index reflects the frequency concentration interval  $[-\pi, \pi]$  and the last one is for the time concentration  $[-\tau, \tau]$  respectively [28]. Among several ways, one way to characterize Slepian functions is to represent them as the eigenfunctions of an integral operator,

$$\frac{\sigma}{\pi} \int_{-\tau}^{\tau} \varphi_{n,\sigma,\tau} \frac{\sin(\sigma(t-x))}{\sigma(t-x)} dx = \lambda_{n,\sigma,\tau} \varphi_{n,\sigma,\tau}(t)$$

Its Fourier transform, denoted as  $\hat{\varphi}_{0,\pi,\tau}(\omega)$ , has support on  $[-\pi, \pi]$ , has no zeros in  $[-\pi, \pi]$  and is continuous there [30],

$$\hat{\phi}(\omega) := \hat{\varphi}_{0,\pi,\tau}(\omega) = (-1)^n \sqrt{\frac{2\pi\tau}{\pi\lambda_{0,\pi,\tau}}} \varphi_{0,\pi,\tau}\left(\frac{\tau\omega}{\pi}\right) [u(\omega + \pi) - u(\omega - \pi)] \quad (5.1)$$

The scaling function itself and its integer translates,  $\{\phi(t-n) = \varphi_{0,\pi,\tau}(t-n)\}_{n \in \mathbb{Z}}$ , span a space  $V_0 \in S_\pi$ , i.e. they form an unconditional basis for a subspace  $V_0$  of a band limited functions space,  $S_\pi$ . The dual scaling function  $\tilde{\phi}(t)$  can be [29] noted as:

$$\hat{\tilde{\phi}}(\omega) = \hat{\varphi}_{0,\pi,\tau}(\omega) := \frac{\hat{\varphi}_{0,\pi,\tau}(\omega)}{\sum_k |\hat{\varphi}_{0,\pi,\tau}(\omega - 2\pi k)|^2}$$

This choice of  $\{\tilde{\varphi}_{0,\pi,\tau}(t-n)\}$  yields biorthogonality with the scaling function  $\{\phi(t-n) = \varphi_{0,\pi,\tau}(t-n)\}_{n \in \mathbb{Z}}$ , i.e.,

$$\sum_k \tilde{\varphi}_{0,\pi,\tau}(\omega - 2\pi k) (\varphi_{0,\pi,\tau}(\omega - 2\pi k))^* = 1$$

The dual scaling function  $\tilde{\phi}(t)$  is also positive on  $[-\pi, \pi]$ , same as the scaling function  $\phi(t)$ . So with its integer translates  $\{\tilde{\phi}(t-n)\}_{n \in \mathbb{Z}}$ , it forms a Riesz basis for  $\tilde{V}_0 \in S_\pi$ . One can obtain  $\tilde{\phi}(t)$  by inverse Fourier transform [15],

$$\tilde{\phi}(t) = \tilde{\varphi}_{0,\pi,\tau}(t) = (-1)^n \sqrt{\frac{2\pi\tau}{\pi\lambda_{0,\pi,\tau}}} \frac{1}{2\pi} \int_{-\pi}^{\pi} \tilde{\varphi}_{0,\pi,\tau}\left(\frac{\tau\omega}{\pi}\right) e^{j\omega t} d\omega$$

The dual function is obtained first in the frequency domain using the biorthogonality criteria, and then the time domain correspondence is obtained from an inverse transform. Unfortunately as it is noticed, there is no closed form expressions for neither Slepian functions or the dual function that is formed from them. They can be only obtained through a computational procedure and even then, only at specific points. This might seem to be a drawback but as we are interested in signal expansions for real data, we have benefitted from a computational procedure better than a closed form expression. Moreover, it has been shown that once we arrive at the filters  $h[n], \tilde{h}[n]$  need for waveforms,  $\phi(t), \tilde{\phi}(t)$  will be suspended, and the same is true for wavelets  $\psi(t), \tilde{\psi}(t)$  and their associated filters  $g[n], \tilde{g}[n]$  [10].

One can easily verify that, if  $\phi(t - n)$  is a Riesz basis of  $V_0$ , and  $\phi(2t - n)$  is a Riesz basis of  $V_j$ , then the same is true for  $\tilde{\phi}(2t - n)$  of  $\tilde{V}_j$ . Since both  $\phi(t)$  and  $\tilde{\phi}(t)$  have a low-pass character, the projection spaces  $V_j$  are called coarse spaces. These dual Riesz bases of compactly supported Slepian wavelets give rise to exact reconstruction schemes with finite length synthesis filters that are different than the analysis filters. We now need to show the filters that will perform the projection operator on to coarse scale spaces  $V_j$  and  $\tilde{V}_j$ . Multiresolution leads to a hierarchical scheme for computation of these coefficients [13]. Iterated low-pass filters' output will converge to our scaling functions,

$$\hat{\phi}(\omega) = (2\pi)^{1/2} \prod_{j=1}^{\infty} \hat{h}(2^{-j}\omega)$$

$$\hat{\tilde{\phi}}(\omega) = (2\pi)^{1/2} \prod_{j=1}^{\infty} \hat{\tilde{h}}(2^{-j}\omega)$$

Here the first channel filters are denoted as  $h$  and  $\tilde{h}$  and their Fourier transform as,

$$\hat{h}(\omega) = 2^{-1/2} \sum_n h[n] e^{-j\omega n}$$

$$\hat{\tilde{h}}(\omega) = 2^{-1/2} \sum_n \tilde{h}[n] e^{-j\omega n}$$

Since  $\{\phi(t-n)\}_{n \in \mathbb{Z}}$  and  $\{\tilde{\phi}(t-n)\}_{n \in \mathbb{Z}}$  are unconditional bases of  $V_0$  and  $\tilde{V}_0$  respectively, and  $V_0 \subset V_1$  similarly  $\tilde{V}_0 \subset \tilde{V}_1$ , hence we can decompose,

$$\begin{aligned}\phi(t) &= \sqrt{2} \sum_{-\infty}^{\infty} h[n] \phi(2t-n) \\ \tilde{\phi}(t) &= \sqrt{2} \sum_{-\infty}^{\infty} \tilde{h}[n] \tilde{\phi}(2t-n)\end{aligned}\tag{5.2}$$

These equations are named as *Refinement Equations* in wavelet literature. Slepian scaling and dual functions are one possible solution for the refinement equations. We would like to make an interesting observation for the Slepian functions in here: we know if  $\phi(t)$  is a solution of the refinement equation (5.2) with a particular  $h_0(k)$ ,  $\phi(t) * \phi(t)$  will be the solution with convolved coefficients  $h_0(k) * h_0(k)$ . This yields in an interesting case for Slepian functions as depicted in the Fig. 35a: the convolution of Slepian functions generates a dyadic structure which could be exploited to generate the basis for the dyadic scales. In other words, basis functions are self similar at different scales.

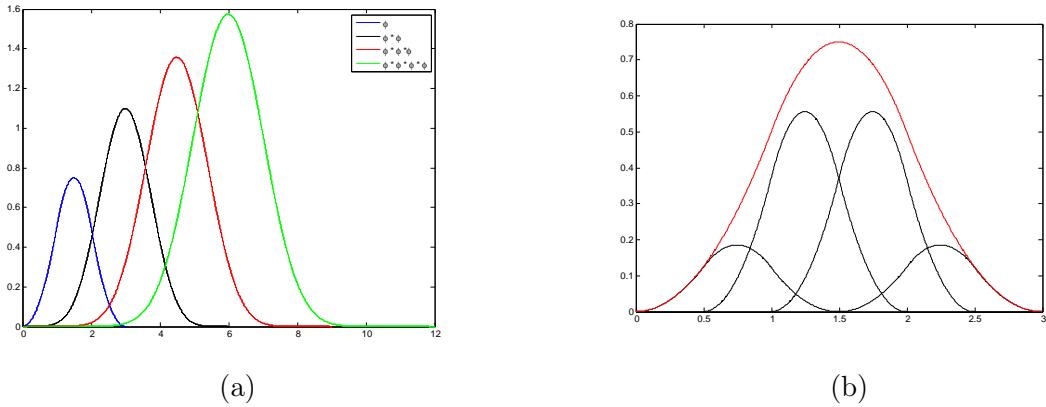


Figure 35: (a) First Slepian function and convolutions of it with itself, (b) Refinement Equation verification

The Fourier transform of the refinement equations will yield the filter associated with the scaling functions,

$$\begin{aligned}\hat{\phi}(\omega) &= \hat{h}(\omega/2)\hat{\phi}(\omega/2) \\ \hat{\tilde{\phi}}(\omega) &= \hat{\tilde{h}}(\omega/2)\hat{\tilde{\phi}}(\omega/2)\end{aligned}\tag{5.3}$$

Note that a recursive relation can be obtained for Eq. 5.3,

$$\begin{aligned}\hat{\phi}(\omega) &= \hat{h}\left(\frac{\omega}{2}\right)\hat{\phi}\left(\frac{\omega}{2}\right) \\ &= \hat{h}\left(\frac{\omega}{2}\right)\overbrace{\hat{h}\left(\frac{\omega}{4}\right)\hat{\phi}\left(\frac{\omega}{4}\right)} \\ &\vdots \\ &= \prod_{j=1}^{\infty}\hat{h}\left(\frac{\omega}{2^j}\right)\end{aligned}$$

In other words, scaling functions appear in the limit of and infinite iteration [72]. In order for this infinite product to converge we need to have  $\hat{h}(0) = 1 = \hat{\tilde{h}}(0)$  which is satisfied for Slepian scalings. Using Eq. 5.3

$$\hat{h}(\omega/2) = \frac{\hat{\varphi}_{0,\pi,\tau}(\omega)}{\hat{\varphi}_{0,\pi,\tau}(\omega/2)}, \quad |\omega| < \pi$$

We can simplify this relation using the multi structure behavior of Slepian functions. By changing the scale in the integral equation Eq.(5.1) one can obtain [29],

$$\sqrt{2}\varphi_{0,\sigma,\tau}(2t) = \varphi_{0,2\sigma,\tau/2}(t)\tag{5.4}$$

Using this relation among scales and Eq.5.1, we revisit Eq.5.3,

$$\hat{h}(\omega/2) = \frac{\varphi_{0,\pi,\tau}(\tau\omega/\pi)}{\varphi_{0,2\pi,\tau/2}(\tau\omega/\pi)}, \quad |\omega| < \pi$$

Finally the filter coefficients are,

$$h_n = \frac{1}{4} \int_{-\pi}^{\pi} \frac{\varphi_{0,\pi,\tau}(\tau\omega/\pi)}{\varphi_{0,2\pi,\tau/2}(\tau\omega/\pi)} e^{-j\omega n} d\omega\tag{5.5}$$

Similarly we can derive the dual filter coefficients  $\tilde{h}_n$  in terms of  $\tilde{\varphi}_{0,\pi,\tau}(t)$ . We now can construct Slepian wavelets  $\psi$  and  $\tilde{\psi}$  by considering the complement of  $\tilde{V}_j$  in  $\tilde{V}_{j+1}$  and  $V_j$  in  $V_{j+1}$  respectively. We can do a similar deduction to one in Eq.5.2 for wavelets,

$$\psi(t) = \sqrt{2} \sum_n g[n+1] \phi(2t-n) \quad (5.6)$$

$$\tilde{\psi}(t) = \sqrt{2} \sum_n \tilde{g}[n+1] \tilde{\phi}(2t-n) \quad (5.7)$$

The second channel filters are given below in terms of the first channel in order to satisfy the perfect reconstruction conditions [13] as,

$$g[n] = (-1)^{n+1} \tilde{h}[-n], \quad \tilde{g}[n] = (-1)^{n+1} h[-n] \quad (5.8)$$

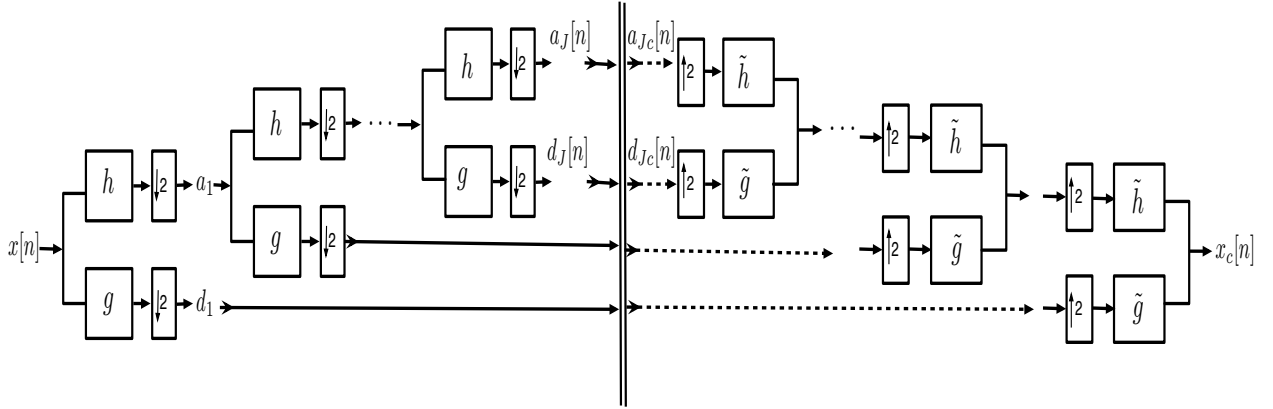


Figure 36: Wavelet Transform with filter banks

Plugging Eq.5.8 into Eq.5.6 the relationship between wavelet functions and scaling filters are obtained as follows,

$$\psi(t) = \sqrt{2} \sum_n (-1)^n \tilde{h}[-n-1] \phi(2t-n)$$

$$\tilde{\psi}(t) = \sqrt{2} \sum_n (-1)^n h[-n-1] \phi(2t-n)$$

Given the set of bases  $\psi, \tilde{\psi} \in B_\pi$  defined as above, we can express all  $x(t) \in B_\pi$  as,

$$x(t) = \sum_{j,n} \langle x(t), \tilde{\psi}_{j,n}(t) \rangle \psi_{j,n}(t) = \sum_{j,n} \langle x(t), \psi_{j,n}(t) \rangle \tilde{\psi}_{j,n}(t)$$

Here  $\psi_{j,n}(t) = 2^{-j/2}\psi(2^{-j}t - n)$ . We previously called the product  $d_j = \langle x, \tilde{\psi}_{j,n} \rangle$  detail coefficient. As we illustrated in Fig. 36 filter banks make possible to implement this transform without the need of continuous wavelet and scaling waveforms. Starting with a biorthogonal filter and using the iterated filter bank method we can calculate the Slepian wavelet transform. Finite length filters  $h[n], \tilde{h}[n], g[n], \tilde{g}[n]$  give the approximation and detail coefficients.

The Slepian scaling functions of different length and their associated wavelets, dual functions and filters are shown in the following Figures (37-38-39). Some comments about these figures:

- In the simulations, we obtain biorthogonal Slepian scalings using  $\pi$  band limited DPSS sequences of different length. The Matlab R20013a function  $dpss(N, NW, k)$  is used. Here  $N$  is the sequence length,  $NW$  is the time half bandwidth product, and the last index  $k$  indicates how many DPSS sequences are generated. We used for the scaling function the first DPSS, with  $NW \approx 1/2$  with a different size of  $N$ .
- We construct dual Slepian bases  $\tilde{\phi}$  by starting with a biorthogonal filter bank, and then used the iterated filter bank method.
- As it can be seen from Fig. 39, all of the filters are symmetric, so neither one is orthogonal except Fig. 39 (a). They have linear phase and hence no phase distortion is caused by filtering.
- All of the filters have finite length, and the bases have compact support.
- All of the proposed filters satisfy perfect reconstruction conditions. We showed in the following for one of them that is length-8 analysis filter  $h = [0 \ 0 \ 0.1768 \ 0.5303 \ 0.5303 \ 0.1768 \ 0 \ 0]$ , and length-8 synthesis filter

$$\tilde{h} = [0.06 \ 0.19 \ 0.15 \ 0.99 \ 0.99 \ 0.15 \ 0.19 \ 0.06]$$

- Double shift orthogonality:  $\sum_k h[k]\tilde{h}[2n - k] = \delta[n]$ , i.e.

$$\text{conv}(h, \tilde{h}) = [0 \ 0 \ 0.01 \ 0 \ 0.09 \ 0 \ 0.58 \ 1.00 \ 0.58 \ 0 \ 0.09 \ 0 \ 0.011 \ 0 \ 0]$$

$$\begin{aligned}
& - \sum_k h[k] \tilde{g}[2n - k] = 0 \\
& - \sum_k \tilde{h}[2k - n'] h[n - 2k] = \delta[n] + \sum_m \tilde{g}[2m - n'] g[n - 2m] = \delta[n - n']
\end{aligned}$$

$$conv(h, \tilde{h}) + conv(g, \tilde{g}) = [0 \ 0 \ 0 \ 0 \ 0 \ 0 \ 0 \ 2 \ 0 \ 0 \ 0 \ 0 \ 0 \ 0 \ 0].$$

- Smoothness of the Slepian scaling function generated by  $h$ . It is measured with  $s = -\frac{1}{2} \log_2 |\lambda_{max}|$  [11] where  $\lambda_{max}$  is the maximum non-special eigenvalue of transition matrix  $T = (\downarrow 2)2H_0H_0$ . The following are some  $s$  values obtained by the proposed filters  $h$ .

$$- h = [0.125 \ 0.375 \ 0.375 \ 0.125] \Rightarrow s = 2.5.$$

$$\begin{aligned}
- h = [0.0005 \ 0.0054 \ 0.0269 \ 0.0806 \ 0.1611 \ 0.2256 \ 0.2256 \ 0.1611 \ 0.0806 \ 0.0269 \\
0.0054 \ 0.0005] \Rightarrow s = 5.99.
\end{aligned}$$

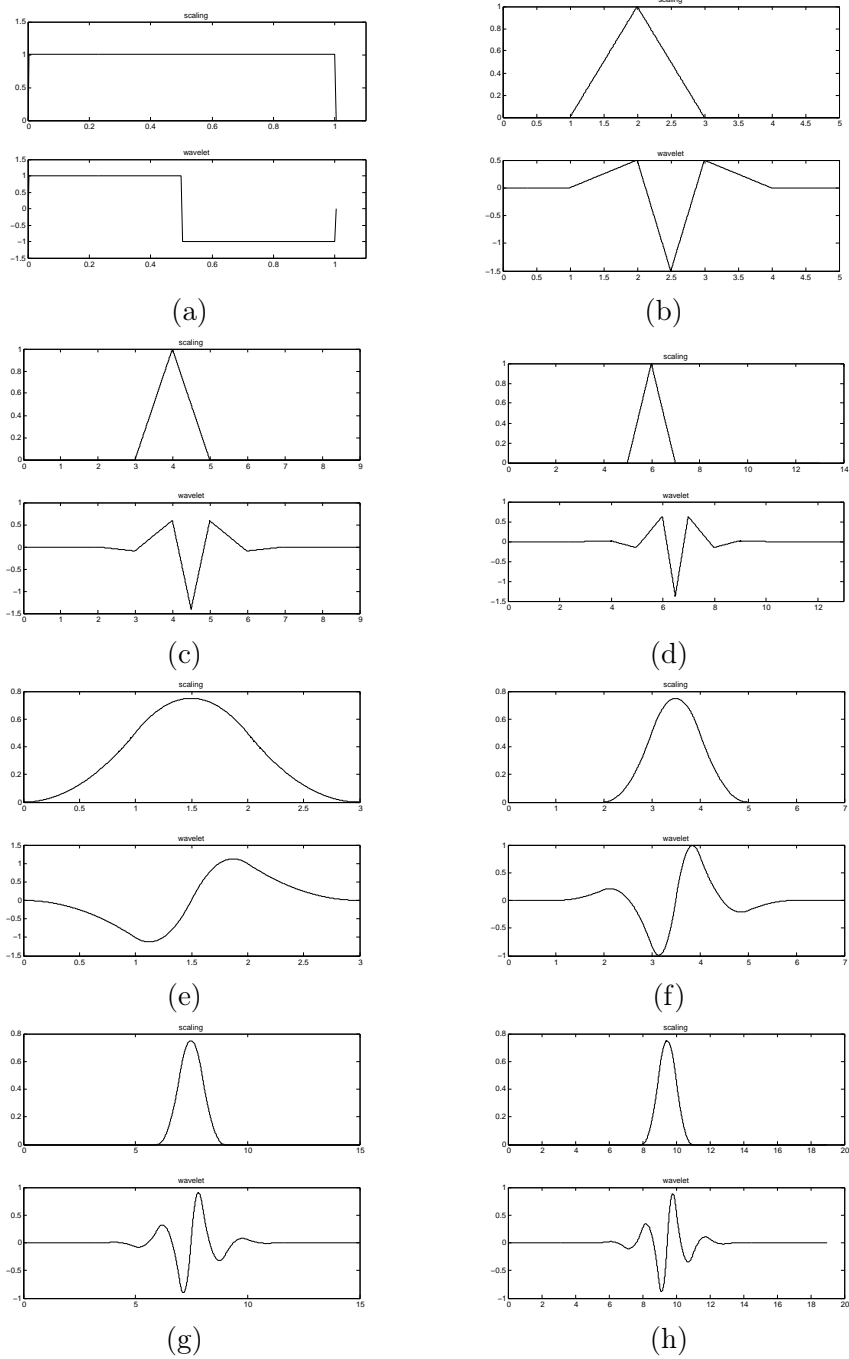


Figure 37:  $\pi$ -bandlimited Biorthogonal Slepian scaling functions  $\phi$  and corresponding wavelets  $\psi$ : (a) N=2 DPSS sequence; (b)-(d) N=3 DPSS sequence; (e)-(h) N=4 DPSS sequence

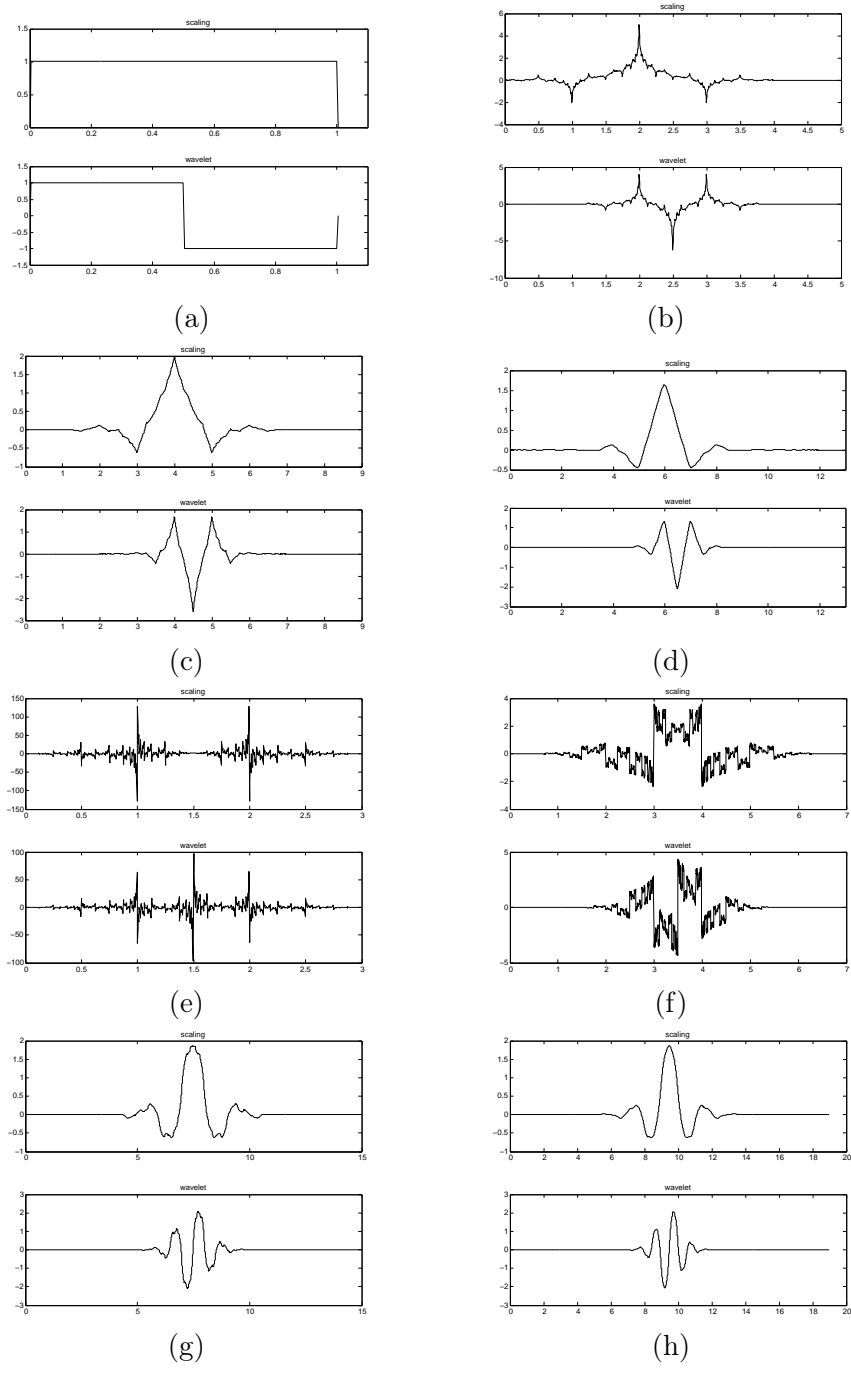


Figure 38: Dual Slepian scaling functions  $\tilde{\phi}$  and wavelets  $\tilde{\psi}$  based on different lengths L: (a) length-2; (b) length-5; (c) length-9; (d) length-13; (e) length-4; (f) length-8; (g) length-16, (h) length-20

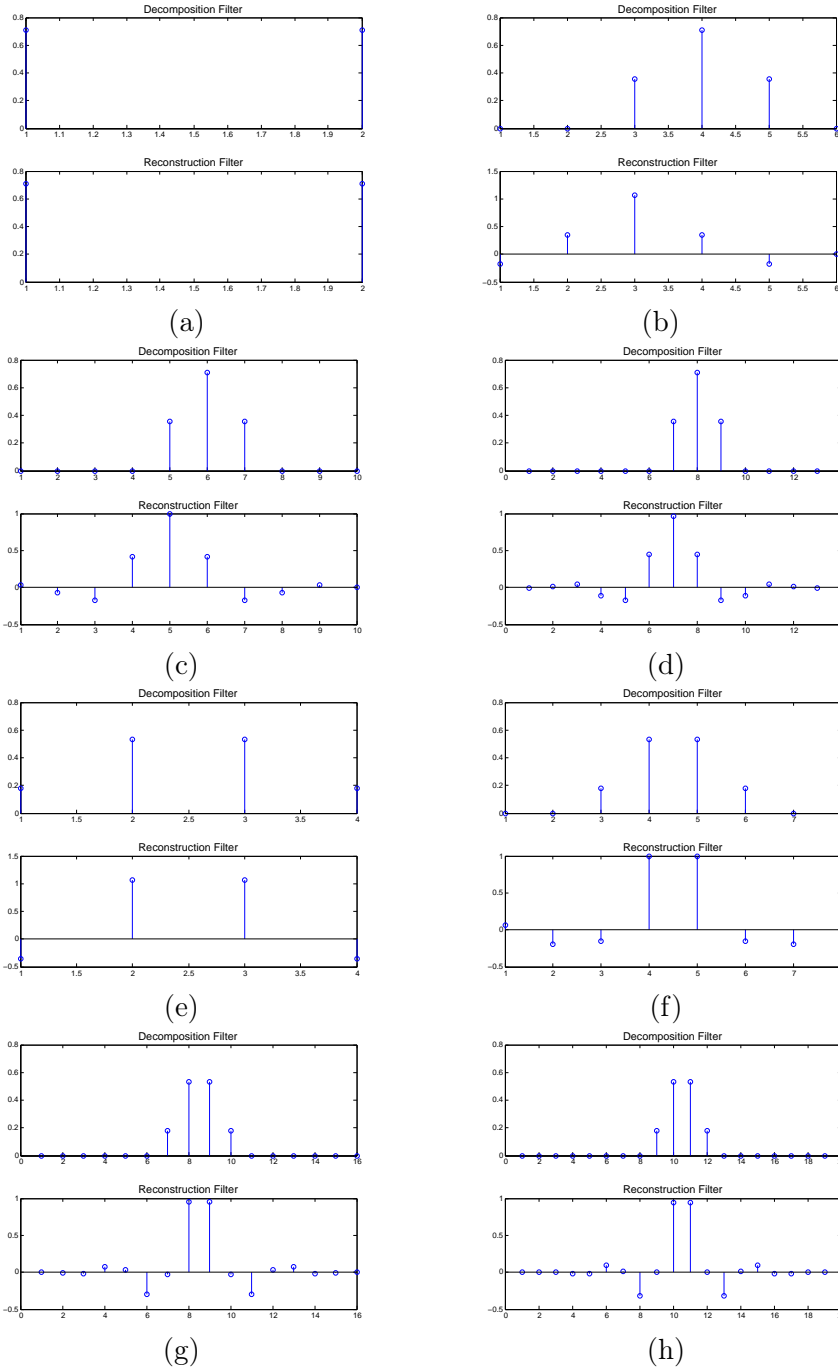


Figure 39: Different lengths decomposition and reconstruction filters: (a)  $2 \times 2$ ; (b)  $3 \times 5$ ; (c)  $3 \times 9$ ; (d)  $3 \times 13$ ; (e)  $4 \times 4$ ; (f)  $4 \times 8$ ; (g)  $4 \times 16$ ; (h)  $4 \times 20$  where  $M \times N$  denotes length- $M$  decomposition filter and length- $N$  reconstruction filter

## 5.2 MULTIREOLUTION ANALYSIS WITH THE SLEPIAN SCALING FUNCTIONS

A multi-resolution structure provides successive approximations that enable us to extract only the relevant details for a particular task. Signals can be expanded on different resolution spaces, where higher resolutions yield more details and low resolution spaces provide coarser approximation. Especially in the processing of sparse signals this feature can be very useful as it may yield efficient representations and compression.  $\pi$ -bandlimited biorthogonal Slepian scalings and wavelets suggested in section 5.1 satisfy all the required properties for multi-resolution analysis (MRA) [17, 29]. These bases are linearly independent, unconditional and not necessarily orthogonal. They are dense in band limited function space  $S_\pi$ , which means that any signal in this space can be approximated finely. The lack of orthogonality is not a problem by itself as long as the basis remains stable. We are interested in MRA spaces that can be formed by the first Slepian function  $\varphi_{0,\pi,\tau}(t)$ , which has the maximum energy concentration on a given interval  $[-\tau, \tau]$  and with frequency concentration,  $[-\pi, \pi]$ , as illustrated by Fig. 40.

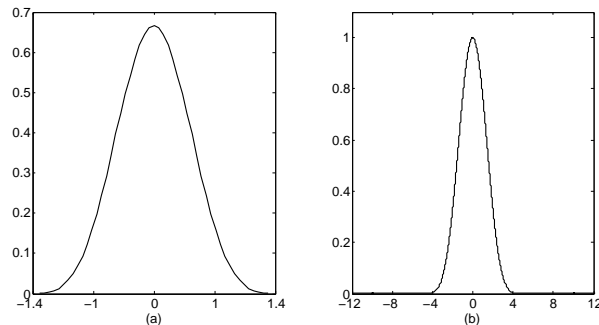


Figure 40: (a) First Slepian function  $\phi(t) = \varphi_{0,\pi,\tau}(t)$  and, (b) its Fourier transform  $\hat{\theta}(\omega)$

It is interesting to notice in Fig. 40 that both  $\phi(t) = \varphi_{0,\pi,\tau}(t)$  and its Fourier transform  $\hat{\phi}(\omega) = \hat{\varphi}_{0,\pi,\tau}(\omega)$  are Slepian functions, so we may use either to obtain Riesz basis of  $V_j$ . This feature of Slepian functions makes them appealing in both domains.

We consider the biorthogonal wavelet bases and illustrate MRA with them. It has been shown by Walter and Shen [15] that Slepian functions are a Riesz basis of the Paley-Wiener space hence they constitute stable basis in approximating band limited functions. This means there exists  $A > 0$  and  $B$  such that any function  $x(t) \in V_0$  can be uniquely and stably decomposed into

$$x(t) = \sum_{n=-\infty}^{\infty} c[n]\theta(t-n) \text{ with}$$

$$A\|x\|^2 \leq \sum_{k=-\infty}^{\infty} \|c[k]\|^2 \leq B\|x\|^2$$

with the same bounds  $A$  and  $B$  at all scales  $2^j$ . The energy equivalence ensure the expansion over  $\{\theta(t-n)\}_{n \in \mathbb{Z}}$  to be numerically stable. And multi-resolution yields, if  $\theta(t-n)$  is a Riesz basis of  $V_0 \Rightarrow \sqrt{2^j} \theta(2^j t - n)$  is a Riesz basis of  $V_j$ .

Before discussing the multi resolution features of this biorthogonal basis, we briefly mention how can we find an orthonormal bases based on Slepian functions. If we could find an orthonormal basis  $\theta(t)$  of  $V_j$ , we could obtain a discrete approximation of  $x$  at any scale  $2^j$  is defined by an orthogonal projection  $A_j x$  on  $V_j$ ,

$$A_j x = \sum_{n=-\infty}^{\infty} \langle x, \theta_{j,n} \rangle \theta_{j,n} \tag{5.9}$$

with  $\theta_{j,n}(t) = \sqrt{2^j} \theta(2^j t - n)$ . Here the inner product gives the coarse approximation coefficients  $a_j[n] = \langle f, \theta_{j,n} \rangle$ . Now we show how can we orthogonalize the Slepian Riesz basis  $\{\theta(t-n)\}_{n \in \mathbb{Z}}$ . While the Slepian scaling function and its integer translates form a non-orthogonal basis (except for  $N = 2$ ), we can apply an orthogonalization procedure [8]. Assume  $\theta \in V_0$  is an orthonormal basis, hence can be expanded using our unconditional basis of  $V_0$  as,

$$\theta(t) = \sum_{n=-\infty}^{\infty} c(n)\phi(t-n).$$

The expansion in the frequency domain  $\hat{\theta}(\omega) = \hat{c}(\omega)\hat{\phi}(\omega)$ , where  $\hat{c}(\omega)$  is a  $2\pi$  periodic Fourier series of finite energy as  $\phi(t-n)$  is a stable basis. Now suppose,

$$s(t) = \sum_{m=-\infty}^{\infty} \theta(m)\theta(t-m).$$

Then  $\{\theta(t-n)\}_{n \in \mathbb{Z}}$  is orthonormal if and only if  $s(n) = s(t)|_{t=n} = \delta(n)$ . If we take the Fourier transform of this equality yields,

$$\sum_{k=-\infty}^{\infty} |\hat{\theta}(\omega + 2\pi k)|^2 = 1 \quad (5.10)$$

Eq. 5.10 can be satisfied if we choose  $\hat{c}(\omega)$  as,

$$\hat{c}(\omega) = \frac{1}{\left(\sum_{k=-\infty}^{\infty} |\hat{\phi}(\omega + 2\pi k)|^2\right)^{1/2}}.$$

Hence we can obtain an orthonormal basis  $\phi$  from a Slepian Riesz basis  $\theta$  as follows,

$$\hat{\theta}(\omega) = \frac{\hat{\phi}(\omega)}{\left(\sum_{k=-\infty}^{\infty} |\hat{\phi}(\omega + 2\pi k)|^2\right)^{1/2}} \quad (5.11)$$

Note that if  $\phi$  were orthonormal to its integer translates,  $\sum_{k=-\infty}^{\infty} \hat{\phi}(\omega - 2\pi k) = 1$  holds and  $\theta(t) = \phi(t)$ . Since  $\sum_{k=-\infty}^{\infty} \hat{\phi}(\omega - 2\pi k)$  is the periodic extension of  $\hat{\phi}(\omega)$  that is positive on  $[-\pi, \pi]$ ,  $\hat{\theta}(\omega)$  is also  $\pi$ -bandlimited and is a Riesz basis of  $V_0$ .

We are interested in MRA spaces that can be formed by the first Slepian function and its biorthogonal pair. This MRA eventually lead us to obtain biorthogonal filters to realize Slepian wavelet expansion. Our constructions, given in Section 5.1, are based on discrete-time filter banks. Expansion of signals in terms of wavelets and perfect reconstruction filter banks are proven to be equivalent forms in signal representation, see Section 2.4. We have adapted the later one where it yields implementable systems.

For simplicity, we first explain MRA based on an orthonormal basis  $\theta$  of band limited functions obtained in Eq.5.11. Then, we arrived at the biorthogonal case. Using a scaling function, wavelet and their dilated versions, we can obtain successive approximations at different scales, as depicted in Fig. 41 [8]. By using  $\theta$ 's scaled version we can build the Riesz basis for different resolutions  $V_j$  and obtain successive approximations as in Eq. 5.9. The

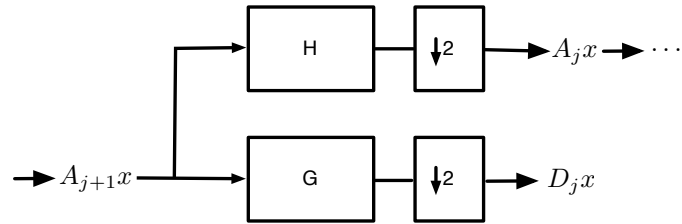


Figure 41: Decomposition of a discrete approximation  $A_{j+1}x$  into an approximation at a coarser resolution and detail  $D_jx$

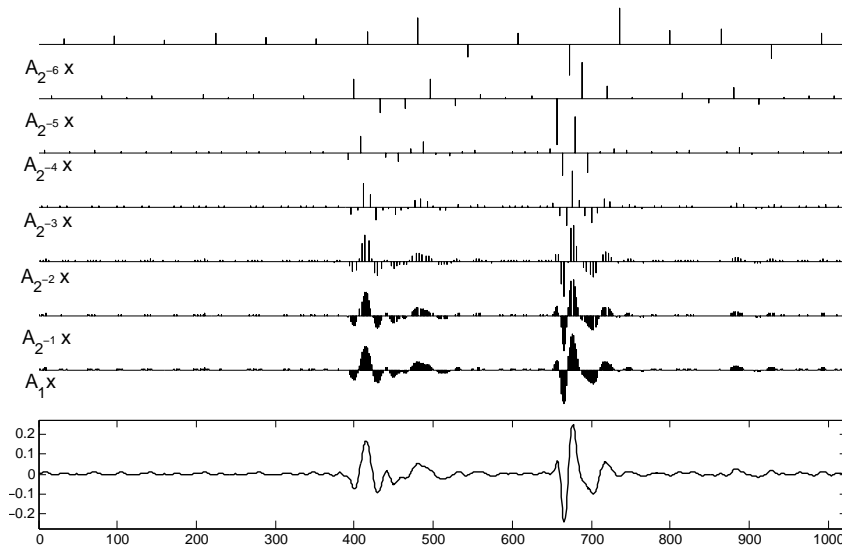
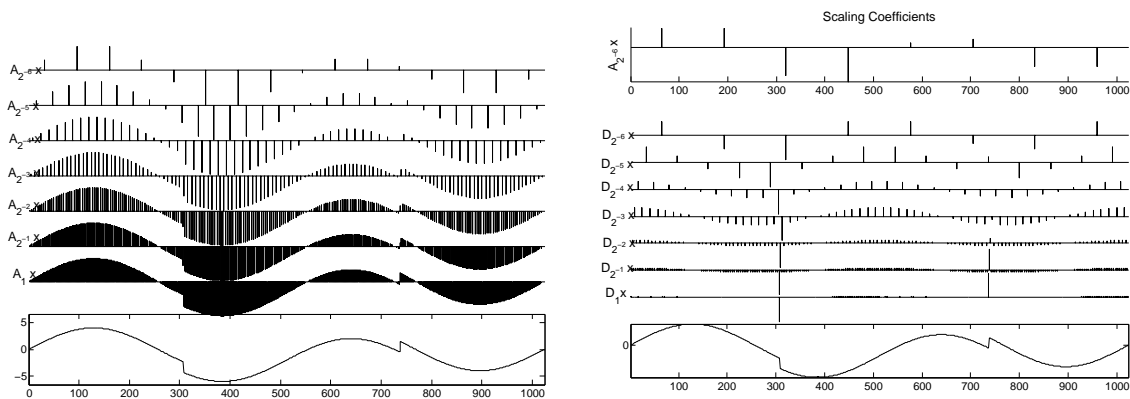


Figure 42: Coarse approximations  $a_j[n]$  at resolutions  $1, 1/2, 1/4, 1/8, 1/16$  and  $1/32$  of the signal shown at the bottom

illustration of coarse approximations of a smooth signal using orthogonal scaling function is shown in Fig. 42. The energy of  $\theta$  is concentrated on  $[-\pi, \pi]$ , so as  $\theta(2^j t)$ 's will be on  $[-\pi/2, \pi/2]$  for  $j < 0$ . Therefore approximation  $a_j[n]$  is a low-pass filtering of  $x$  sampled at intervals  $2^{-j}$ . Fig. 42 depicts a multi resolution approximation at scales  $2^j$ ,  $-6 \leq j \leq 0$ . The reason we choose negative values of  $j$  is, in practice the measuring devices gives only a finite number of samples  $N$ , and each discrete signal  $A_{V_j}x$  ( $j < 0$ ) has  $2^j N$  samples.



(a) Projection on coarse spaces  $V_j$

(b) Projection on detail spaces  $W_j$

Figure 43: Multi-resolution discrete approximations of an discontinuous signal: (a) Coarse approximations  $A_j x$  with different resolution scaling function, (b) Detail approximation with wavelets. The top gives the coarse approximation at resolution  $1/32$

We have also shown these approximations on an irregular signal in Fig. 43a. Although a multi resolution approximation can entirely be performed using the scaling function  $\theta_{j,n}(t)$ , as in Fig. 43a, there is still information between the spaces  $V_{j-1}$  and  $V_j$  that may not be captured by  $\theta_{j,n}(t)$  due to its low-pass behavior. Although captured, may require higher resolution. In our simulation Fig. 43a, it is around resolution  $1/8$  that we can notice the discontinuity. Here we need to find another basis that will pick up the oscillation where

the scaling functions provides the averages. This basis is called the wavelet. They will help to carry the details that are needed to increase the resolution of approximation. Also the efficiency of the basis can be judged by their ability to approximate with few non-zero coefficients. In applications such as compression, coding, and noise removal this aspect becomes important. The uncaptured information lays in the space between  $V_j$  and  $V_{j+1}$ . If

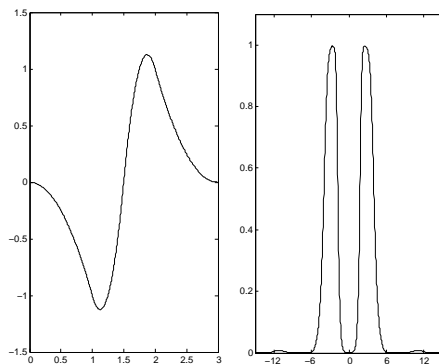


Figure 44: Wavelet function  $\psi(t)$  and, Right: its Fourier transform  $\hat{\psi}(\omega)$

we can form a space  $W_j$  that will complement  $V_j$  in  $V_{j+1}$ , we could capture the information inbetween. A wise way to define this space is for it to be perpendicular to  $V_j$  so that there is no redundancy. And the basis of these complementary space are called *wavelets*, see in Fig. 44. The wavelet  $\psi(t)$  corresponding to a scaling function  $\theta(t)$  and its translates spans the space  $W$  thus,

$$A_{j+1}x = A_jx + D_jx$$

The orthogonal projection onto the wavelet space  $W_j$  now can be calculated as in Eq.5.9,

$$D_j = \sum_{n=-\infty}^{\infty} \langle x, \psi_{j,n} \rangle \psi_{j,n} \tag{5.12}$$

$$d_j[n] = \langle x, \psi_{j,n} \rangle \tag{5.13}$$

Both in Eq.5.9 and Eq.5.12 the approximation coefficients in Eq.5.9 can be found using convolution:

$$d_j[n] = \langle x, \psi_{j,n} \rangle = \int_{-\infty}^{\infty} x \psi(2^j t - n) dt \quad (5.14)$$

In Fig. 43(b) wavelet coefficients  $d_j[n]$  at scales  $2^j$  and the remaining coarse approximation  $a_j[n]$  is plotted.

->  $V_j$  : all combinations of scaling at that scale  $\phi(2^j t - k)$

->  $W_j$  : all combinations of wavelets  $\psi(2^j t - k)$

->  $V_{j+1} = V_j + W_j$  recursively  $V_{j+1} = V_0 + \sum_{i=0}^j W_i$ .

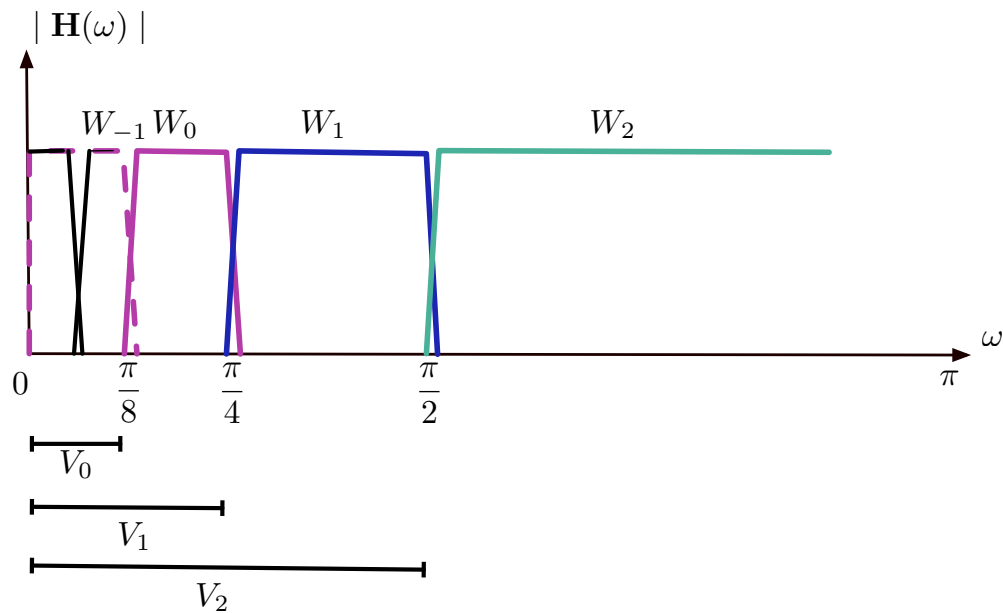


Figure 45: Frequency splitting in a  $j = 2$  scale approximation

We see from Fig. 44 that  $\hat{\psi}(\omega)$  is concentrated on  $[-2\pi, -\pi] \cup [\pi, 2\pi]$  so it captures the gap in the frequency left by scaling. As  $\psi(t)$  has a high pass characteristic, Eq.5.14 can be regarded as high-pass filtering of the signal. There are many ways to choose basis  $\psi(t)$  that is orthogonal to  $\phi(t)$ . One of the criteria is informally implied above as well, we expect wavelets to pick up oscillations, so they should have zero-average. Then, we can construct an orthonormal basis of  $W_j$  by dilating and shifting it. Note also that the Slepian scaling

function that has time support  $[-1, 1]$  generates a direct orthogonal basis, yet we have shown it is equivalent to the Haar basis, see Fig. 37(a).

Using scaled wavelets and scaling function a given signal can be represented by a coarse approximation and added details,

$$\begin{aligned}
A_J x &= A_{J-1} x + D_{J-1} x \\
&= A_{J-2} x + D_{J-2} + D_{J-1} x \\
&\vdots \\
&= A_0 x + \sum_{j=0}^J W_j x = \sum_{j=-\infty}^{\infty} W_j
\end{aligned}$$

Applying successive approximations recursively the space of any given band limited signal  $S_\pi$  can be spanned by spaces of successive details at all resolutions, i.e.  $S_\pi = \sum_{j \in \mathbb{Z}} W_j$ . An example of decomposition of  $V_2$  into successive octave bands,  $V_2 = \sum_{j=-\infty}^{j=2} W_j$ , is shown in Fig. 45. Dual (non-orthogonal) Slepian bases generate two different approximation spaces,  $V_j$  and  $\tilde{V}_j$ , which are associated with the scaling basis  $\phi(t-n)_{n \in \mathbb{Z}}$  and  $\tilde{\phi}(t-n)_{n \in \mathbb{Z}}$  respectively. The scaling function itself and its integer translates span a space  $V_0$ , i.e.  $\{\phi(t-n) = \varphi_{0,\pi,\tau}(t-n)\}_{n \in \mathbb{Z}}$  is an unconditional basis for  $V_0$ . A Riesz basis  $\phi_j(t)$  of  $V_j$  can be transformed into a Riesz basis of  $V_{j+1}$  by scaling. By dilation of  $\phi(t)$  with a coefficient  $2^j$  and translation we can successively build Riesz bases for different resolution spaces,  $V_j$ . Since  $\phi(t)$  has a low-pass character, the projection to resolution spaces  $V_j$  can be interpreted as low pass filtering followed by a uniform sampling at the rate  $2^j$ . Approximation on the coarse space  $V_j$  can be expressed by a projection operator  $A_j$  as follows,

$$A_j x = \sum_{n=-\infty}^{\infty} \langle x, \phi_{j,n} \rangle \tilde{\phi}_{j,n} = \sum_{n=-\infty}^{\infty} \langle x, \tilde{\phi}_{j,n} \rangle \phi_{j,n}$$

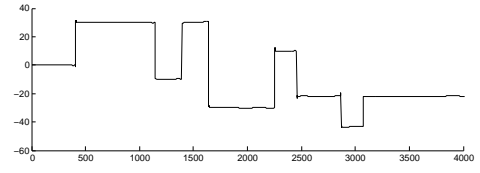
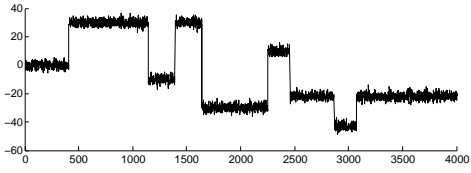
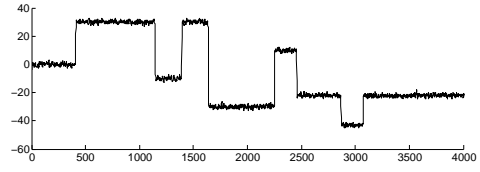
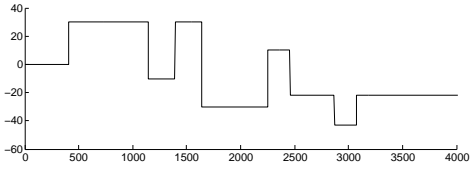
where  $\phi_{j,n} = \sqrt{2^j} \phi(2^j t - n)$ . Complement spaces, aka wavelet spaces, are defined perpendicular to those coarse spaces as  $\tilde{W}_j \perp V_j$  and  $W_j \perp \tilde{V}_j$  to capture the information between the nested spaces of  $V_j$  and  $\tilde{V}_j$ , e.g  $V_{j-1} \subset V_j$ . Approximation on the detail space  $W_j$  can be expressed by a projection operator  $D_j$  as follows,

$$D_j x = \sum_{n=-\infty}^{\infty} \langle x, \psi_{j,n} \rangle \tilde{\psi}_{j,n} = \sum_{n=-\infty}^{\infty} \langle x, \tilde{\psi}_{j,n} \rangle \psi_{j,n}$$

where  $\psi_{j,n} = \sqrt{2^j}\psi(2^j t - n)$ . In order for the wavelet to be able to pick up the oscillations, it should have zero average. All the opposed wavelets do so, see Fig. 37.

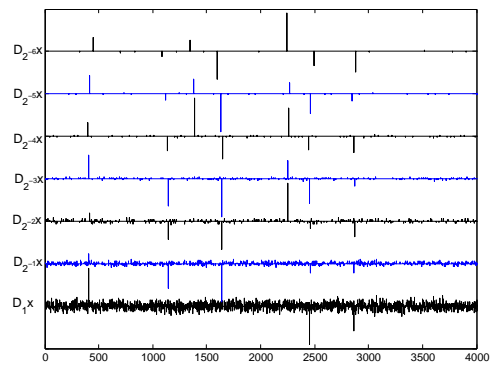
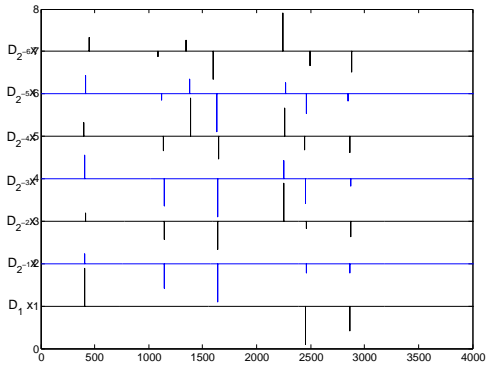
In the following we demonstrate and evaluate the performance of Slepian wavelets with different examples.

- Example 1: Wavelets give a representation that can discriminate the signal from the noise by concentrating the signal energy over a few coefficients. It is possible to outperform Wiener Filtering which is optimal in the presence of non-Gaussian noise. We can obtain smoothing by thresholding wavelet coefficients in Fig. 46d [73]. We have performed the simulation using a length-2 Slepian biorthogonal scaling function. The signal and Wiener Filtering algorithm is obtained using Wavelab Version 850 software [74].
- Example 2: We can improve the approximation under noise by choosing the basis depending on the signal behavior. Wavelet bases can pick up the local irregularities very fast in a globally smooth signal, as shown in the following Fig. 47. Enhancement of a signal by thresholding wavelet coefficients may lead to approximations as good as the ones incorporating prior knowledge. Fourier denosing gets rid of high frequencies, yielding a smoother signal, but is that the exact signal? We might have throw away part of the signal and kept the noise. We can't help it if we don't know what that noise is, and in this case Wiener filtering gives the best answer if we assume time-invariance. How would we use wavelets to enhance signals? We take the wavelet transform to look at the coefficients. We would like to keep the projection onto  $V_0$  which is the space spanned by the scaling function. We kept that as a smooth average part, as most of the signal is there for regular signals. The irregular sections will start to show up in finer scales, and we can completely ignore them or threshold them to get nicer results as in Fig. 48. Wavelet coefficient decay fast for regular functions if the wavelet has a compact support and sufficient vanishing moments [75].
- Example 3: Similar to previous example, we can use the scale aspect of the wavelets to completely separate out the noise Fig. 49.



(a)

(b)



(c)

(d)

Figure 46: (a) Top: Piecewise constant function, Bottom: Gaussian White noise added ( $SNR = 21.8dB$ ); (b) Top: Wiener Filter estimation ( $SNR = 26.6dB$ ), Bottom: Estimation reconstructed from thresholded wavelet coefficients of Slepian length-2 wavelet ( $SNR = 38.9dB$ ); (c) Slepian wavelet transform of the clean signal: (d) Slepian wavelet transform of noisy signal

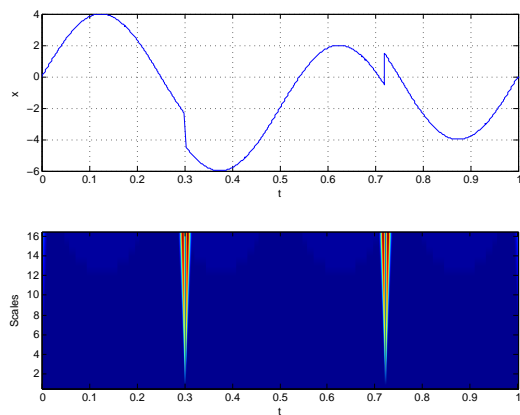


Figure 47: Slepian wavelet transform of a smooth signal with short live irregularities

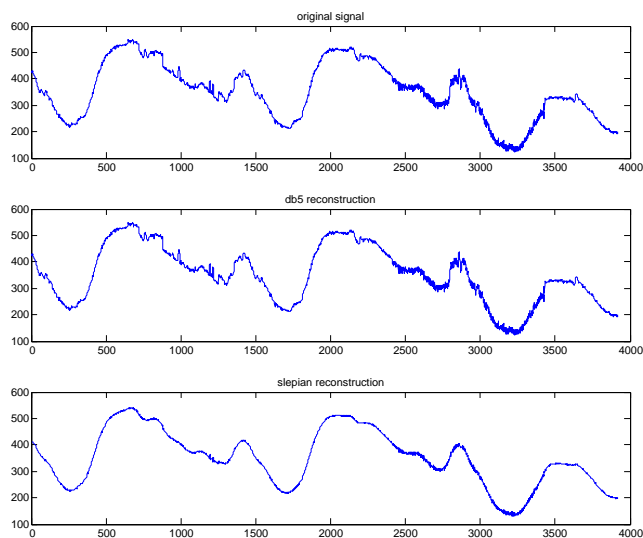


Figure 48: Wavelet Enhancement:(a) Noisy signal, (b)Reconstruction with Daubechies length-5 wavelets, (c) Reconstruction with Slepian length-5wavelets

- Example 4: We illustrate the ability of Slepian wavelets to efficiently approximate piecewise smooth signal, Fig. 50. This piecewise smooth signal is generated using Wavelab [74] which is a library of Matlab routines for wavelet analysis. Smooth signals can be ap-

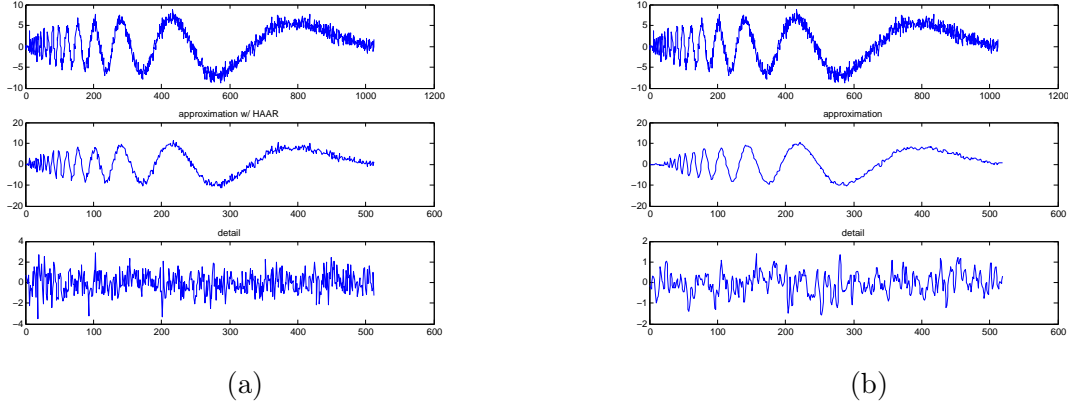


Figure 49: Wavelet denoising (a) with Haar wavelet, Top: Noisy chirp signal, Middle: Coarse approximation, Bottom: Details; (b) with Slepian wavelet Top: Noisy chirp signal, Middle: Coarse approximation, Bottom: Details

proximated as a partial sum of low frequency sinusoidal waves. Fourier approximation is obtained by projection, using the orthonormal basis of  $L^2[0, N]$ ,  $\{\frac{1}{\sqrt{N}}e^{j\frac{2\pi kt}{N}}\}_{k \in \mathbb{Z}}$ . In this approximation important errors occur in the neighborhood of the singularities, Gibbs phenomenon, see in Fig. 50b. As it would be expected from an infinite support basis, the error in this approximation will decrease as the number of the basis increase, i.e.  $K$ . Also for smoother  $x(t)$  decay of the approximation error is faster. But the Gibbs ringing remains. We observed that long length Slepian wavelet (length-20) exhibits similar behavior around singularity regions Fig. 50c. This can be managed by refining the scale or changing the support of the wavelet. While shortest length Slepian wavelet (length-2), Fig. 50d gave better approximation of uniformly smooth signal, changing the length to 7 resulted in more precise approximation Fig. 50e.

- Comment: Using the irregular sampling grid obtained by wavelets we can outperform these results in general class of signals. These results suggest that we may also obtain non-

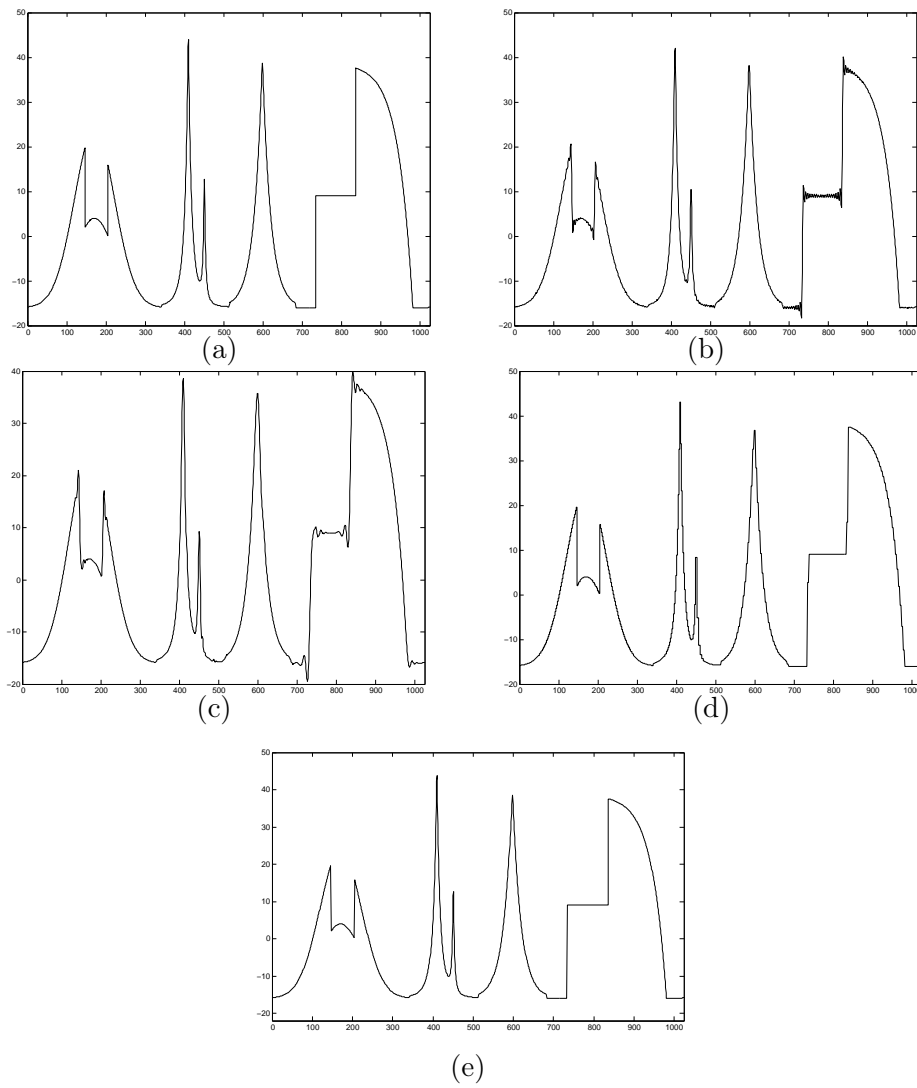


Figure 50: Piecewise regular signal representation: (a) original signal; (b) Fourier basis approximation (notice the Gibbs ringing at the discontinuities in the original signal); (c)  $Length - 20$  Slepian wavelet (Gibb's ringing still present); (d)  $Length - 2$  Slepian wavelet (there is smoothing at the discontinuities); (e)  $Length - 7$  Slepian wavelet

linear approximations by projecting signals over  $M$  vectors chosen adaptively within the basis and extend the basis dictionary. If we know the singularities and break points of the signal of the signal we can form better approximations, using non-linear approximation with different size slepian wavelets. Let  $\psi_k(t) = \psi(N_k, \Omega_k)$  then the expansion of  $x(t)$  using  $K$  low frequency sinusoidal waves is,

$$\hat{x}(t) = \frac{1}{N} \sum_{|k| < K/2} \langle x, \psi_k \rangle \psi_k$$

Since the Slepian functions provide high-energy concentration, they are promising candidates for wavelet basis where the efficiency of the transform is directly related to the time-bandwidth localization of the basis. Here the efficiency means that the sparsity in the transform domain. It increases as we use well-localized functions, hence the transform results in reduced redundancy and high compression.

### 5.3 INCORPORATING SLEPIAN WAVELETS INTO ASYNCHRONOUS DECOMPOSERS

In this section, we will show how to reconstruct signals from non-uniform samples using Slepian wavelets, and relate the coefficients in different scales to derive a multi resolution analysis. Non-uniform samples have appeared at the output of the asynchronous decomposer and we have shown that as long as the average rate of samples is equal to Nyquist rate, reconstruction is possible with Slepian functions and its modulated versions as bases. In order to have stable solutions to this oftenly ill-posed problem, we have adapted regularization techniques before. Differently in here, we incorporate Slepian wavelets into the synthesis part to reconstruct the time-sparse signal signal from non-uniform samples. The implementation is performed with the perfect reconstruction Slepian biorthogonal filters we have introduced in the previous section.

We have shown that modulated Slepian functions enables time-frequency (TF) tiling as illustrated by Fig. 51. In order to efficiently approximate other types of signals, such as the ones that have oscillatory behavior, different types of bases can be constructed. The efficiency of representation depends on the ability of the basis concentrates the signal energy over a few coefficients. In addition to effectiveness, the speed and computation cost of approximation is a matter of interest where we aim our algorithms to be used in real-time, low-powered sensors (bio-or enviromental).

As the TF behavior of the non-stationary signals changes we would like to design to have adaptive TF properties. Wavelet bases are particularly efficient in representing piecewise smooth functions, as it can be observed in the illustration Fig. 45 that the frequency resolution increases. Higher resolution in frequency is achieved by dilations. This is a result of the flow in wavelet transform filters, see Fig. 36, they iterate on the low-frequency output. We wanted to exploit this behavior. As mentioned earlier, using more localized Slepian bases as in the modulated ones, or using redundant time-frequency dictionaries, accuracy can be increased. However, we want to capture the variations of the signal without increasing computational complexity. Our decomposition schemes, analysis part of Fig.29, already captures the time content of the signal with asynchronous signal dependent algorithms. We can see

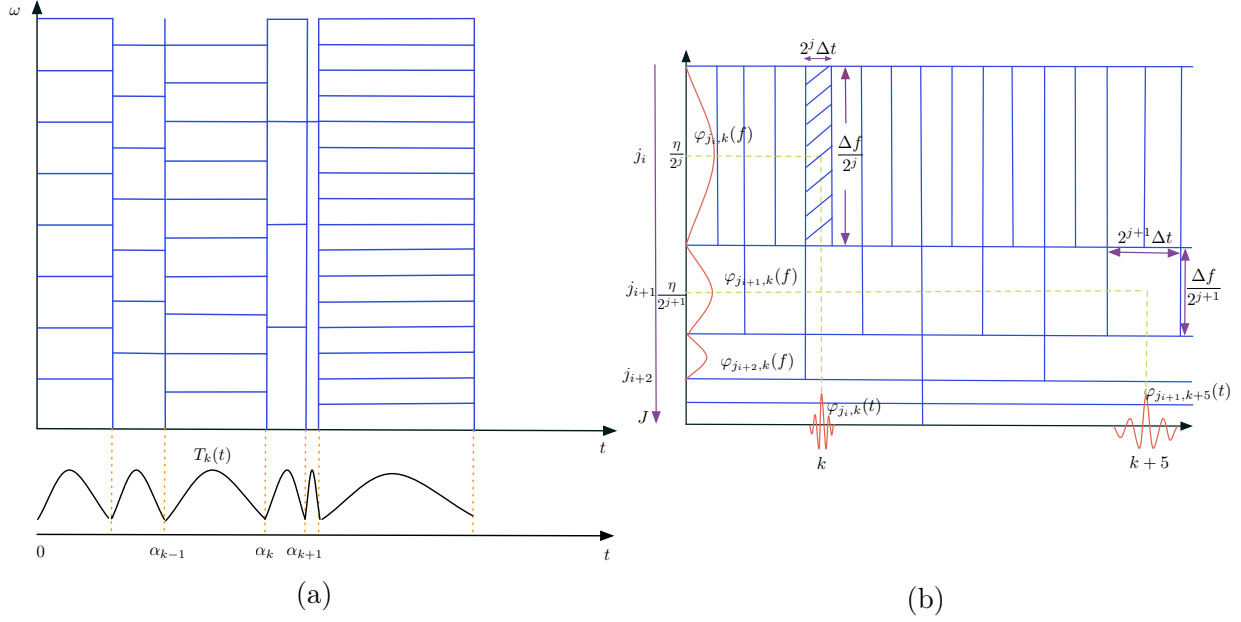
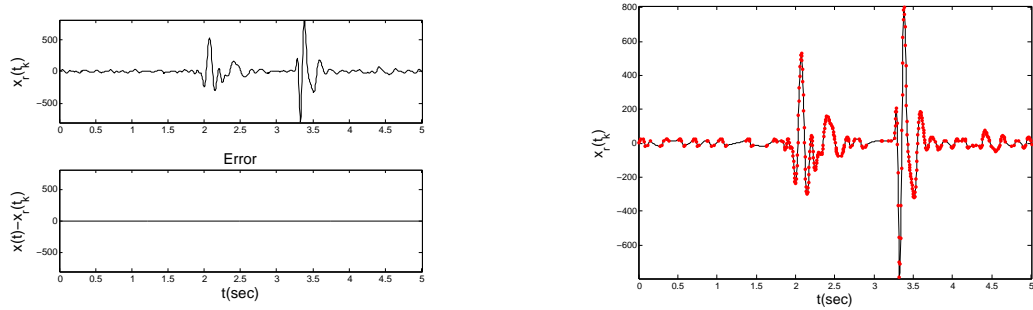


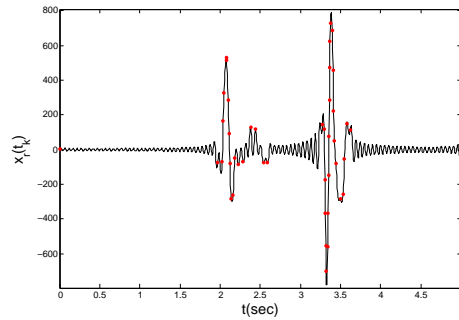
Figure 51: Heisenberg rectangles that indicate where the energy of the basis is mostly concentrated (a) A local Slepian basis divides the time axis with smooth windows where modulation translates these windows in frequency: (b) Wavelet basis divides the frequency into octave bandwidths

from Fig. 53b that samples are drawn where the signal activity is high. Moreover, parallel filter banks provides frequency localization. Under given circumstances Slepian wavelets have proven to be efficient in piecewise smooth signal can perform very well without even needing many scales as we shown in the following simulation on heart sounds. First, as a verification of perfect reconstruction we simulate biorthogonal Slepian filter banks using uniform samples, see Fig.52a. Indeed, any length Slepian filter we suggested in Fig. 39 provides perfect reconstruction. Rather than uniformly, if we collect non-uniform samples satisfying Nyquist criteria, in Fig.52b we obtain  $SNR = 24.3dB$  performance. When we decrease the sample size drastically, such as 14% as in Fig.52c we could obtain  $9.9dB$  performance.



(a) Perfect Reconstruction with uniform samples; top: original signal, bottom: reconstruction error

(b) Reconstruction from non-uniform samples drawn at a rate equivalent to Nyquist rate  $SNR = 24.3dB$



(c) 14% of samples give  $SNR = 9.9dB$

Figure 52: Biorthogonal Slepian wavelet basis performance on sparse signal

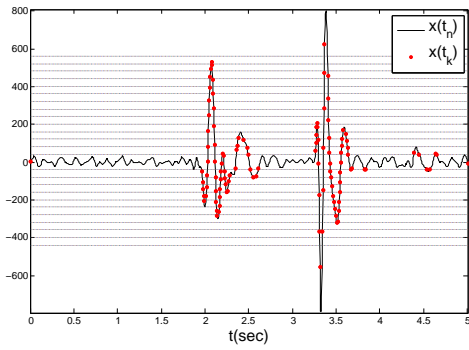
In the following two simulations we examine the behavior of short-length and long-length biorthogonal filter implementations in the recovery of sparse signals from non-uniform samples. In particular we look at length-2 and length-20 filters. In Fig. 53c we observe the

Gibbs phenomenon on the edge of sharp changes when we use longer Slepian wavelets. Reconstruction in the high density sample regions is almost perfect as expected. To the contrary in Fig. 53d short wavelets outperform in high-frequency regions, though they perform poorly on the regions where sample density is low. This is mitigated if we have more samples in this silent region where overall sample size is lower by 42%, see in Fig. 54d. Although overshooting is still present in the simulation Fig. 54b, interpolation performance is acceptable for very low, 21%, sample density. Based on the presented results, we can state that Slepian wavelet based reconstruction is suitable for sparse signals from non-uniform samples. Particularly accurate results have been obtained when we use localized reconstruction in each branch. We expect that further improvements can be achieved by changing the wavelet length.

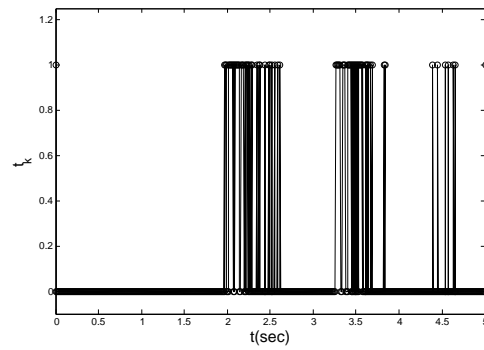
## 5.4 CONCLUSIONS

- The motivation for working with Slepian functions is that they are compactly supported in both frequency and time domains. They are smooth, well behaved functions in the region of concentration and hence Slepian wavelet approximations construct smooth approximations with fast asymptotic decay.
- $\pi$ -bandlimited Slepian wavelet representation satisfies all the required properties of MRA analysis, such as the fact that Slepian MRA analysis is dense in  $\pi$ -bandlimited signal space, i.e. we can approximate any  $\pi$ -bandlimited functions as closely as we want.
- We observed that some well-known wavelets can be obtained with Slepian wavelets. For instance, when  $N = 2$  it is a piecewise constant multi resolution approximation and when  $N = 4$  it is cubic box spline. Also the conventional Shannon wavelets can be easily modified to obtain Slepian wavelet representation of analog signals as they are related,
- Slepian wavelets have finite support and are implementable with FIR filters.
- The proposed biorthogonal filters have linear phase which makes them favorable in applications where data do not allow phase distortion such as in image processing.

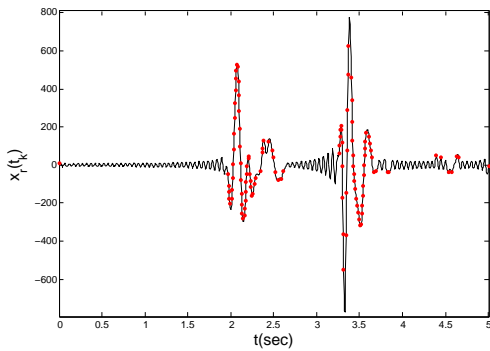
- We have shown that Slepian wavelet techniques are applicable on non-uniformly spaced data. Biorthogonal Slepian wavelet reconstruction is suitable for proposed asynchronous decomposition scheme. As an example, we obtained accurate reconstruction of heart sounds from sparse samples.



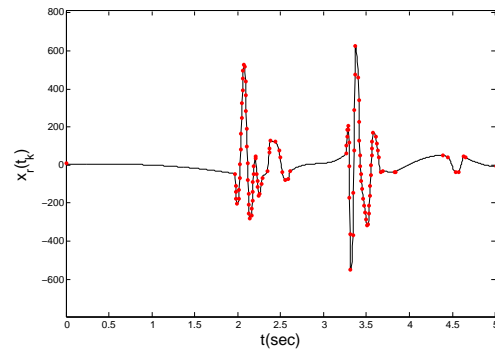
(a)



(b)

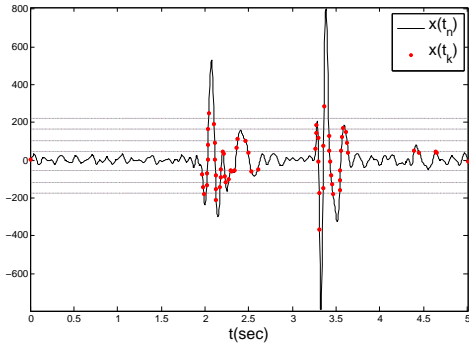


(c)

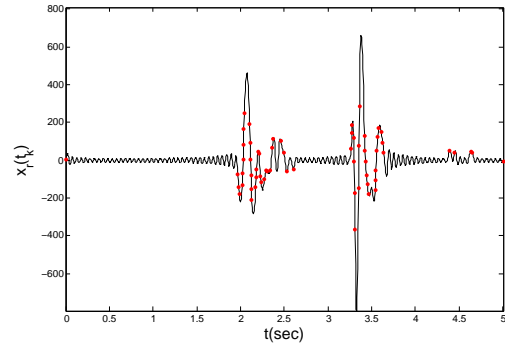


(d)

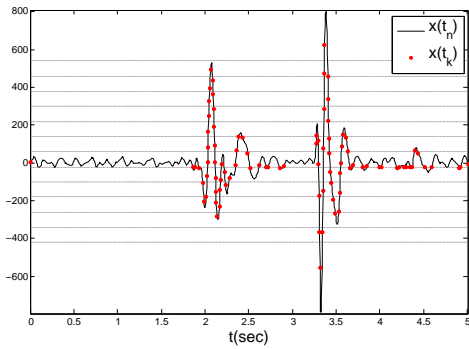
Figure 53: A sparse data: (a) the original signal with samples, 38% samples; (b) Sample positions; (c) Interpolation with long-length Slepian wavelets,  $SNR = 14.2dB$  ( $N = 17$ ,  $W = \pi$  rad/sec); (d) Interpolation with short-length Slepian wavelets,  $SNR = 11.6dB$  ( $N = 4$ ,  $W = \pi$  rad/sec)



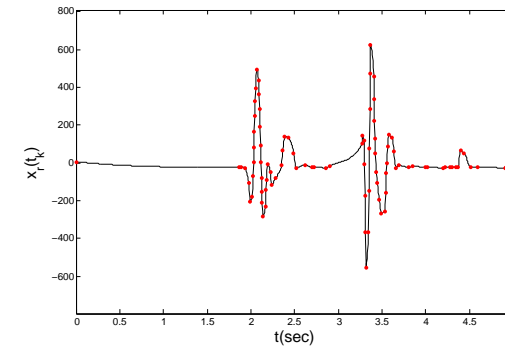
(a)



(b)



(c)



(d)

Figure 54: A sparse data: (a) the original signal with samples, 21% samples; (b) Interpolation of samples in (a) with long-length Slepian wavelets,  $SNR = 11.4dB$  ( $N = 17$ ,  $W = \pi$  rad/sec); (c) the original signal with samples, 42% samples; (d) Interpolation of samples in (c) with short-length Slepian wavelets  $SNR = 11.6dB$  ( $N = 4$ ,  $W = \pi$  rad/sec)

## 6.0 FUTURE WORK

- On the promise of our results on Slepian wavelets we would like to look further in application areas, especially image processing, where linear phase and smoothness are important.
- We have studied the  $\pi$ -bandlimited signal case for Slepian wavelets. We would like to extend the expansion to a more general class of signals.
- Perform the implementation of the proposed asynchronous decomposers in real time.

One does, often, not know *a priori* which scale the relevant information is located in. One common aspect of biomedical signals is that the information of interest is often a combination of features that are well localized temporarily or spatially (e.g spikes and transients in EEG) and others that are more diffuse (small oscillations, bursts). This requires the use of analysis methods sufficiently versatile to handle events that can be at opposite extremes in terms of their time frequency localizations. The overall goal is how can we find an accurate representation for sparse signals and that can be computed fast. Our scheme automatically adapts to different components of a signal, enabling it to look at brief, high frequency components as well as long-lived low frequency components. The resulting waveforms in each branch tell which components of the analyzing function will be dominant in order to best reconstruct the signal. One can literally reconstruct the signal adding up the dominant components at different scales. Based on the presented results, we can state with high confidence that asynchronous processing of sparse information results in signal-dependent effective representation of sparse information, and scaled Slepian bases are suitable in the reconstruction and analysis steps.

## BIBLIOGRAPHY

- [1] M. Kurchuk and Y. Tsvividis, “Signal-dependent variable-resolution clockless A/D conversion with application to continuous-time digital signal processing,” *IEEE Trans. Circuits and Syst. I: Regular Papers*, vol. 57, pp. 982–991, May 2010.
- [2] Y. Tsvividis, “Event-driven data acquisition and digital signal processing: a tutorial,” *IEEE Transactions on Circuits and Systems II: Express Briefs*, vol. 57, no. 8, pp. 577–581, 2010.
- [3] K. Guan, S. Kozat, and A. Singer, “Adaptive reference levels on a level-crossing analog-to-digital converter,” *EURASIP J. Advances in Signal Proc.*, pp. 1–11, doi:10.1155/2008/513706, January 2008.
- [4] Y. Tsvividis, “Digital signal processing in continuous time: a possibility for avoiding aliasing and reducing quantization error,” *IEEE International Conference on Acoustics, Speech, and Signal Processing, 2004. Proceedings. (ICASSP '04).*, vol. 2, pp. ii–589–92, 2004.
- [5] Y. Tsvividis, “Mixed-domain systems and signal processing based on input decomposition,” *IEEE Transactions on Circuits and Systems I: Regular Papers*, vol. 53, no. 10, pp. 2145–2156, 2006.
- [6] A. Lazar and L. Toth, “Time encoding and perfect recovery of bandlimited signals,” *IEEE International Conference on Acoustics, Speech, and Signal Processing, 2003. Proceedings. (ICASSP '03)*, vol. 6, pp. VI–709–12, 2003.
- [7] S. Senay, L. Chaparro, M. Sun, and R. Sciabassi, “Adaptive level-crossing sampling and reconstruction,” in *18th European Signal Proc. Conf. (EUSIPCO)*, August 2010.
- [8] S. Mallat, *A Wavelet Tour of Signal Processing*, Academic Press, Burlington, MA, 2008.
- [9] I. Daubechies, “Orthonormal bases of compactly supported wavelets,” *Communications on Pure and Applied Mathematics*, vol. 41, pp. 909–996, November 1988.
- [10] M. Vetterli and J. Kovačević, *Wavelets and Subband Coding*, Prentice Hall, Signal Processing Series, Englewood Cliffs, NJ, 1995.

- [11] G. Strang and T. Nguyen, *Wavelets and Filter Banks*, Wellesley-Cambridge Press, October 1996.
- [12] C. Burrus, A. Gopinath, and H. Guo, *Introduction to wavelets and wavelet transforms: A Primer.*, Prentice Hall, Upper Saddle River, N.J., August 1998.
- [13] J. Feauveau A. Cohen, I. Daubechies, “Biorthogonal bases of compactly supported wavelets,” *Communications on Pure and Applied Mathematics*, vol. 45, no. 5, pp. 485–560, 1992.
- [14] R. Gao and R. Yan, *Wavelets: Theory and Applications for Manufacturing*, Springer, New York, December 2011.
- [15] X. Shen and G. Walter, “Wavelets based on prolate spheroidal wave functions,” *Journal of Fourier Analysis and Applications*, vol. 10, no. 1, pp. 1–26, 2004.
- [16] S. Mallat, “A theory for multiresolution signal decomposition: the wavelet representation,” *IEEE Transactions on Pattern Analysis and Machine Intelligence*, vol. 11, no. 7, pp. 674–693, 1989.
- [17] S. Mallat, “Multiresolution approximation and wavelet orthonormal bases of  $\ell_2$ ,” *Trans. Amer. Math. Soc.*, vol. 315, no. 1, pp. 69–87, September 1989.
- [18] R. J. Duffin and A. C. Schaeffer, “A class of nonharmonic fourier series,” *Trans. Amer. Math. Soc.*, , no. 72, pp. 341–366, 1952.
- [19] Haar A., “Zur theorie der orthogonalen funktionensysteme,” *Math. Annal.*, vol. 69, pp. 331–371, 1910.
- [20] L. Chaparro, E. Sejdic, A. Can, O. Alkishriwo, S. Şenay, and A. Akan, “Asynchronous representation and processing of nonstationary signals : A time-frequency framework,” *Signal Processing Magazine, IEEE*, vol. 30, no. 6, pp. 42–52, Nov 2013.
- [21] E. Menaka, S.S. Kumar, and M.Bharathi, “Change detection in deforestation using high resolution satellite image with haar wavelet transforms,” in *2013 IEEE International Conference on Green High Performance Computing (ICGHPC)*, March 2013, pp. 1–7.
- [22] A. Can, E. Sejdić, and L. Chaparro, “Asynchronous sampling and reconstruction of sparse signals,” in *Proceedings of the 20th European Signal Processing Conference (EUSIPCO)*, August 2012, pp. 854–858.
- [23] D. Slepian, “Some comments on fourier analysis, uncertainty and modeling,” *SIAM Review*, vol. 3, pp. 379–393, July 1983.
- [24] D. Slepian and H. Pollak, “Prolate spheroidal wave functions, fourier analysis and uncertainty–I,” *Bell Syst. Tech. J.*, vol. 40, no. 1, pp. 43–63, 1961.

- [25] H. Landau and H. Pollak, “Prolate spheroidal wave functions, fourier analysis and uncertainty–II,” *Bell Syst. Tech. J.*, vol. 40, no. 1, pp. 65–84, 1961.
- [26] D. Slepian, “Prolate spheroidal wave functions, fourier analysis and uncertainty–IV: Extensions to many dimensions; generalized prolate spheroidal functions,” *Bell Syst. Tech. J.*, vol. 43, no. 6, pp. 3009–3057, 1964.
- [27] G. Walter, “Prolate spheroidal wavelets: Differentiation, translation, and convolution made easy,” *Journal of Fourier Analysis and Applications*, pp. 73–84, 2005.
- [28] G. Walter and X. Shen, “Recovery of digitized signals using slepian functions,” in *IEEE International Conference on Acoustics, Speech, and Signal Processing (ICASSP)*, April 2003, vol. 6.
- [29] X. Shen, Y. Guo, and G. Walter, “Slepian semi-wavelets and their use in modeling of fading envelop,” in *IEEE Topical Conference on Wireless Communication Technology*, October 2003, pp. 250–252.
- [30] G. Walter and X. Shen, “Sampling with prolate spheroidal wave functions,” *Sampling Theory in Signal and Image Proc.*, vol. 2, pp. 25–52, Jan. 2003.
- [31] G. Walter and X. Shen, “Periodic prolate spheroidal wavelets,” *Numerical Functional Analysis and Optimization*, vol. 26, no. 7-8, pp. 953–976, 2005.
- [32] R. Gopinath and C. Burrus, “Wavelet transforms and filter banks,” in *In Wavelets: A Tutorial in Theory and Applications*, San Diego, CA, 1991, pp. 603–654, Academic Press.
- [33] P. Vaidyanathan, *Multirate Systems and Filter Banks*, Prentice Hall, 1993.
- [34] J. Kovačević and M. Vetterli, “Design of multidimensional nonseparable regular filter banks and wavelets,” in *In Proc. IEEE Int. Conf. Acoust., Speech, and Signal Proc.*, San Francisco, CA, March 1992, pp. 389–392.
- [35] R. Crochiere, S. Webber, and J. Flanagan, “Digital coding of speech in sub-bands,” *Bell Syst. Tech. J.*, vol. 55, no. 8, pp. 1069–1085, October 1976.
- [36] M. Smith and S. Eddins, “Subband coding of images with octave band tree structures,” *In Proc. of the Intl. Conf. on Acous., Speech and Signal Processing*, pp. 1382–1385, 1987.
- [37] M. Smith, *Exact Reconstruction Analysis/Synthesis Systems and Their Application to Frequency Domain Coding*, Ph.D. thesis, Georgia Institute of Technology, 1984.
- [38] M. Smith and T. Barnwell III, “Exact reconstruction for tree-structured subband coders,” *IEEE Trans. Acoust., Speech, and Signal Proc.*, vol. 34, no. 3, pp. 431–441, June 1986.

- [39] F. Mintzer, “Filters for distortion-free two-band multirate filter banks,” *IEEE Trans. Acoust., Speech, and Signal Proc.*, vol. 33, no. 3, pp. 626–630, June 1985.
- [40] M. Vetterli, “Splitting a signal into subsampled channels allowing perfect reconstruction,” in *In Proc. IASTED Conf. on Appl. Sig. Proc. and Dig. Filt.*, Paris, June 1985.
- [41] M. Vetterli, “Filter banks allowing perfect reconstruction,” *Signal Proc.*, vol. 10, no. 3, pp. 219–244, April 1986.
- [42] M. Vetterli and C. Herley, “Wavelets and filter banks: Theory and design,” *IEEE Trans. on Signal Processing*, vol. 40, no. 9, September 1992.
- [43] P. Vaidyanathan, “Quadrature mirror filter banks, m-band extensions and perfect reconstruction techniques,” *IEEE ASSP Mag.*, vol. 4, no. 3, pp. 4–20, January 1987.
- [44] L. Cohen, *Time–frequency Analysis: Theory and Applications*, Prentice-Hall, New York, 1995.
- [45] M. Priestley, *Spectral Analysis and Time Series*, Academic Press, London, 1981.
- [46] A. Kayhan, A. El-Jaroudi, and L. Chaparro, “Evolutionary periodogram for nonstationary signals,” *IEEE Transactions on Signal Processing*, vol. 42, pp. 1527–1536, 1994.
- [47] A. Kayhan, A. El-Jaroudi, and L. Chaparro, “Data adaptive evolutionary spectral estimation,” *IEEE Transactions on Signal Processing*, vol. 43, pp. 204–213, January 1995.
- [48] F. Marvasti, *Nonuniform Sampling: Theory and Practice*, Kluwer Academic/Plenum Publishers, New York, 2001.
- [49] A. Lazar and L. Toth, “Perfect recovery and sensitivity analysis of time encoded bandlimited signals,” *IEEE Trans. Circuits and Syst. – I: Regular Papers*, vol. 51, pp. 2060–2073, Oct. 2004.
- [50] K. Guan and A. Singer, “A level-crossing sampling scheme for non-bandlimited signals,” in *IEEE Intl. Conf. Acoustics, Speech and Sig. Proc.*, 2006, pp. III–381–383.
- [51] S. Senay, L. Chaparro, and L. Durak, “Reconstruction of nonuniformly sampled time-limited signals using Prolate Spheroidal Wave Functions,” *Signal Processing*, vol. 89, pp. 2585–2595, 2009.
- [52] N. Sayiner ad H. Sorensen and T. Viswanathan, “A level-crossing sampling scheme for A/D conversion,” *IEEE Transactions on Circuits and Systems II: Analog and Digital Signal Processing*, April 1996.
- [53] J. Mark and T. Todd, “A nonuniform sampling approach to data compression,” *IEEE Trans. Communications*, vol. 29, pp. 24–32, Jan. 1981.

- [54] A. Lazar, E. Simonyi, and L. Toth, “An overcomplete stitching algorithm for time decoding machines,” *IEEE Trans. Circuits and Syst. – I: Regular Papers*, vol. 55, pp. 2619–2630, October 2008.
- [55] A. Can, E. Sejdić, and L. Chaparro, “An asynchronous scale decomposition for biomedical signals,” in *EEE Sig. Proc. in Medicine and Biol. Symp*, 2011, pp. 1–6.
- [56] E. Sejdić, “Segmentation of dual-axis swallowing accelerometry signals in healthy subjects with analysis of anthropometric segmentation of dual-axis swallowing accelerometry signals in healthy subjects with analysis of anthropometric effects on duration of swallowing activities,” *IEEE Trans. on Biomedical Engineering*, vol. 56, no. 4, pp. 1090–1097, 2009.
- [57] Y. Eldar and T. Michaeli, “Beyond bandlimited sampling,” *IEEE Signal Processing Magazine*, vol. 26, no. 3, pp. 48–68, 2009.
- [58] P. Hansen, *Rank-Deficient and Discrete Ill-Posed Problems: Numerical Aspects of Linear Inversion*, SIAM, Philadelphia, 1998.
- [59] S. Şenay, J. Oh, and L. Chaparro, “Regularized signal reconstruction for level-crossing sampling using slepian functions,” *Signal Processing*, vol. 92, pp. 1157–1165, 2012.
- [60] D. Donoho, “Compressed sensing,” *IEEE Trans. Info. Theory*, vol. 52, pp. 1289–1306, Apr. 2006.
- [61] L. Cohen, “Time-frequency distributions: A review,” *Proc. IEEE*, July 1989.
- [62] S. Mallat and Z. Zhang, “Matching pursuits with time-frequency dictionaries,” *IEEE Trans. on Signal Processing*, vol. 41, no. 12, December 1993.
- [63] E. Sejdić, M. Luccini, S. Primak, K. Baddour, and T. Willink, “Channel estimation using dpss based frames,” *IEEE Intl. Conf. Acoust., Speech and Sig. IEEE Intl. Conf. Acoust., Speech and Sig. Proc.*, pp. 2849–2852, 2008.
- [64] J. Oh, S. Senay, and L. Chaparro, “Signal reconstruction from nonuniformly spaced samples using evolutionary slepian transform-based pocs,” *EURASIP Journal on Advances in Signal Processing*, 2010.
- [65] E. Roza, “Analog-to-digital conversion via duty-cycle modulation,” *IEEE Trans. Circuits and Syst. — II: Analog and Dig. Sig. Proc.*, vol. 44, pp. 907–914, Nov. 1997.
- [66] H. Choi and D. Munson, “Analysis and design of minimax-optimal interpolators,” *IEEE Transactions on Signal Processing*, vol. 46, no. 6, pp. 1571–1579, 1998.
- [67] A. Neumaier, “Solving ill-conditioned and singular linear systems: A tutorial on regularization,” *SIAM Review*, vol. 40, pp. 636–666, 1998.

- [68] E. Sejdić, A. Can, L. Chaparro, C. Steele, and T. Chau, “Compressive sampling of swallowing accelerometry signals using time-frequency dictionaries based on modulated discrete prolate spheroidal sequences,” *EURASIP J. Advances Sig. Proc.*, vol. 101, 2012.
- [69] E. Sejdic and J. Jiang, “Selective regional correlation for pattern recognition,” *IEEE Transactions on Systems, Man and Cybernetics, Part A: Systems and Humans*, vol. 37, no. 1, pp. 82–93, 2007.
- [70] G. Walter and T. Soleski, “Prolate spheroidal wavelet sampling in computerized tomography,” *Sampling Theory in Signal and Image Proc.*, vol. 1, no. 1, pp. 0–50, January 2005.
- [71] D. Mondal and D. Percival, *Statistical Challenges in Modern Astronomy V*, chapter Slepian wavelet variances for regularly and irregularly sampled time Slepian wavelet variances for regularly and irregularly sampled time series, pp. 403–418, Springer-Verlag, New York, 2012.
- [72] G. Strang, in *Lecture Notes in Control and Information Sciences*, vol. 219, chapter Creating and comparing wavelets, pp. 143–153, Springer Berlin Heidelberg, June 26-28 1996.
- [73] D. Donoho and I. Johnstone, “Ideal denoising in an orthonormal basis chosen from a library of bases,” *Comptes Rendus Acad. Sci. Ser. I*, vol. 319, no. 1317-1322, 1994.
- [74] J. Buckheit and D. Donoho, *Wavelab and Reproducible Research*, Springer-Verlag, 1995.
- [75] I. Daubechies, “Ten lectures on wavelets,” *SIAM, CBMS series*, April 1992.